BEHAVIOR OF SURFACTANT MIXTURES AT SOLID/LIQUID AND OIL/LIQUID INTERFACES IN CHEMICAL FLOODING SYSTEMS

FINAL REPORT

Reporting Period:	09/01/2001 to 08/31/2004
Contract Date:	09/01/2001
Principle Author:	Prof. P. Somasundaran
Date Report Issued:	November 20, 2004
DOE Award Number:	DE-FC26-01BC15312
Principal Investigator	Prof. P. Somasundaran
Submitting Organization	Office of Projects and Grants Columbia University in the City of New York 1210 Amsterdam Avenue, Mail Code 2205 Room 254 Engineering Terrace New York, NY 10027
Contracting Officer's Representative	H.V. Weyland U.S. Department of Energy, National Petroleum Technology Office One West Third Street, Suit 1400 Tulsa, Oklahoma 74101-3519

DISCLAIMER

ABSTRACT

The aim of the project is to develop a knowledge base to help the design of enhanced processes for mobilizing and extracting untrapped oil. We emphasize evaluation of novel surfactant mixtures and obtaining optimum combinations of the surfactants for efficient chemical flooding EOR processes. In this regard, an understanding of the aggregate shape, size and structure is crucial since these properties govern the crude oil removal efficiency. During the three-year period, the adsorption and aggregation behavior of sugar-based surfactants and their mixtures with other types of surfactants have been studied.

Sugar-based surfactants are made from renewable resources, nontoxic and biodegradable. They are miscible with water and oil. These environmentally benign surfactants feature high surface activity, good salinity, calcium and temperature tolerance, and unique adsorption behavior. They possess the characteristics required for oil flooding surfactants and have the potential for replacing currently used surfactants in oil recovery.

A novel analytical ultracentrifugation technique has been successfully employed for the first time, to characterize the aggregate species present in mixed micellar solution due to its powerful ability to separate particles based on their size and shape and monitor them simultaneously. Analytical ultracentrifugation offers an unprecedented opportunity to obtain important information on mixed micelles, structure-performance relationship for different surfactant aggregates in solution and their role in interfacial processes. Initial sedimentation velocity investigations were conducted using nonyl phenol ethoxylated decyl ether (NP-10) to choose the best analytical protocol, calculate the partial specific volume and obtain information on sedimentation coefficient, aggregation mass of micelles. Four softwares: OptimaTM XL-A/XL-I data analysis software, DCDT+, Svedberg and SEDFIT, were compared for the analysis

of sedimentation velocity experimental data. The results have been compared to that from Light Scattering. Based on the tests, Svedberg and SEDFIT analysis were chosen for further studies.

Surface tension and density measurements were performed to determine critical micellar concentrations (cmc), and partial specific volumes of n-dodecyl-β-D-maltoside (DM), nonyl phenol ethoxylated decyl ether (NP-10) and their 1:1 mixtures at 25°C. The effects of temperature and surfactant mixing on micellization and partial specific volumes were also studied. It was found that the partial specific volume is concentration dependent and sensitive to changes in temperature. Surface tension results revealed no interaction between the two surfactants in mixed micelles. Partial specific volume measurements also indicated no interaction in mixed micelles. A scrutiny of partial specific volumes of four sugar-based surfactants revealed that conformational changes upon micelle formation are responsible for the large deviation from the theoretical calculation. The information generated is used for the study of surfactant aggregate mass distribution in mixed systems. Such information is useful for identifying optimum surfactant systems in chemical flooding enhanced oil recovery processes.

From sedimentation equilibrium experiments in analytical ultracentrifugation technique, two types of micelles were identified for the nonionic polyethylene oxide surfactant (NP-10) and its mixtures with the sugar-based surfactant, dodecyl maltoside. Our study showed, for the first time, that small micelles coexist with large micelles at high concentrations due to unique structures of the surfactant although classical thermodynamic theory supports only one type of micelle. Initial dynamic light scattering results support the results for the same mixed surfactant system from analytical ultracentrifuge equilibrium technique. The implication of this finding lies in the fact that efficiency of oil recovery can be improved due to the large micellar size, its polymer-like fluidity and possible reduced adsorption on solids.

Micelles of the nonionic surfactants DM, NP-10 and their mixtures are found to be asymmetrical in shape at cmc. Interestingly, unlike ionic surfactants, the micellar growths of the nonionic surfactants were found to begin at concentrations immediately above cmc. The results also give evidence the coexistence of two types of micelles in nonyl phenol ethoxylated decyl ether solutions and its mixtures with n-dodecyl-β-D-maltoside while only one micellar species is present in n-dodecyl-β-D-maltoside solutions. Type I micelles are primary micelles at cmc while type II micelles are elongated micelles.

Reduced adsorption of surfactants on rocks is essential for them to be cost effective in enhanced oil recovery (EOR) by chemical flooding. Keeping this objective in mind, the adsorption of nonionic-anionic mixtures of n-dodecyl-β-D-maltoside (DM) and sodium dodecyl sulfonate ($C_{12}SO_3$) on alumina was studied under various conditions. At pH 7, molar ratio of DM to sulfonate changes do not have any significant effect on the mixture adsorption on alumina, even though the addition of salt did decrease their adsorption due to the reduced electrostatic attraction between oppositely charged surfactant and the solid. Solution pH showed a remarkable effect on the mixture adsorption: under acidic conditions, synergistic adsorption was observed for both DM and sulfonate, however, under basic conditions, interestingly there were only antagonistic or competitive effects between the sulfonate and the DM species. Competitive adsorption on minerals is relevant for obtaining reduced surfactant loss for efficient chemical flooding processes.

As it is our aim to develop structure-property relationships for adsorption that can be used in general, a preliminary model for the adsorption of the above mixed surfactants at the solid liquid interfaces was developed. Also, a model for micellization behavior of binary surfactant mixtures in solution is proposed. This model considers asymmetric behavior of micellization in

binary surfactant mixtures and predicts the changes in the structures of mixed micelles with concentration that are dependent on the overall ratio of the surfactant components and their chemical characteristics. Indeed there is a need to delineate the relationship between aggregate structures and chemical compositions of the surfactants, due to the important role played by aggregates as determined by their structures in interfacial properties such as wettability.

TABLE OF CONTENTS

LIST OF FIGURES

LIST OF TABLES

INTRODUCTION

There is considerable amount of oil trapped, together with water and gas, in reservoirs made up of porous and permeable rocks after the traditional oil production. Various chemical methods have been under development in order to recover the additional oil. These methods have been in general inadequate due to the high costs of the processes as well as significant loss of chemicals by adsorption on reservoir minerals and precipitation. There is a need to develop innovative and cost-effective reagent schemes to increase recovery from domestic oil reservoirs. It was our aim to design and evaluate efficient novel mixtures of surfactants for enhanced oil recovery. The key criterion for the successful application of the techniques using candidate surfactants is minimal loss of surfactants by adsorption and precipitation.

It is well known that surfactants can interact to form aggregates in solution (micelles) and at interfaces (hemimicelles) and these phenomena can have drastic effects on rock wettability and hence oil recovery processes. However, there is almost no information on such interactions in the case of mixtures and on changes in the aggregate structures due to perturbations in the system properties. Our recent work has shown that the aggregation behavior of some surfactant mixtures is quite unusual both in solutions and at the solid-liquid interfaces: more than one type of mixed micelles can form and possibly co-exist in mixed surfactant solutions. This finding has both theoretical and practical implications. It has potential for applications to minimize interfacial tension between oil and the flooding media to facilitate oil liberation and, at the same time, to reduce adsorption of surfactants on reservoir rocks.

There is no information in the literature, to our knowledge, on the relationship between the micro and nano-structures or performance of mixed surfactant aggregates and the chemical structure of the components in the mixtures. Also, there are no models with predictive capability

for the formation of mixed micelles, co-existing or otherwise. In this research, formation of aggregates in mixed systems and the effects of that on processes relevant to oil recovery were investigated. Major emphasis was placed on the relationships between surfactant mixture parameters (type, mixing ratio) and the aggregates properties (shape, composition and structure of mixed micelles and hemimicelles). Based on these results, a model which can predict the formation and changes in surfactant aggregates in their mixtures was developed.

A major hurdle in the analysis of mixed surfactant systems is the lack of information on the type of complexes and aggregates formed between various components and the lack of techniques for deriving such information. For the first time, we developed analytical ultracentrifuge technique for monitoring the mixed surfactant systems to derive information on the type of complexes and aggregates formed between various components. Information from analytical ultracentrifuge technique was used to reveal the relationship between distribution of surfactant species and aggregates and performance of the surfactants and their mixtures. Both dynamic and equilibrium information, such as the weight, shape and types of micelles, can be obtained with analytical ultracentrifuge from sedimentation velocity and equilibrium experiments.

Protocols for analytical centrifugation were established and preliminary analytical ultracentrifuge tests were conducted to identify the best analytical method. Partial specific volume of surfactants, as one of the fundamental parameters, play an important role in obtaining some dynamic and equilibrium information, such as weight, shape and types of micelles, from sedimentation velocity and equilibrium experiments. They were determined by both theoretical calculation methods and density measurements. The effects of temperature, mixing and micellization process (several key variables in enhanced oil recovery processes) on partial

specific volumes were investigated. It was found that the partial specific volume is concentration dependent and sensitive to changes in temperature. Such information is useful for identifying optimum surfactant systems used in EOR.

Solution and micellization behavior of sugar-based n-dodecyl-β-D-maltoside (DM), nonyl phenol ethoxylated decyl ether (NP-10) and their mixtures have been studied by surface tensiometry, dynamic light scattering, ultrafiltration, analytical ultracentrifuge sedimentation velocity and equilibrium techniques. Micellar size, shape and structures of above-mentioned systems were determined in dilute concentration regimes. Cryo-TEM images of those surfactants and their mixtures were taken to visualize the micelles.

Two types of micelles are detected to coexist in NP-10 solutions and its mixtures with DM while only one micellar species is present in individual DM solutions. The molecular structures of DM and NP-10 are responsible for the differences in the micellar shapes of single surfactants and their mixtures. Both the relative hydrocarbon / hydrophilic chain length and the flexibility of the hydrophilic groups contribute to the packing parameters and hence the excess free energy. From the concentration range below the cmc to above the cmc, these nonionic micelles were identified to grow from non-spherical into cylindrical shape. The information on aggregation of surfactants is particularly important for identifying optimum oil displacement condition because of their role in determining wettability.

Adsorption behavior of sodium dodecylsulfonate (sulfonates are one of the most commonly used surfactants in chemical flooding), sugar-based n-dodecyl-β-D-maltoside (DM) and their mixtures on alumina at different molar ratios has been investigated in the dilute concentration regimes. The effects on the adsorption of above mentioned mixture systems have been studied in terms of solution pH change, solution salinity and surfactant mixing ratios. Dramatic changes on

adsorption properties have been observed in DM/Sulfonate mixture system, with change in the solution pH from acidic to basic conditions. These findings are helpful for providing valuable information and for the study of mechanisms of EOR by chemical flooding and for the utilization of surfactant mixture systems in EOR by means of synergistic/antagonistic micellization and adsorption properties.

EXPERIMENTAL

MATERIALS

Surfactants:

Several typical ionic and nonionic surfactants were selected for this study. Non-ionic sugar-based n-decyl-β-D-glucoside and n-dodecyl-β-D-maltoside (DM) (>95% purity by thin layer chromatography) from Calbiochem (<0.05% dodecanol), n-dodecyl-β-D-maltotrioside (DTM) (>99.8% purity by HPLC) from Anatrace, and nonionic nonyl phenol ethoxylated decyl ether (NP-10) (>99% purity by HPLC) from Nikko Chemicals were used as received. The structure of n-dodecyl-β-D-maltoside is shown in Figure 1. The above nonionic surfactants enable study of the effects of surfactant structure such as chain length of the hydrophobic tail and size of hydrophilic headgroups on mixed aggregates formation. Anionic sodium dodecyl sulfonate ($C_{12}SO_3$) of greater than 99% purity from TCI Chemicals, Japan was also used as received. All surfactants used for the study are listed in table 1.

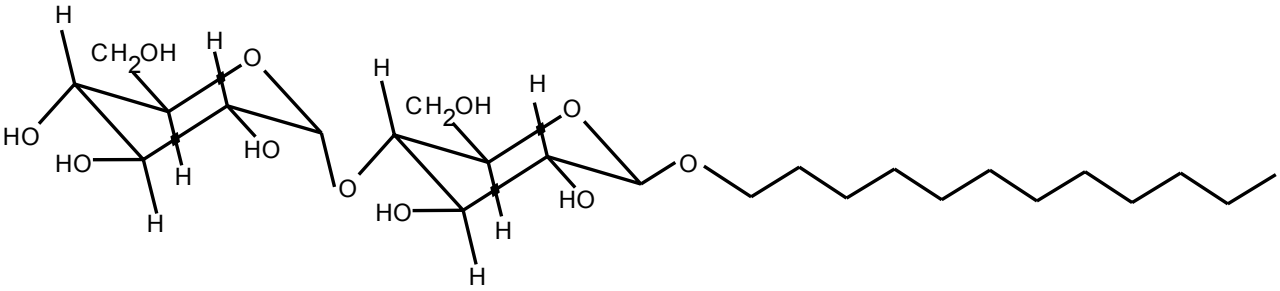

Figure 1. The chemical structure of sugar-based surfactant n-dodecyl-β-D-maltoside.

Mineral Samples:

Alumina AKP-50 obtained from Sumitomo had a mean diameter of 0.2 μm. The BET specific surface area measuring using nitrogen with a Quantasorb system was 10.8 m^2/g and the isoelectric point (iep) was 8.9. Silica obtained from Geltech was of a mean diameter of 0.1 μm and the specific surface area of 12.21 m^2/g and the iep was around 2. These solids were chosen

because of their low solubility and relative surface homogeneity with considerable amounts of information available in the literature.

Table 1. Surfactants used and their formulas.

Surfactant	formula
Sodium dodecyl sulfonate	$C_{12}H_{23}SO_3Na$
Polyethoxylated nonyl phenol	$C_9H_{19}(C_6H_4)(CH_2CH_2O)_nH$
n-alkyl-β-D-glucopyranoside	$CH_3(CH_2)_n[C_6H_{10}O_5]OH$
n-alkyl-β-D-maltoside	$CH_3(CH_2)_n[C_6H_{10}O_5]_2OH$

Other Chemicals:

HCl and NaOH, used for pH adjustment, were of A.C.S. grade certified (purity > 99.9%), from Fisher Scientific Co. To study the salt effect on adsorption, A.C.S. certified NaCl from Fisher Scientific Co. was used as received. Pyrene, a fluorescence probe, was obtained from Aldrich Chemicals and recrystallized from ethanol. Refractive index matching liquid, mixture of cis and trans decalin (>98% purity), was purchased from Acros Organics. It was used to reduce light bending at the glass interfaces in dynamic light scattering experiments.

Water used in all the experiments was triple distilled, with a specific conductivity of less than $1.5\mu\Omega^{-1}$ and was tested for the absence of organics using surface tension measurements.

METHODS

Adsorption experiments

Adsorption experiments were conducted in capped 20 ml vials. 2 gram samples were mixed for 2 hours with 10 ml of triple distilled water at room temperature. The pH was adjusted as

desired and then 10 ml of the surfactant solution was added and equilibrated further for 16 hours with pH adjustment. The samples were centrifuged for 30 minutes at 5000 rpm and clear supernatant was then pipetted out for analysis. Adsorption density was calculated based upon surfactant depletion from the solutions.

Ultrafiltration experiments

All ultrafiltration tests were done at room temperature (23±2°C) using Amicon membrane filters, specified to exclude molecules with molecular weights greater than 10,000 from single and mixed surfactant micellar solutions. The filtration was carried out by conditioning the filter with a 5 ml solution for an hour prior to the loading of the same solution. The filter was then centrifuged under 3000rpm for 30 minutes to obtain the supernatant.

Analytical Techniques

In adsorption experiments, sodium dodecylsulfonate concentration was determined using a two-phase titration method using a cationic surfactant as the titrating solution. Concentration of the sugar-based surfactant after adsorption was determined by measuring the total organic carbon (TOC) in the sample using a Shimazu Total Organic Carbon Analyzer, or by colorimetric method through phenol-sulfuric acid reaction. In the case of surfactant mixtures, the total surfactant concentration was measured by TOC method, while the sulfonate concentration was measured by the two-phase titration, and sugar-based surfactant by the colorimetric method.

In ultrafiltration experiments, NP-10 concentration was analyzed by determining UV absorbance at 223 or 275 nm using a Shimadzu 1201 UV-vis spectrophotometer. The total concentration of surfactant mixtures was determined using TOC, and the concentration of DM was calculated by subtracting the concentration of NP-10 from the total concentration.

Surface Tension

Surface tension measurements of the individual surfactant and their mixed solutions were made by the Wilhelmy plate method with the correction factors. The pull exerted on the plate was determined by a Cahn microbalance (Model LM 600). The entire assembly was kept in a draft-free plastic cage at 25±0.2ºC. Before each measurement, the plate was burnt to red and then cooled down to remove residual organics. The plate was in contact with the surfactant solution for 30 minutes to allow equilibrium prior to the measurement. Surface tension of triple distilled water was measured at 25ºC prior to each set of experiments.

Cloud Point measurement

Solutions of nonyl phenol ethoxylated decyl ether were heated in a water bath to cloud and then cooled down slowly. The temperature at which the solution became transparent was taken as the cloud point, i.e., phase transition temperature. A Brinkmann PC/600 colorimeter was used to determine the cloud point. Measurements were repeated at least three times for each sample and the accuracy was controlled within 0.1ºC.

Cryo-TEM

The sample was prepared at 25ºC in a humid environment to avoid loss of water by placing a drop of the surfactant solution on a TEM grid covered by a holey carbon film. A thin film of solution was constructed on the grid by blotting out the excess solution. The grids were immediately plunged into liquid ethane at its freezing temperature so that the micellar structures are fixed. The vitrified samples were examined at approximately -175ºC in a JEOL 1200EX TEM at 100kV accelerating voltage at the University of Rhode Island. The images were acquired

with a TVIPS TemCam-F224 slow scan CCD digital camera at 2048 × 2048 pixel resolution at magnifications ranging from 30,000X to 50,000X.

Dynamic light scattering experiments

Dynamic light scattering (DLS), known also as quasi elastic light scattering (QELS) and photon correlation spectroscopy (PCS), was used to analyze fluctuations in the intensity of the scattered light in the short time scale of microseconds to milliseconds caused by the diffusional or Brownian motion of the scattering particles (Figure 2). The light scattering depends on a number of factors including the difference between refractive index of the particles and the suspending liquid, the particle size and shape, the viscosity of the suspending medium, the wavelength and power of the incident light, and the angle of measurement.

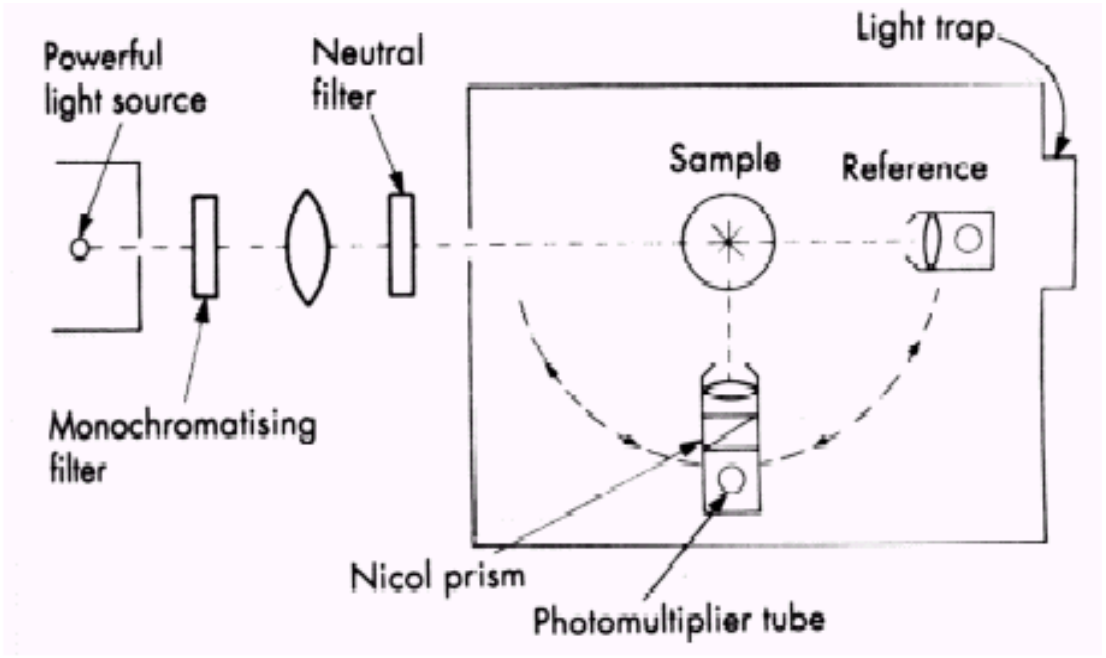

Figure 2. Schematics of light scattering apparatus.

DLS can typically measure the hydrodynamic diameter in the range of 2 nm up to 1000 nm, the translational diffusion coefficient, and the diffusional virial coefficient. The accuracy and

precision of DLS vary based on the type of dispersion analyzed. For dust free samples, the precision is a few percent. Most experimental samples are not ideal, and involve polydispersity and dust contamination. Typical scatterings can be up to ±10%.

The presence of contaminant dust particles is probably the most significant factor affecting the accuracy and precision. The effects of dust can be addressed through extensive cleaning and filtration in the preparation of the samples and for some instruments, a software dust filter is used to eliminate scattered light intensities that suddenly increase in magnitude due to dust.

In the simplified case of two-particle systems, the incident monochromatic laser light is scattered by two particles that are separated by a distance, d [1]. The scattered light then travels to the photomultiplier tube and is converted to an electrical signal. The scattered wave fronts can have constructive or destructive interference according to the equation: $d \sin \theta = m\lambda$, where d is distance between particles, θ is angle of scattering, m is constant, and λ is wavelength.

If m is an integer, then the optical interference is positive while if it is a half integer, the optical interference is destructive. The intensity of the scattered light I(t) varies from zero to two times the case for single particle scattering. A typical experimental sample has from $10^{7\text{-}8}$ particles so that there is random fluctuation between the two extremes. How fast the rate of variation in fluctuations varies determines the size of the particles.

The translational diffusion coefficient is determined from the scattering intensity time correlations function (TCF): $G2(t) = A + Bg_1^2(t)$

where A and B are constants and g_1^2 is the electric field TCF, given as

$$g_1 = \left| < E^*(0)E(t) > \right| / \left| < E^*(0)E(0) > \right|$$

E(0) and *E(t)* are the electric field amplitudes at zero time and delay time *t*. The asterisk denotes the conjugate complex quantity. The TCF shows an exponential-like decay to a base line *A*, and *B* is an efficiency parameter that is characteristic of the "signal to noise" ratio. Because of the exponential-like decay for $g_1(t)$, one can analyze the TCF via a cumulatant expansion given by [1]:

$$\ln g_1(t) = -\Gamma_1 t + (\Gamma_2 / 2!)t^2 - (\Gamma_3 / 3!)t^3 + \ldots$$

where $\Gamma=\Gamma_1, \Gamma_2, \Gamma_3, \ldots$ are the first, second, third, etc. cumulants. The theory of dynamic light scattering yields for the first cumulant measured at a certain concentration that

$$\Gamma_1 / q^2 = D_c(q)$$

where $\boldsymbol{D_c(q)}$ is an apparent, angular-dependent diffusion coefficient at concentration c.

The slope of the apparent translational diffusion coefficient versus particle concentration gives k_d, the diffusional virial coefficient from the following relationship neglecting higher terms:

$$D(q) = D_0(1 + k_d C + \ldots)$$

where *C* is concentration,

k_d is the diffusional virial coefficient,

k_d is defined as:

$$k_d = 2A_2 M_w - k_f - 2v_2$$

where A_2 is the second virial coefficient,

M_w is the molecular weight,

k_f is concentration dependence of the friction factor,

v_2 is the particle specific volume.

All surfactant solutions were filtered through 0.2 μm Nalgene™ pore size filter (Nalge Nunc International Co.) using a B-D syringe to remove dust. The first 5 ml filtered solution was

discarded to avoid dilution of the filtrate due to the adsorption of surfactant on the filter membrane.

Dynamic light scattering experiments were performed using the Brookhaven research grade system with a BI-9000 AT correlator and BI-200 SM geniometer with a detection angle of 90 degree. The water-cooled argon laser light source from Lexel Laser Inc. was used at a wavelength of 488 nm. The measurements were carried out at 25 ± 1^0C. The correlation function was measured and then analyzed using a cumulant analysis.

Partial specific volume measurements

Approach of Durchschlag and Zipper [2,3] was adopted to obtain the theoretical partial specific volume based on Traube's additivity principle and concept of volume increments for atoms. All the calculated partial specific volumes are at 25^0C.

Empirically, partial specific volume was obtained by determining the density difference over concentration. Densities of surfactant solutions were measured with an Anton Paar DMA 5000 densitometer. The principle involved measurement of the period of oscillation of a U-shape tube with the sample inside. The accuracies of the density and temperature data were $\pm5\times10^{-6}$g/cm^3 and $\pm0.01^0$C, respectively. The instrument was calibrated at atmospheric pressure (1013 mbar) with air and Anton Paar's standard water (=0.99820 ± 0.000010 g/cm^3 at 20^0C). Acetone was used to rinse the U-tube between measurements and was dried by pumping filtered air into U-tube.

Partial specific volume played an important role in the determination of micellar mass by analytical ultracentrifuge in that the quantity directly measured by sedimentation experiment was the buoyant mass, $M(1-\bar{\nu}\rho)$. If the solute concentration is determined on a mass/volume basis, the digital densitometer can measure the partial specific volume to a deviation within 0.2%.

Analytical ultracentrifuge

The Optima XL-I analytical ultracentrifuge (Beckman Coutler) [4] with integrated optical system can measure solute concentration distributions in one or more sample solutions at high centrifugal forces. The data can yield many important thermodynamic and hydrodynamic properties of surfactant aggregates or macromolecules and their interactions. The system can analyze dilute as well as concentrated samples.

The XL-I optical system contains two detectors: UV absorbance and interference optical systems. Absorbance optical system uses a UV/Vis spectrophotometer to monitor concentration by absorption of light at wavelengths from 190-800 nm. The interference optical provides a cell image in which the total concentration is determined from the refractive index difference between the test sample and the reference sample at each radial position as indicated by the vertical displacement of a set of evenly spaced horizontal fringe. Figure 3 shows the optical systems of the analytical ultracentrifuge [5]. A xenon flashlamp serves as the light source. The lamp is fired as the sector of interest passes over the detector. A toroidally-curved diffraction grating selects single-wavelength light onto the sample. Since the intensity of light from the flash lamp varies somewhat from pulse to pulse, light from the diffraction grating is normalized by reflecting a small percentage onto a detector located at the virtual focal point of the monochromator system. Monochromatic light passes through the sample cell, which is bounded by two quartz windows. This cell contains both a sample sector and a solvent sector so that the intensity of light transmitted through the sample can be expressed with reference to the solvent, as measured by a photomultiplier tube positioned beneath the rotor. A lens-slit assembly moves as a unit to provide radial scans of these sectors.

The absorbance optical system is based on the fact that many macromolecular solutes absorb incident radiation at particular wavelengths. For solutes obeying Beer's law, the absorption is linearly related to the molecular concentration. Thus, the radial distribution of the solute of interest, C(r), is readily determined from a radial scan of optical density.

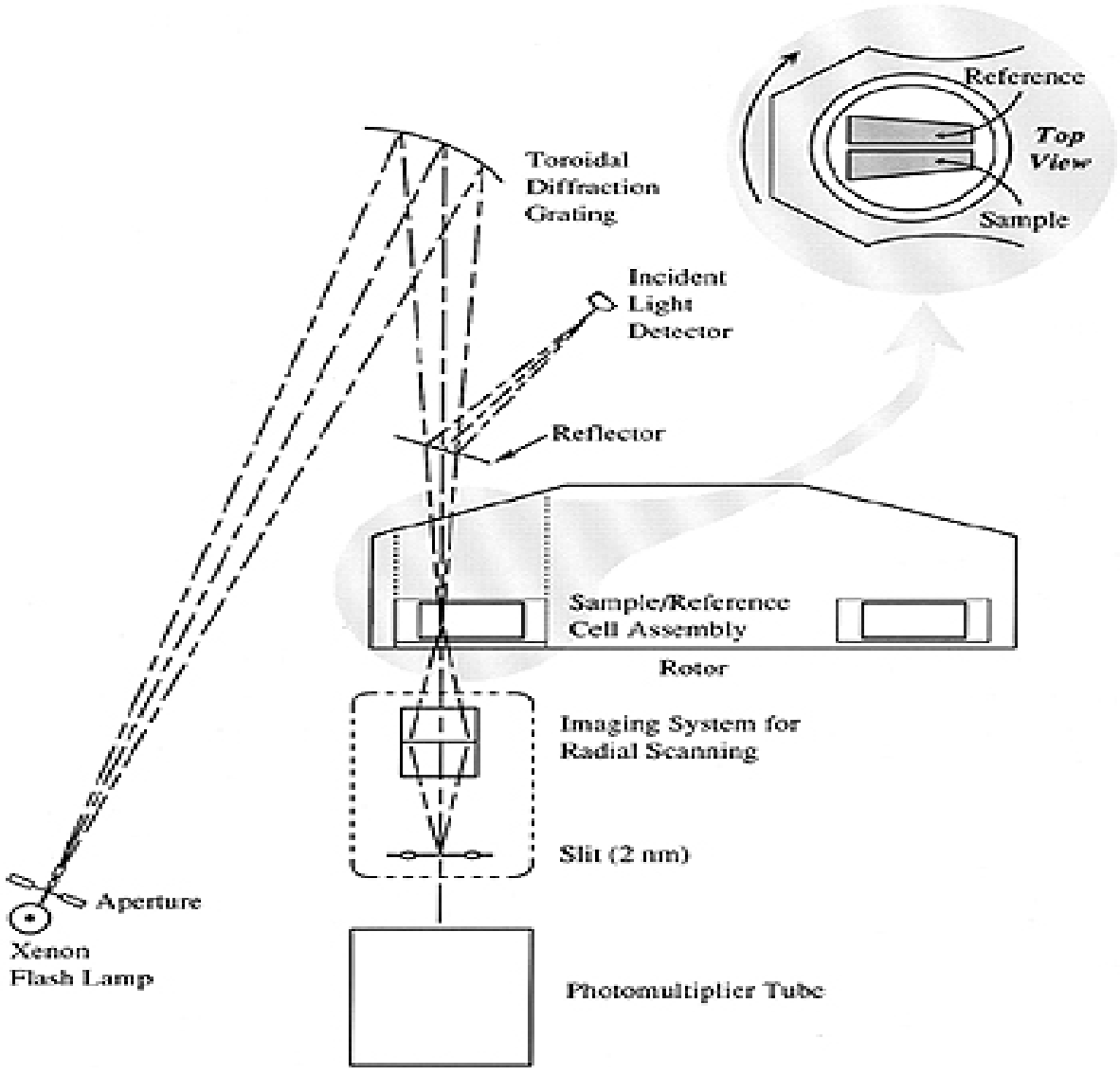

Schematic diagram of the optical system of the Beckman Optima XL-A Analytical Ultracentrifuge From "Analytical Ultracentrifugation, Vol. I", Beckman Instruments, Inc.

Figure 3. Optical system of the Beckman Optima XL-A AUC.

The experiment begins with the sample mixed uniformly throughout the cell, so that a plot of concentration vs radius is a horizontal line (C(r) = constant). As sedimentation proceeds, molecules are depleted from the top of the solution column. This results in the formation of a trailing boundary for the concentration distribution.

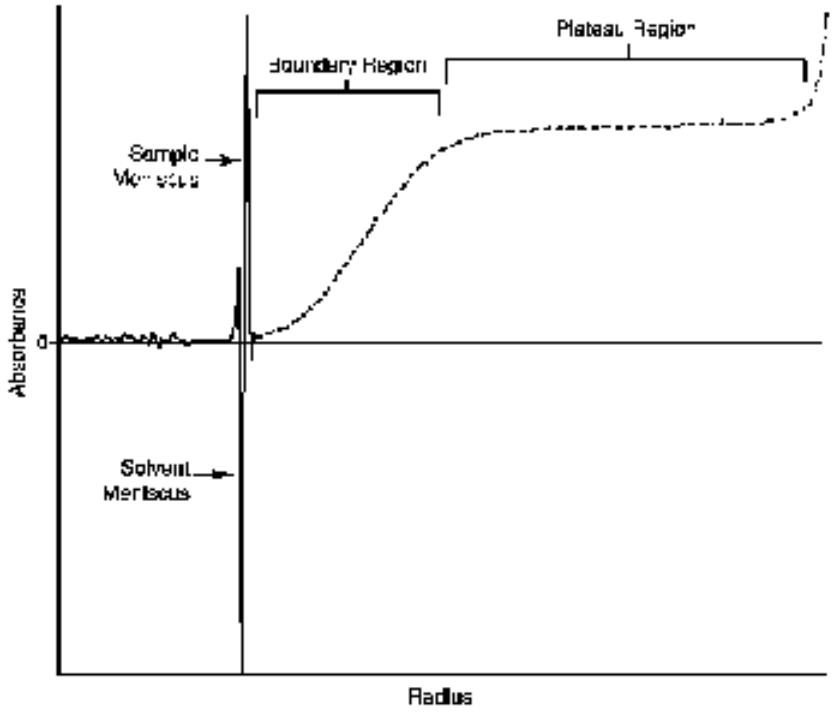

Figure 4. Typical boundary sedimentation data.

Figure 4 presents the absorbance of a solute in the sample sector compared to the reference sector. Sharp peaks result from the refraction of light away from the photomultiplier by the menisci in each sector. The remainder of the data consists of the boundary region in which the solute concentration increases rapidly to a reasonably constant value in the plateau region. Most of the information in a sedimentation velocity experiment is taken from analysis of the boundary. For example, the boundary will be sharp for a simple sedimentation involving one component. The sedimentation coefficient can be derived from the motion of the boundary midpoint. As an alternative representation, the data may be presented as the derivative of the concentration

function, or dC/dr. In this representation, each boundary segment appears as a discrete peak. The sedimentation coefficient is obtained from the radial motion of these peaks. The relative concentration of each sample component is determined from the area under each peak.

One feature of the plateau region is worth noting. Particles of greater radii will move faster than the smaller ones, thus pulling away from the latter as seen in Figure 5. In addition, as the experiment progresses, particles beginning near the outermost portion of the solution column will be pulled against the outer wall of the sample cell, and will be replaced by particles from nearer the center of rotation. These latter particles enter a progressively increasing volume as they migrate outward through the sector-shaped cavity, and thus become more dilute.

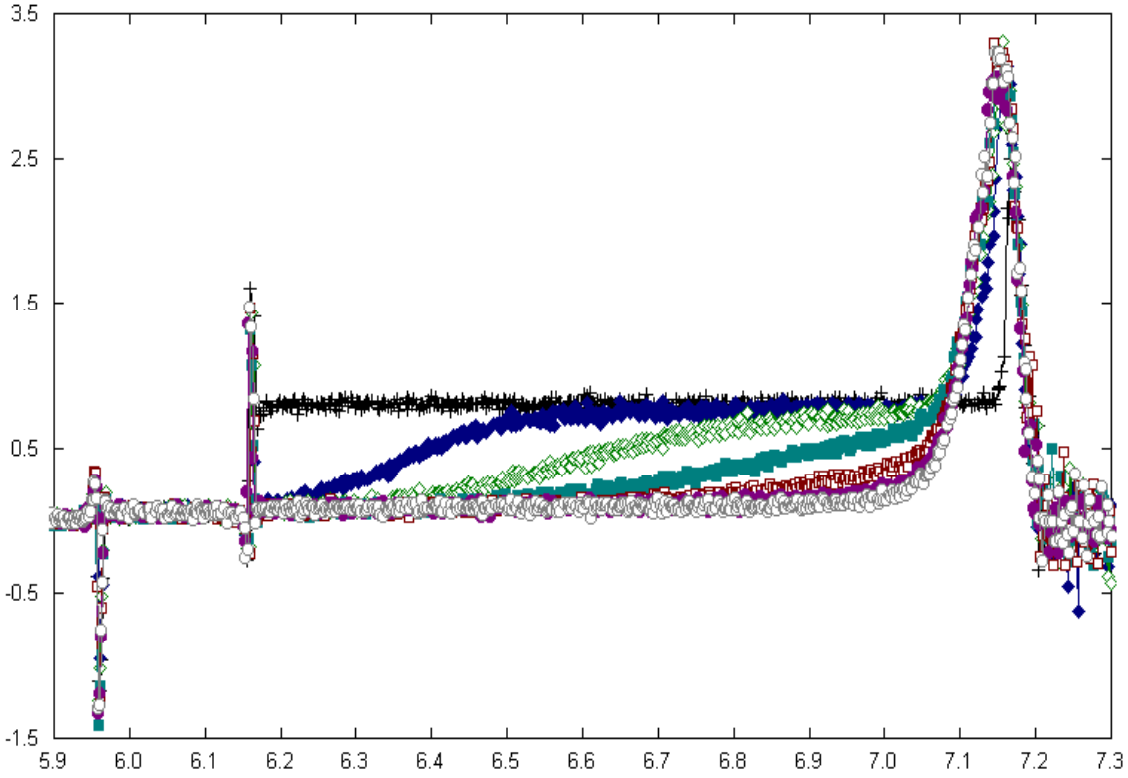

Figure 5. **Shifting boundaries at different rotation time. As sedimentation starts, the solute is distributed evenly along the radius. Boundary shifts gradually to the bottom of the cell with time.**

Analytical ultracentrifuge sedimentation equilibrium

The sedimentation equilibrium experiments require several criteria [6]:

a. The sedimentation equilibrium is reached if the concentration distribution did not change with time.

b. The equilibrium distribution depended only on the buoyant molecular weight and not in anyway on the shape of particles in solution.

c. Sedimentation equilibrium experiment can provide information such as the state of aggregation.

$$\frac{\partial C}{\partial t} = \frac{1}{r}\frac{\partial}{\partial r}\left[rD\ \frac{\partial C}{\partial r} - s\omega^2 r^2 C \right] = 0$$

The equilibrium equation was derived from Lamm equation:

Where, $\partial C/\partial r$ is the solute concentration gradient, r is the radius, D is the diffusion coefficient, s is sedimentation coefficient, $\omega^2 r$ is centrifugal force field strength, c is the solute concentration and M is the molecular weight

Since $1/r \neq 0$, the Lamm equation could be expressed as:

$$D\frac{\partial C}{\partial r} = s\omega^2 r\ \ Cdr$$

Separating variables and integrating the equation,

$$C_r = C_a \exp[\frac{s\omega^2}{2D}(r^2 - a^2)]$$

where a is the radial reference distance, and C_a is the solute concentration or absorbance at a.

From the Svedberg equation:

$$\frac{s}{D} = \frac{M(1-\bar{\nu}\rho)}{RT}$$

where M is the molecular weight of macromolecule or aggregation mass of the surfactant micelles, ρ is solvent density, v bar is the partial specific volume, R is the gas constant and T is the absolute temperature.

Thus, $$C_r = C_a \exp\left[\frac{\omega^2}{2RT} M(1-v\rho)(r^2 - a^2)\right]$$

From the assumption that sedimentation and diffusion have reached a state of equilibrium, the following equation can be derived for equilibrium:

$$\frac{M(1-\bar{v}\rho)\omega^2}{2RT} = \frac{d\ln C}{dr^2}$$

A plot of lnC versus r^2 should give a straight line with a slope related to M. A straight line was achieved only with a single, ideal species. The line was not linear if multiple species, aggregation or nonideal species were present. It is clear that the concentration of macrosolute with radial distance is nonlinear with respect to the parameter of interest, the buoyant molecular weight $M(1-\bar{v}\rho)$.

Data analysis generally involves nonlinear least squares regression.

While in an ideal solution, the solute species are point particles, occupying no volume, and interact only through collisions. Real solutions of macromolecules will exhibit thermodynamic nonideality because of the excluded volume effect of macromolecules, which usually occupy a significant fraction of the volume. This case was especially severe for particles of high masses and extended shapes. Nonideality occurred often with charged macromolecules since the electrostatic force act over long distances.

Nonideality is concentration dependent, being larger at high concentrations. Quantitatively, the nonideality can be measured through the relationship between apparent M and concentration, using virial coefficients:

$$M_{app} = \frac{M}{1 + BMC + \ldots}$$

$$\frac{1}{M_{app}} = \frac{1}{M} + BC + \ldots$$

where M_{app} is the apparent molecular weight obtained from the data, B is the second virial coefficient and C is the weight concentration of the centrifuged sample. The minimum of B was in the range of $10^{-5} - 10^{-6}$.

Probably the best test for the homogeneity with respect to mass is based on the residuals following minimization of the sum of squared scatterings. If the data is fitted to a single ideal solute model, the residual is randomly distributed if the solution is ideal. Upward residuals indicate aggregation and downward residuals nonideality.

Sedimentation equilibrium experiments were performed in a Beckman Coulter Optima™ XL-I analytical ultracentrifuge equipped with both absorbance and interference optical detectors [5]. A six-sector cell and sapphire windows [7] were used for sedimentation equilibrium experiments. The aluminum cell was counter-balanced on an An-60 Ti rotor.

In the sedimentation equilibrium experiment, the sample solutions were subjected to centrifugation at speeds ranging from 3,000 to 40,000 rpm. "Subtract data" command in Optima® XL-I data analysis software "Origin 4.0" was used to detect the equilibrium state. The blank noise was removed using software WinReed and then the new data set were sent back to Optima® XL-I data analysis software "Origin 4.0" to do the analysis. All experiments were done at temperature of 25 ± 0.1^0C.

Analytical ultracentrifuge sedimentation velocity

The micellar masses were calculated from Svedberg equation [8] and then were converted to the aggregation numbers.

$$\frac{s}{D} = \frac{M(1 - \bar{v}\rho)}{RT}$$

where s is the sedimentation coefficient, D is the diffusion coefficient, M is the micelle weight, $\bar{v}$ is the partial specific volume of micelles, R is gas constant and T is absolute temperature.

The Stokes-Einstein equation leads to the hydrodynamic radii [8,9]:

$$r_H = \frac{k_B T}{6\pi\eta D_0}$$

where k_B is the Boltzmann constant and η is the viscosity of the solvent, i.e. water.

The hypothetical minimum radius of spherical micelle, r_0, is defined as [8,9]:

$$r_0 = \left(\frac{3M\bar{v}}{4\pi N}\right)^{\frac{1}{3}}$$

where N is the Avogadro's number.

The transnational frictional coefficient, f, is obtained using the above relation [8,9],

$$D = \frac{RT}{Nf}$$

It should be noted that f depends on the shape of the particle. The frictional coefficient f_0, of a sphere taking up the same volume, is calculated from the equation [8,10]:

$$f_0 = 6\pi\eta r_0$$

where η is the viscosity of the solvent, r_0 is the hypothetical spherical radius.

The ratio of f/f_0 comprise of the shape and hydration contributions [8,10]:

$$\frac{f}{f_0} = \frac{f}{f_{shape}}\left(1 + \frac{\delta\bar{v}_s}{\bar{v}}\right)^{\frac{1}{3}}$$

where the f_{shape} is the frictional coefficient due to the geometrical asymmetry, δ is the hydration and $\bar{v}_s$ is the density of the solvent.

From the f/f_{shape}, the shape of micelles can be evaluated using the above equations [8,9]:

For prelate ellipsoid,

$$\frac{f}{f_{shape}} = \frac{(1-\alpha^2)^{\frac{1}{2}}}{\alpha^{\frac{2}{3}} \ln\left(1+\frac{(1-\alpha^2)^{\frac{1}{2}}}{\alpha}\right)}$$

For oblate ellipsoid,

$$\frac{f}{f_{shape}} = \frac{(\alpha^2-1)^{\frac{1}{2}}}{\alpha^{\frac{2}{3}} \tan^{-1}(\alpha^2-1)^{\frac{1}{2}}}$$

where α is the maximum axial ratio, $\alpha=a/b$.

Sedimentation velocity experiments were performed in a Beckman Coulter Optima® XL-I analytical ultracentrifuge equipped with both absorbance and interference optical detectors [5]. A 12 mm two-sector aluminum cell and quartz windows were used for velocity experiments. The aluminum cell was counter-balanced in an An-60 Ti rotor.

In sedimentation velocity experiment, the rotor speed was set at 40,000 rpm. The velocity experiment is run after the vacuum reached 1-2 micron Hg. Software SEDFIT 84 developed by Peter Schuck was used to obtain sedimentation coefficient distribution, c(s), from sedimentation velocity data [10, 11]. The sedimentation coefficients were obtained from John Philo's software DCDT+[12-14].

RESULTS AND DISCUSSION

Experimental schemes of analytical ultracentrifuge

Basically, analytical ultracentrifuge(AUC) has four experimental schemes [15]:

1) sedimentation velocity experiment,

2) sedimentation equilibrium run,

3) density gradient run,

4) synthetic boundary experiment.

Sedimentation velocity experiment and sedimentation equilibrium run are the commonly used methods.

1. Generally, sedimentation velocity experiment is carried out at high centrifugal fields. When separation of mixture takes place, one can detect a step-like concentration profile. Each step corresponds to one species. Also, the sedimentation of molecules can be monitored. From the sedimentation velocity experiment, one can obtain information such as the rate of movement of a solute in a centrifugal field, an apparent weight average sedimentation coefficient, an apparent sedimentation coefficient diffusion function g(s*) from the time derivative of the concentration profile, a weight average diffusion coefficient and an estimated molecular weight (M). From the velocity of the sedimenting boundary, one can determine the sedimentation coefficient *s* according to:

$$s = \frac{\ln(r / r_m)}{\omega^2 t}$$

where r is the position of the moving boundary, r_m the radial distance of the meniscus, t the time and ω the angular velocity. The sedimentation coefficient is a concentration and pressure dependent quantity, which can be obtained by appropriate correction or the extrapolation to zero

concentration. A plot of ln(r/rm) vs. $\omega^2 t$ is a line with the slope equal to the sedimentation coefficient. The sedimentation coefficient is measured in the Svedberg (S) unit where $1S=10^{-13}$ s. The molar mass of the sample can be calculated according to the Svedberg equation:

$$M = \frac{sRT}{D(1-\bar{v}\rho)}$$

where D is the diffusion coefficient, M the molar mass of the sample, $\bar{v}$ the partial specific volume, ρ the solvent density, R the gas constant and T the absolute temperature.

2. Sedimentation equilibrium experiment is performed either at moderate or at high centrifugal fields. The concentration gradient contains information about the molar mass of the sample, the second osmotic virial coefficient or interaction constants in the case of interacting systems. The advantage is that the detection of the concentration gradient is possible without disturbing the chemical equilibrium even for weak interactions. Sedimentation equilibrium analysis allows one to determine the following properties: macromolecular structure (molecular weight, or weight-average molecular weight if there is heterogeneity), association properties of macromolecules in solutions (stoichiometry, reversibility and association constant), heterogeneity (dissimilar non-self-associating components present) and nonideality (non-associative interactions between molecules due to shape or charge).

$$c(r) = c(a)\exp[M(1-\bar{v}\rho)\omega^2(r^2 - a^2)/2RT]$$

where *c(r)* is the concentration at radial position r, *c(a)* the concentration at the meniscus, *a* the radial distance of the meniscus, R gas constant and T absolute temperature.

3. Density gradient experiment is based on possible separation due to chemical structure in a density gradient medium. Either high-density salts or substances like sucrose are dissolved in

water or a mixture of two organic solvents with very different densities is used. The sample will sediment/float to a position where its density matches that of the gradient. In the case of mixtures, this leads to a banding of the components due to their chemical structure/density.

4. Synthetic boundary experiment relies on the changes of a boundary between solution and solvent with time at low centrifugal fields where no sedimentation of the sample occurs. Such experiments require special cells where the solvent is layered upon the solution column under the action of a certain centrifugal field. Diffusion coefficient distribution could be derived in a single synthetic boundary experiment.

Theoretical calculation of partial specific volume of surfactants

Svedberg equation is the basis of analytical ultracentrifuge technique. Thus partial specific volume is a very important parameter. There are two ways to obtain the partial specific volume: theoretical calculation and by densiometer. Calculation method is fast and accurate for single component systems and systems with inorganic salts. Experimental method is especially useful for mixed systems.

So far, calculation method is chosen because only hydrodynamic properties of single surfactant are measured. Helmut Durchschlag and Peter Zipper's approach [2,3] is adopted to calculate the partial volumes of surfactants and their mixtures in aqueous solutions. The method is based on Traube's additivity principle and concept of volume increments for atoms. This calculation procedure is developed for some special increments/decrements for co-volume, ring formation, ionization and linking tabulated volumes of inorganic ions.

Partial molar volumes, $\overline{V_c}$, is defined as:

$$\overline{V_c} = \sum V_i + V_{CV} + \sum V_{RF} - \sum V_{ES}$$

where *Vi* is the volume increment for any atom or atomic group, V_{CV} the correction due to the covolume, V_{RF} and V_{ES} take into account the decrease in volume caused by ring formation and ionization (electrostriction), respectively.

The partial specific volume, $\overline{\nu_i}$ of the ith component of a solution is defined as the change in total volume, ∂V, per unit mass upon adding an infinitesimal amount, ∂g_i, of component i at constant temperature, *T*, and pressure, *P*, and masses in grams, g_j, of all other components *j*:

$$\overline{v}_i = (\partial V/\partial g_i)_{T,P,g_j} \qquad (j \neq i)$$

The partial specific volume, is defined in an analogous way by substituting the number of grams, *g*, by the number of moles, *n*:

$$\overline{V}_i = (\partial V/\partial n_i)_{T,P,n_j} \qquad (j \neq i)$$

Usually, partial specific volumes, $\overline{\nu}$, are given in cm^3/g, and partial molar volumes, $\overline{V}$, in cm^3/mol. These two are related by:

$$\overline{\nu}_i = \overline{V} / M_i$$

where M_i is the molar mass of the ith component, in g/mol.

Reported experimental partial specific volumes of surfactants generally vary between 0.7 and 1.2 cm_3/g, depending on the nature of surfactants and the micellar state. The effect of micellization on the partial specific volume is also taken into account by introducing an additional volume increment V_{mic}. V_{mic} is influenced by various parameters (e.g., chain length and surface charge, shape and structure of micelles, aggregation number, CMC values, interaction between surfactants, solvent and co-solvents). The volumes of surfactants above CMC generally exceed the value below CMC by 0-6%. However, for most nonionic surfactants, no correction for micellization is necessary.

Partial specific volume of nonyl phenol ethoxylated decyl ether (NP-10) is calculated according to the above method.

Table 2. Calculation of the partial specific volume of NP-10 Surfactant at 25°C

Name	V_C (cm3/mol)	M (g/mol)	ν_C (cm3 /g)
NP-10	606.5	658.9	0.920

Compared to values in literature [16], experimentally determined value for partial specific volume of Triton N-101 (a mixture between NP-9 and NP-10) is 0.922. The calculated result is very close to the experimental result.

It should be noted that the partial volumes are only valid for aqueous solutions at 25°C. Application of volumes at different temperatures requires the use of a temperature correction. For substances in aqueous solutions, temperature coefficient of 2-10 $\times 10^{-4}$ $cm^3g^{-1}K^{-1}$ has been reported in the literature, therefore, a value of 5 $\times 10^{-4}$ $cm^3g^{-1}K^{-1}$ for temperature correction may be used.

Data analysis softwares for analytical ultracentrifugation

Lamm equation is the basic equation for sedimentation velocity data analysis software. It describes the evolution of concentration distribution C(r, t) of a species with sedimentation coefficient s and diffusion coefficient D in a sector-shaped volume and in centrifuge field $\omega^2 t$. It is a partial differential equation:

$$\frac{dc}{dt} = \frac{1}{r}\frac{d}{dr}[rD\frac{dc}{dr} - s\omega^2 r^2 c]$$

1. OptimaTM XL-A/XL-I data analysis software [4]

A customized OptimaTM XL-A/XL-I data analysis software is used for velocity and equilibrium experiments. The experimental analysis of sedimentation velocity experiments provides four models such as transport, second moment, sedimentation time derivative and flotation time derivative. The transport method measures the total amount of solute transported across a boundary chosen in the plateau region of the data set. An advantage of the transport method is that it can be used to calculate a *s* value from early files in an experiment, because it does not require that the meniscus to be depleted of the solute. However, a more accurate analysis of the interference data can be obtained using the second moment method. The second moment method must use data with a flat lower plateau, indicating that the solute has moved away from, or become depleted at, the meniscus region of the cell.

Sedimentation time derivative analysis is used to calculate apparent sedimentation coefficient distribution functions, *g(s*)*, from the time derivative of the concentration profile of all particles in a system. In systems where particles are less dense than the solution they are suspended in, they float up from the bottom of the cell, and the flotation time derivative analysis is used to determine the density distribution for the system. Molecular weight could not be determined by this analysis because sedimentation does not occur.

Sedimentation time derivative method is the most commonly used method in sedimentation velocity experimental data analysis. The molar mass, diffusion coefficient and sedimentation coefficient of 6×10^{-4}M NP-10 micelles are analyzed by time derivative method. Experimental conditions are below:

* Rotor speed: 40K rpm

* Scan No. used in the analysis: 20

* Detector: UV 273 nm and RI

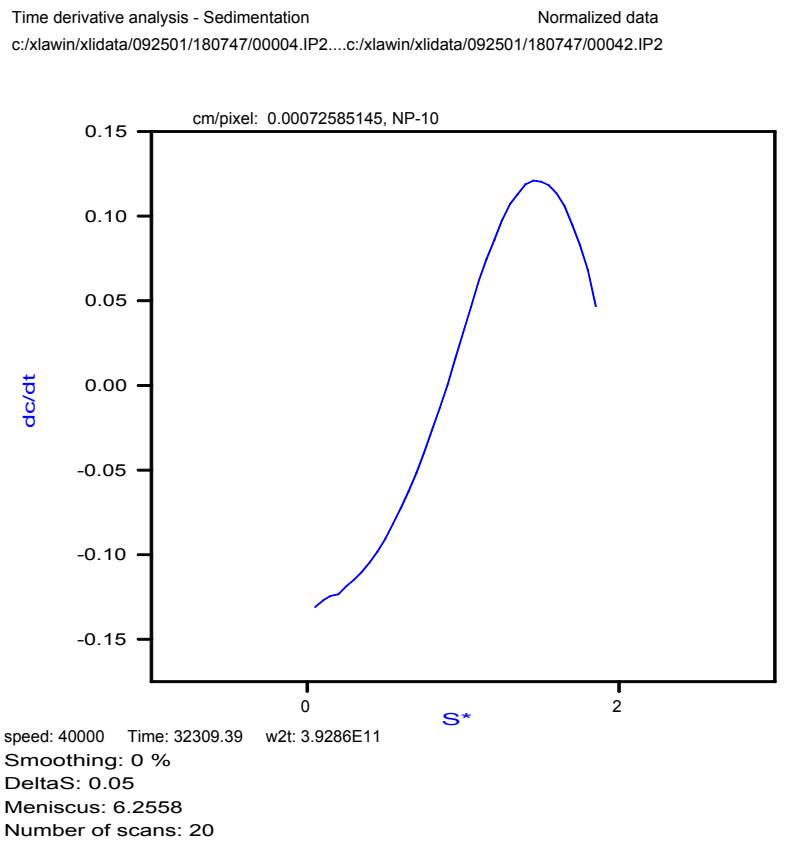

Figure 6. dc/dt vs. s* plot for sedimentation time derivative method.

Figure 6 shows results obtained for sedimentation time derivative method. Here, s* denotes apparent sedimentation coefficient. Because the software does not eliminate the diffusion effect, this sedimentation coefficient is not the real sedimentation coefficient. A Gaussian's distribution could be applied for the apparent sedimentation coefficient as shown in Figure 7.

Figure 8 shows the overlay of two curves. Results for the *g(s*)* are shown here: S*=1.40S, M=138KDa, D*=9.39e-8. From this aggregation mass, the aggregation number is expected to be 209.

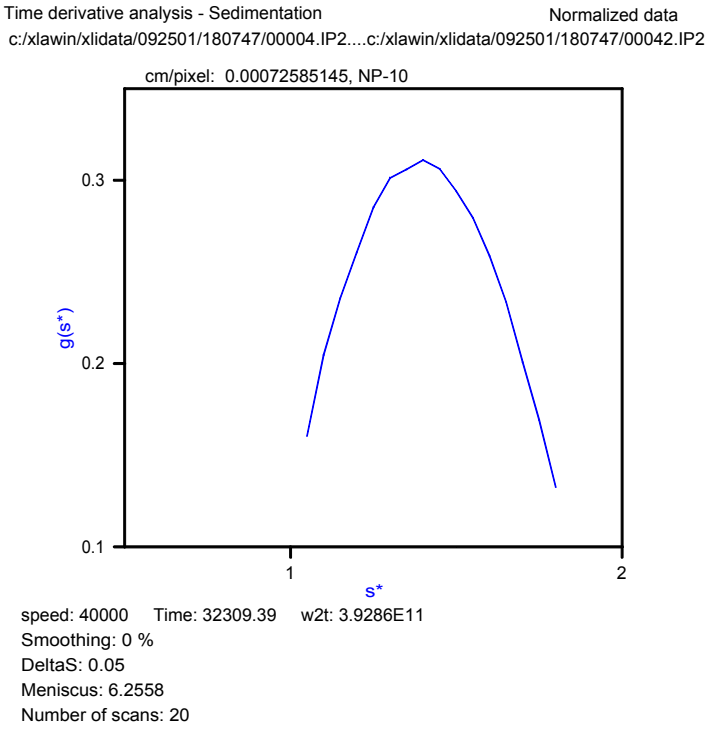

Figure 7. Gaussian's fit curve of apparent sedimentation coefficient.

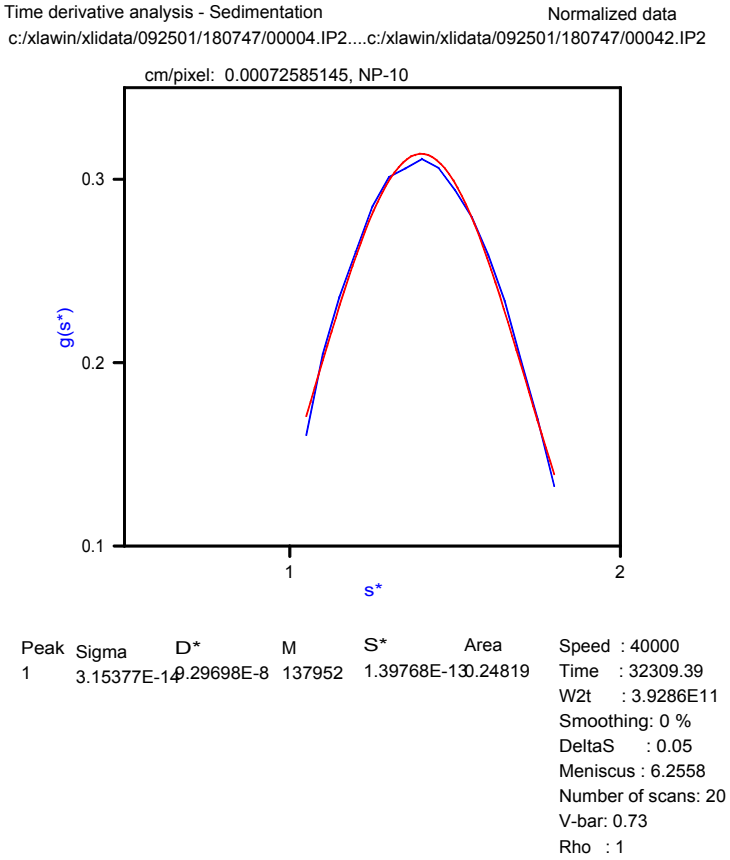

Figure 8. Comparison of Gaussian's distribution results with experimental results.

Disadvantages of OptimaTM XL-A/XL-I data analysis:

a. It is very difficult to obtain g(s*) results for surfactant systems by this software. Gaussian distribution is the default analysis method. One of the virtue of Gaussian distribution is that the time difference dc/dt eliminates the time invariant noise usually encountered in interference optical data. However, the resolution of Gaussian distribution is poor.

b. This software sets partial specific volume and solvent density as default values. The partial specific volume is the same as that of proteins - 0.73 cm3/g and the solvent density is the same as that of water. The partial specific volume of the surfactant is quite different from that of protein.

c. Back diffusion effect is very severe in surfactant systems due to the small micellar size. The sedimentation coefficient distribution g (s*) using time derivative method does not eliminate the back diffusion effect. A small portion among the whole scans (usually less than 40 scans) has to be chosen to do analysis to keep the diffusion coefficient constant. Thus, the apparent sedimentation coefficient and molecular mass results do not reflect the real values.

2. DCDT+ software

DCDT+, developed by John Philo [12], directly fit the dc/dt curves [rather than g(s*)] to obtain the s and D (or M) values. This gives significantly more accurate results [~1% error in M instead of errors up to 10% through fitting g(s*)]. Fitting to dc/dt also provides an improved ability to resolve multiple species, and avoids some of the problems that g(s*) has with low molecular weight species. The function used to fit the dc/dt curves is the analytical time derivative of the modified Fujita-MacCosham function, which is the approximate analytical solution of Lamm equation. This software allows input of partial specific volume and solution density. The maximum scan number is 99.

Modified Fujita-MacCosham function is described as below: This function gives the concentration c at any time t and radial position r in terms of dimensionless parameters

$$\tau \equiv 2 s \omega^2 t \qquad x \equiv (V / V_0)^2 \qquad \varepsilon \equiv 2D / s\omega^2 r_0^2 \qquad Z = ln(x)$$

and z = ln(x), from the formula:

$$C = \frac{C_0 e^{-\tau}}{2}\left\{\begin{array}{c} 1 - erf\left[\dfrac{\tau - z}{2\sqrt{\varepsilon\tau}}(1+\alpha\tau)\right] \\ -\dfrac{2}{\sqrt{\pi}}\left(\dfrac{\tau}{\varepsilon}\right)^{1/2}\exp\left(\dfrac{-(\tau-z)^2}{4\varepsilon\tau}(1+\beta\varepsilon\tau)\right) \\ +\left(1+\dfrac{\tau+z}{\varepsilon}\right)\left(1-erf\left[\dfrac{\tau+z}{2\sqrt{\varepsilon\tau}}\right]\right)\exp\left(\dfrac{z}{\varepsilon}\right) \end{array}\right\}$$

where C_0 is the loading concentration, r_0 is the meniscus position, and *erf()* is the error function.

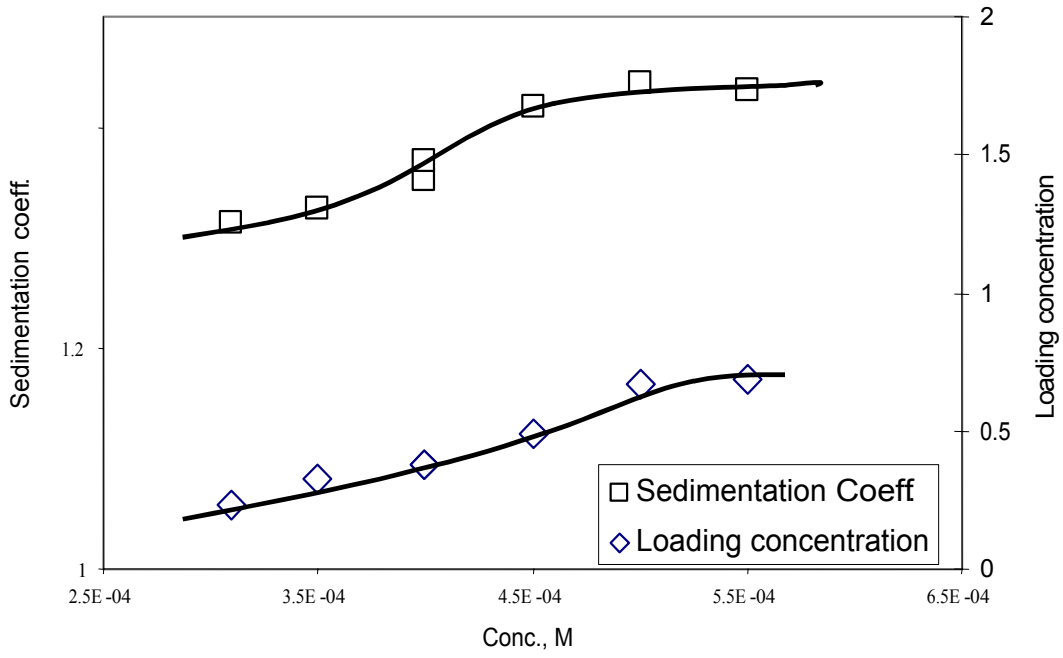

Figure 9. Effect of concentration on the loading concentration and sedimentation coefficient.

Figure 9 shows that both loading concentration and sedimentation coefficient are linear with concentration. These trends agree with the theoretical prediction. By inputting the partial specific volume of NP-10, the aggregation masses are less than that from OptimaTM XL-A/XL-I data analysis software. The results are closer to the result observed by other techniques such as light scattering [17]. Light scattering shows that the aggregation number of NP-10 is around 100.

3. Svedberg software

SVEDBERG is particularly good for quantitative results and for resolving small amounts of minor species (e.g. 5-10% of a dimer). Its superior resolution over the DCDT method arises from the fact that it can fit data over a broad time range. Compared to g(s*) analysis with DCDT, SVEDBERG provides superior accuracy for s values, especially for small proteins (5-50 kDa), and significantly more accurate results for D or M of larger proteins (>100 kDa) [<~1% error instead of errors up to ~10% through fitting g(s*)].

For multi-species fits SVEDBERG also allows the user to constrain the properties of the species with respect to one another, forcing the constrained species to have hydrodynamic properties, which are in ratios appropriate for small oligomers. These constraints can significantly enhance the ability to resolve minor species (and also the accuracy of the results for the major species).

The aggregation mass of NP-10 is determined by DCDT+ and Svedberg methods. The results are shown in Table 3. Taking an average aggregation mass (denoted as M) over the measured concentrations, two averages could be obtained for DCDT+ and Svedberg methods, respectively. The average aggregation masses are 83.9 KDa by DCDT+ and 73.3 KDa by Svedberg. From the plot of aggregation masses from DCDT+ and Svedberg as functions of

concentration (Figure 10), it is clear that the results by Svedberg have less fluctuation than those by DCDT+.

Table 3: Comparison of aggregation mass of NP-10 by DCDT+ and Svedberg methods

C	C0	s	M, DCDT+	M, Svedberg
3.1E-04	0.23	1.314	98.7	75.41
3.5E-04	0.327	1.326	77.39	76.13
4.0E-04	0.376	1.352	93.85	90.21
4.0E-04	0.38	1.37	77.7	68.7
4.5E-04	0.488	1.419	78.37	66.08
5.0E-04	0.669	1.439	89.95	63.28
5.5E-04	0.69	1.434	71.31	

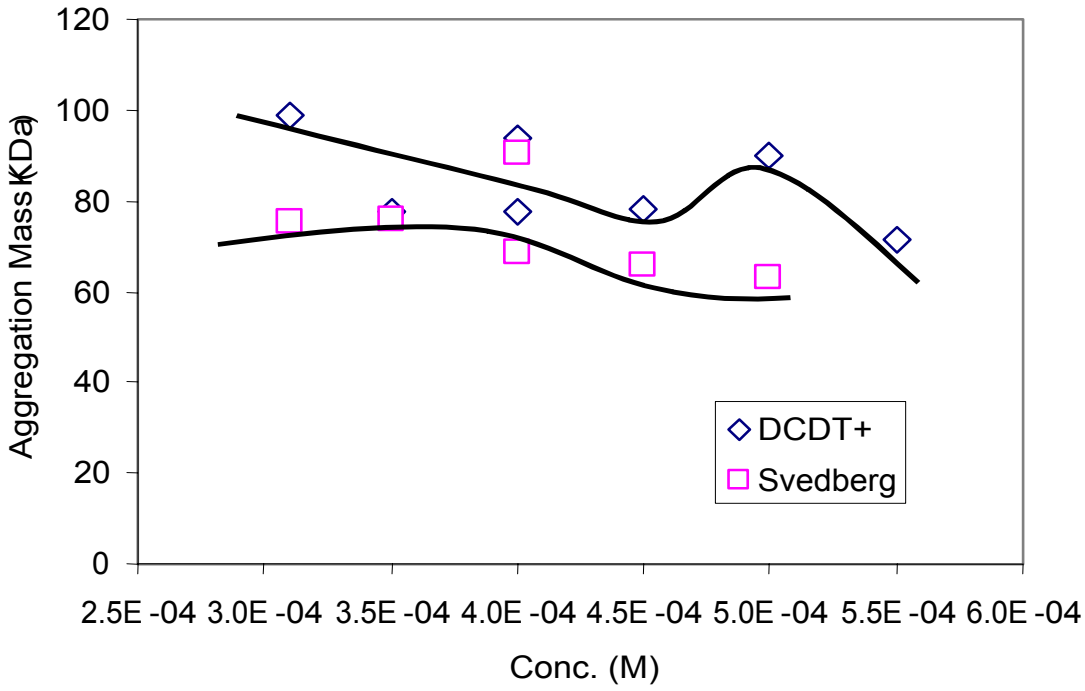

Figure 10. Aggregation masses from DCDT+ and Svedberg as a function of concentration.

From the average aggregation masses by DCDT+ and Svedberg, the aggregation number is calculated by dividing the average aggregation masses by molecular weight. They are 127 by DCDT+ and 111 by Svedberg. The result by Svedberg is closer than DCDT+ to the results from Light Scattering.

Although Svedberg is more reliable than DCDT+, this software also has some shortcomings. DCDT+ uses only limited results to get the final results, while Svedberg could be applied in the whole range. However, it is possible that no result comes out of Svedberg, i.e., no convergence. As mentioned before, back-diffusion effect due to small molecular weight is responsible for such failures.

4. SEDFIT software

The last software to be introduced is SEDFIT. Although this software has not been applied to our practical analysis, it is claimed that this software is more powerful than others. First, this software treats the results with continuous size-distributions with many known variants for sedimentation velocity analysis with maximum entropy regularization. Second, this software has the most analytical models including discrete non-interacting species, self-associating systems (1-2, 1-3, 1-2-4, 1-4-8), non-ideal sedimentation apparent sedimentation coefficient distribution, ls-g*(s) and van Holde-Weischet analysis G(s) (both for absorbance and interference data). Third, this software makes all sedimentation velocity models for **direct** boundary modeling with algebraic noise elimination. Fourth, the software could also be used to analyze data from sedimentation equilibrium experiments by continuous size-distribution models.

The advantage of this software is:

1. Back diffusion effect is taken into account in this case. The outer fitting limit does not need to be set before the bottom to cut off the back-diffusion from the bottom. In principle, it is

not necessary and should not be done when dealing with small molecules that show a significantly larger back-diffusion. In this case, the back-diffusion does contain significant information and should not be ignored.

2. More parameters such as partial specific volume, density, viscosity with unit as poise, **frictional ratio** is calculated by this software. Thus the aggregation mass, sedimentation coefficient and even the shape of micelle can be obtained by SEDFIT.

From the above discussion, the Svedberg and SEDFIT softwares are found to be better than the other two softwares for analyzing the sedimentation velocity. The results indicate that analytical ultracentrifuge is a novel and powerful technique for studying mixed surfactant systems.

Mixtures of sugar-based surfactant and nonionic surfactant in solution

Surface tension of n-dodecyl-β-D-maltoside(DM) with Nonyl phenol ethoxylated decyl ether (NP-10) and their 1:1 molar ratio mixtures was measured at pH 6.5 and 25°C and data were shown in Figure 11 as a function of concentration.

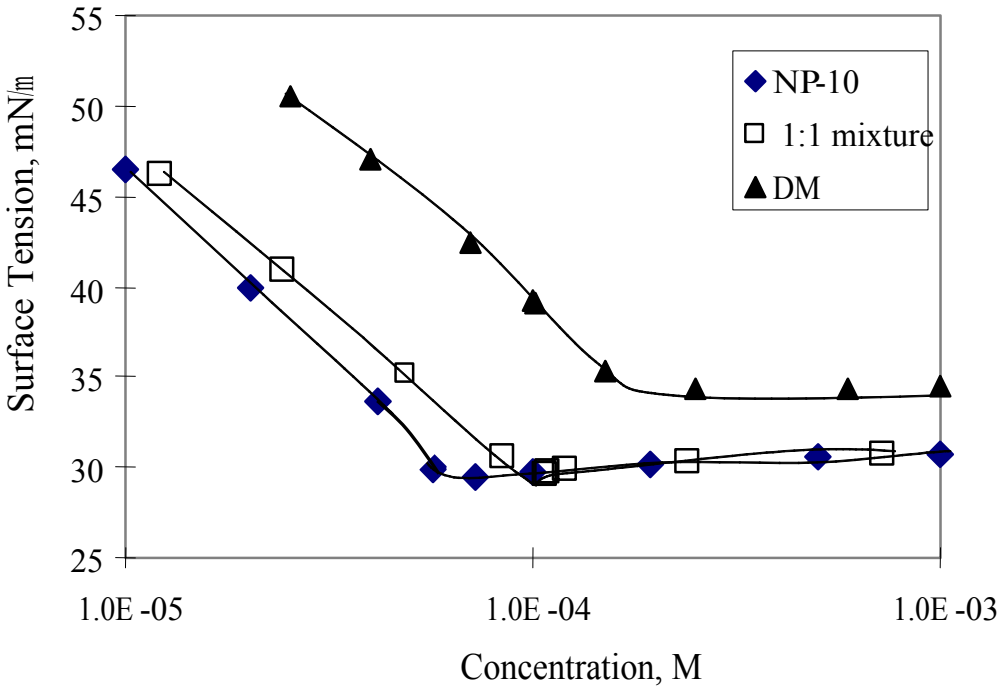

Figure 11. Surface tension of n-dodecyl-β-D-maltoside (DM) and Nonyl phenol ethoxylated decyl ether (NP-10) and their 1:1 molar ratio mixtures.

Table 4. Surface activity parameters obtained from surface tension measurement

	$cmc*10^4$ (M)	γ_{min} (mN/m)	$\Gamma_{max}*10^6$ (mol/m^2)	A_{min} ($Å^2$)	ΔG_{mic} (kJ/mol)
DM	1.8	34.3	3.37	49.3	-31.3
DM (ref. 1)	1.5	36.23	3.32	49.9	-31.8
Mixtures	0.96	29.6	3.28	50.7	-32.9
NP-10	0.62	29.5	3.78	43.9	-34.0

Relevant data such as the critical micelle concentrations (cmc), the mole fraction of DM in the monolayer and in the mixed micelles, and the interaction parameters β for the mixtures in micelles and at air/water interface, maximum adsorption Γ_{max}, area per molecule A_{min} and free energy of micellization ΔG_{mic} are listed in Table 4 and 5.

Cmc is obtained from the intersection before and after cmc in surface tension curve. The strength of interaction between these two surfactants was determined by the interaction parameter, β. A negative interaction parameter corresponds to synergism while a positive interaction parameter indicates antagonism.

Table 5. Interaction parameter β at air/water interface and in micelles, and mole fraction of DM in the monolayer and the micelles at cmc

interaction parameter at the air/water interface	-1.23
mole fraction of DM at the air/water interface	0.28
interaction parameter in the micelle	0.22
mole fraction of DM in the micelle	0.24

From surface tension data, it is seen that NP-10 is more surface active than DM and the mixed micelle is NP-10 dominant at cmc. Our data are very close to the results reported in the literature [18]. The interaction parameter between DM and NP-10 in the mixed micelle is close to zero (β=0.22). This suggests that there is no interaction between these two molecules in the micelles and that the system is ideal. This phenomenon is normal for *nonionic* surfactant interaction. It has been reported in our previous investigation that the interaction between DM and C12EO5 is ideal. At the air water interface, the hydrophilic group stays in water and the hydrophobic group stretches out to air. The stronger interaction at the air/water interface may result from the hydrogen bonding of EO groups (which is the hydrophilic group of NP-10 surfactant and points toward the water upon forming monolayer) and the sugar group (which is the hydrophilic group of DM and anchors inside the water with the carbon chain reaching away from the water surface) with water molecules. On the other hand, the phenol group in NP-10 molecule is directed towards air and facilitates the formation of monolayers.

Data for cmcs of DM, NP-10 and their mixtures were used to calculate concentration normalized to cmc for partial specific volume determination and estimation.

Partial specific volumes of DM, NP-10 and 1:1 mixtures by density experiments

By definition, partial specific volume is the volumetric change upon adding one gram of material to water. Its unit is cm^3g^{-1}. The partial specific volume is obtained experimentally using two methods. The first one is used more frequently [19]:

$$\bar{\nu} = \frac{1}{\rho_0}\left(1 - \frac{d\rho}{dC}\right)$$

c is surfactant volumeric concentration in g/ml. ρ and ρ_0 are the densities of the solution and solvent, respectively.

The second method calculated apparent molar volume first [20]:

$$V_\sigma = M/\rho - 10^3(\rho-\rho_0)/(m\rho\rho_0)$$

then the partial molar volume $\overline{V_c}$

$$\overline{V_c} = V_\sigma + m(\partial_\sigma/\partial m)_{T,P}$$

V_σ is the apparent molar volume, $\overline{V_c}$ is the partial molar volume, M is molecular weight of the solute, and m is molarity.

Finally, partial specific volume is obtained from:

$$\bar{\nu} = \overline{V_C} \;/\; M$$

The partial specific volumes of DM, NP-10, and their 1:1 mixtures at 25°C are determined from data for density measurement using the above equations.

Figure 12 shows their densities as a function of logarithm of volumetric concentration. The slope of density over concentration decreases in the order of DM, 1:1 mixture and NP-10.

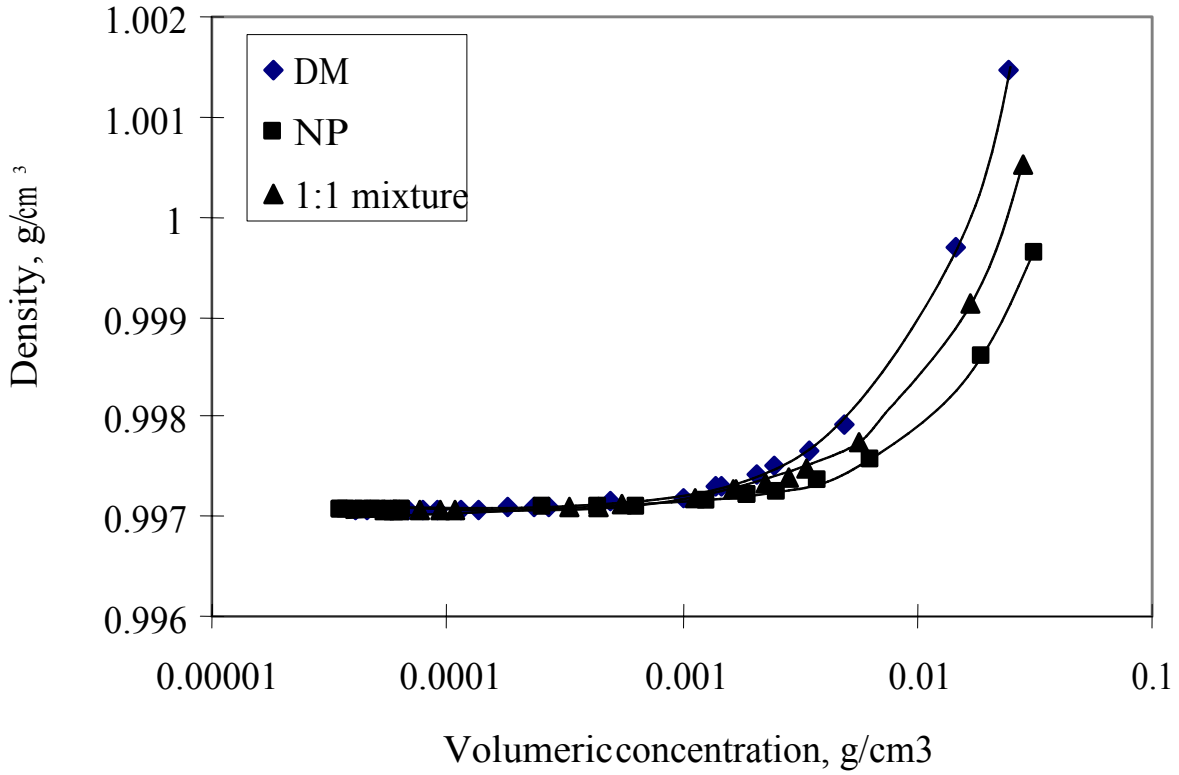

Figure 12. **Density of n-dodecyl-β-D-maltoside (DM) and Nonyl phenol ethoxylated decyl ether (NP-10) and their 1:1 mixtures as a function of logarithm of volumetric concentrations.**

Table 6. Partial specific volumes of n-dodecyl-β-D-maltoside (DM) and Nonyl phenol ethoxylated decyl ether (NP-10) and their 1:1 mixtures in different concentration ranges.

Times cmc	Partial specific volume by dρ/dc method (cm^3g^{-1})		
	DM	1:1 mixtures	NP-10
<1	0.477		0.245
1-10	0.821	0.864	0.899
10-50	0.824	0.881	0.920
>50	0.820	0.879	0.922

The data were analyzed with dρ/dc method first. The partial specific volumes were calculated using above equation and classified into four categories with respect to cmc, i.e., <1, 1-10, 10-50 and >100 times cmc (Table 6).

It is obvious that the partial specific volumes are the lowest at concentrations below cmc. It should be noted that the density of the surfactant solutions does not change with increase in concentration unless the concentration is close to cmc. All the surfactant molecules are evenly distributed in solution at concentrations far below cmc and density of the solutions is the same as that of water. The partial specific volume far below cmc should be higher than 1.0 since the dρ/dc is zero and it is calculated using $1/\rho_0$, which is 0.997043 at temperature of 25^0C. When the concentration is high enough to form micelles in the solution, the self-organized molecular aggregates have a water-free core containing dissolved oxygen. Evidently, micelles do contributes to the sharp increase in density. The current results show that the micelles form in solution at concentrations lower than at which saturated monolayer forms at air/water interface.

The partial specific volumes increase in the range of 1-10 times cmc to 10-50 times cmc. This suggests possible change in packing format in mixed micelles. The differences in partial specific volumes from 1-10 times cmc to 10-50 times cmc are 0.003 for DM, 0.017 for 1:1 mixture and 0.021 for NP-10 respectively. The differences in numbers reveal that the change of micellar shape would follow the order: DM < 1:1 mixture < NP-10.

The partial specific volume at concentrations above 50 times cmc does not change appreciably from that between 10 to 50 cmc. Thus a conclusion could be drawn that partial specific volume is not constant for the same surfactant solution. Micellization has a significant effect on the partial specific volume for nonionic surfactants and their mixtures. The partial specific volume is constant only when the concentration is higher than 10 times cmc.

When analyzing the data with V_σ (apparent molar volume) method, similar trends were obtained as seen in Figure 13.

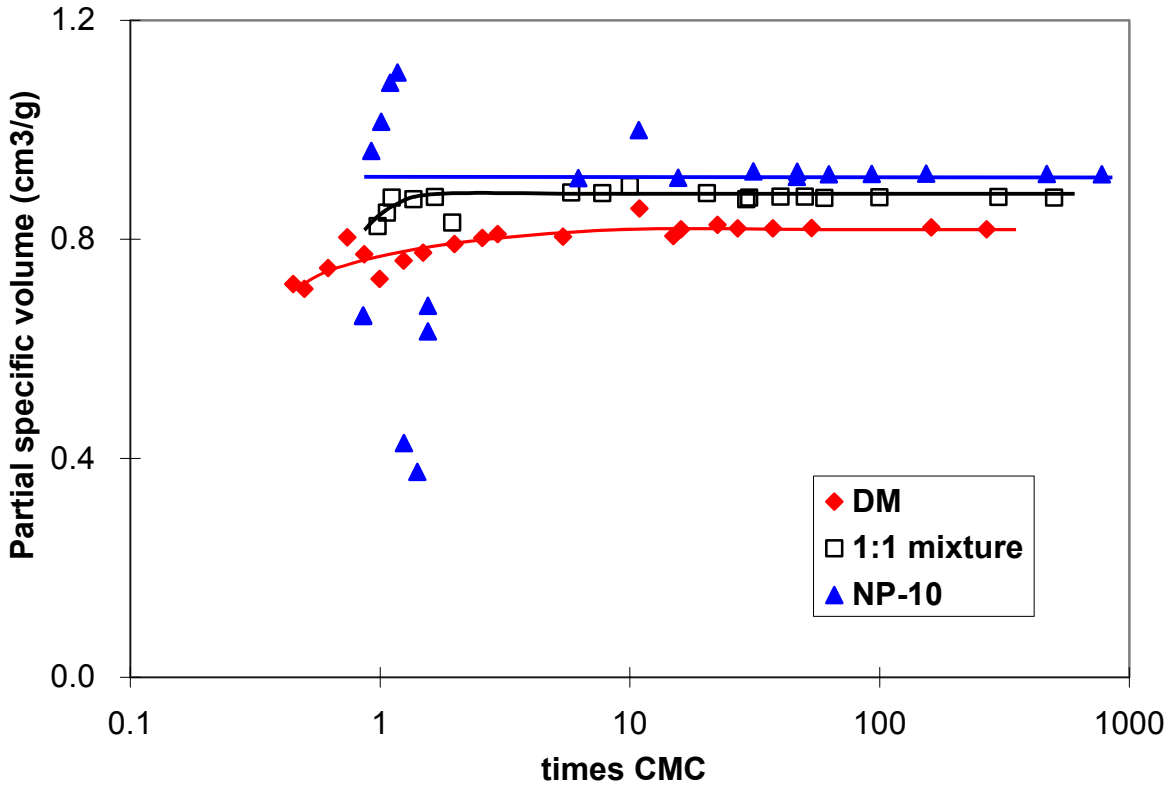

Figure 13. Partial specific volume by V_σ (apparent molar volume) method versus times cmc of n-dodecyl-β-D-maltoside (DM) and Nonyl phenol ethoxylated decyl ether (NP-10) and their mixtures at 25^0C.

These three curves exhibit the same trend showing partial specific volumes are constant at concentrations above 10 times cmc, whereas below cmc, only data for partial specific volume of NP-10 shows scattering. NP-10 has good hydrophilicity and surface activity so that there is very little difference between water and NP-10 in density. This accounts for the scattering of the measured data at low concentrations. When the concentration is between 1-10 times cmc, the partial specific volumes of DM and 1:1 mixture increase with concentration and reach maxima

around 10 times cmc. This may correspond to transition of the packing format of surfactant molecules in mixed micelles with change in concentration. Partial specific volumes of NP-10 scatter at concentration near cmc and become less variant above 6 times cmc. This phenomenon does not exist for the anionic and cationic surfactants with similar hydrocarbon chain length because cmcs of NP-10, DM and their 1:1 mixture are very low (6×10^{-5} – 1.8×10^{-4}M). NP-10 has the highest partial specific volumes among all the three compounds. Thus the difference between densities from low to high concentration is relatively small. This is supported by the fact that the densities of NP-10 solutions are the same as that of water over a wide concentration range. The fluctuation of partial specific volume at different concentration is shown in Table 7.

Table 7. Partial specific volume range of n-dodecyl-β-D-maltoside (DM) and Nonyl phenol ethoxylated decyl ether (NP-10) and their 1:1 mixtures by apparent molar volume method.

Times cmc	Partial specific volume range by V_σ method		
	DM	1:1 mixture	NP-10
<1 (range)	0.71-0.80	0.824	0.660-0.962
1-10 (range)	0.761-0.810	0.830-0.897	0.375-1.105
10-50 (range)	0.806-0.856	0.873-0.885	0.913-0.999
>50	0.818-0.821	0.876-0.878	0.919-0.920

The partial specific volumes in each concentration range excluding maximum and minimum are averaged. The comparison of partial specific volumes derived from V_σ method is made in Table 8.

Table 8. Comparison of partial specific volumes using V_σ method with those using the dρ/dc method.

Times cmc	DM			1:1 mixture			NP-10		
	dρ/dc	V_σ	Δν%	dρ/dc	V_σ	%	dρ/dc	V_σ	Δν%
<1	0.477						0.245		
1-10	0.821	0.802	2.3	0.864	0.879	-1.7	0.899		
10-50	0.824	0.821	0.4	0.881	0.878	0.3	0.920	0.919	0.1
>50	0.820	0.820	0.0	0.879	0.877	0.2	0.922	0.920	0.2

Here the V_σ denotes the apparent molar volume method. The comparison shows that these two methods agree with each other very well at concentrations above 10 times cmc. The agreement manifests that both methods are accurate for determination of partial specific volume. The values from both methods at concentration above 50 times cmc are averaged. The partial specific volumes show the tendency to increase in the order DM < mixture < NP-10. The partial specific volume is a function of the chemical structure, the temperature and micellization. If we examine their chemical structure, n-dodecyl-β-D-maltoside (DM) has 12-carbon chain as hydrophobic tail and 2-sugar groups as hydrophilic head. SANS experiment showed that n-dodecyl-β-D-maltoside (DM) micelle is oblate ellipsoid with a=3.44 and b=2.03 [21]. Nonyl phenol ethoxylated decyl ether (NP-10) has 9-carbon chain and 1 phenol group as hydrophobic part and 10 EO groups as hydrophilic part. Nonyl phenol ethoxylated decyl ether (NP-10) micelle is more asymmetrical with a=5.4 and b=2.8 according to the literature [22]. The bulky hydrophilic head of DM produces very little space between surfactant molecules in the micelles. In contrast, the linear NP-10 structure allows more water molecules in the micelles. Therefore, the partial specific volume of NP-10 is close to that of water. In addition to molecular structure,

strong hydration of NP-10 molecules contributes to the large value in partial specific volume. 1:1 mixture behaves as expected: the partial specific volume is larger than that of DM and smaller than that of NP-10.

Partial specific volumes of DM, NP-10 and their 1:1 mixtures by Durchschlag's calculation method

Partial specific volume could also be calculated theoretically. Method of calculation is fast and accurate for single component systems and systems with inorganic salts. Helmut Durchschlag and Peter Zipper's approach [2, 3] was adopted to calculate the partial specific volumes of surfactants and their mixtures in aqueous solutions. The method is based on Traube's additivity principle and concept of volume increments for atoms. This procedure is developed for increments/decrements for co-volume, ring formation and ionization.

Partial molar volumes, $\overline{V_c}$ is defined as following:

$$\overline{V_C} = \sum V_i + V_{CV} - \sum V_{RF} - \sum V_{ES}$$

Where V_i is the volume increment for any atom or atomic group, V_{CV} is the correction due to the co-volume, V_{RF} and V_{ES} stand for the decrease in volume caused by ring formation and ionization (electrostriction), respectively.

Figure 14 shows the molecular structures of DM and NP-10.

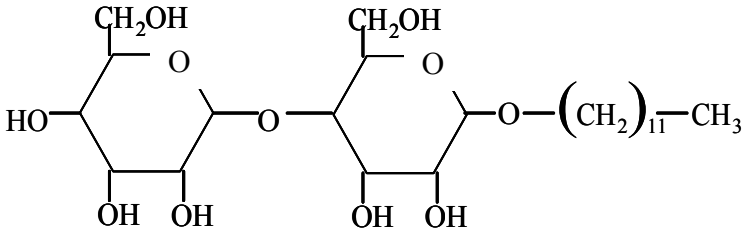

DM $\mathbf{C_{24}H_{46}O_{11}}$ M.W. = 510.6

$\overline{V_c}$ = 24×9.9(C)+46×3.1(H)+4×5.5(O)+2×2.3(O)+5×0.4(O)+12.4(V_{CV})-2×8.1(V_{RF}) = 405cm^3/mol

$\bar{\nu}$ = 0.793 cm^3/g

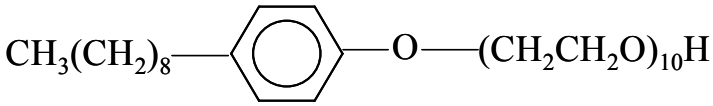

NP-10 $\mathbf{C_{24}H_{46}O_{11}}$ M.W. = 660.9

$\overline{V_c}$ = 35 ×9.9(C)+64×3.1(H)+10×5.5(O)+1×2.3(O)+12.4(V_{CV})-8.1(V_{RF}) = 606.5m^3/mol

$\bar{\nu}$ = 0.918cm^3/g

Figure 14. The molecular structures of n-dodecyl-β-D-maltoside (DM) and nonyl phenol ethoxylated decyl ether (NP-10).

As for the mixture, a simple method is used for the estimating:

$$\bar{\nu} = \frac{\Sigma x_i \overline{V}_{C,i}}{\Sigma x_i M_i}$$

$\overline{V}_{c,i}$ is the sum of partial molar volume of each component, $\sum \boldsymbol{M_i}$ the sum of molecular weights and x_i the molar ratio of one component over the other. For 1:1 DM-NP-10 mixture, the partial specific volume is 0.867. The comparison of dρ/dc, V and Durchschlag's methods are made in Table 9. Data from the literature is also tabulated below.

Table 9. List of partial specific volumes and deviation for DM, NP-10 and their 1:1 mixture by empirical and theoretical methods.

Methods	DM	1:1 mixture	NP-10
dρ/dc	0.820	0.879	0.922
V	0.820	0.877	0.920
Durchschlag's	0.793	0.867	0.918
Δν%	-3.3	-1.3	-0.3
literature value	0.837 [6]		0.922 [7]

The averages of partial specific volumes by dρ/dc & V_σ methods are compared with that obtained by Durchschlag's method. The deviations show that the difference decreases following the order of DM > 1:1 mixture > NP-10. The large difference of DM results from its structure. The hydrophilic group of DM is composed of two sugar rings connected by an oxygen atom to form a β-linkage. The connection of two sugar rings is rigid. It can be seen that the bulky sugar groups not only bring deviation to the partial specific volume of DM, but also influence that of the mixture.

If the average of partial specific volume of DM & NP-10 by dρ/dc & V_σ methods was used to calculate the partial specific volume of mixtures using equation 7, the value obtained is 0.878, which is the same as the average from dρ/dc & V_σ methods. This suggests that there is no interaction between these two molecules in mixed micelles. This finding supports the conclusion from surface tension measurements. The interaction parameter in mixed micelle is close to zero denoting no interaction. Since density measurements are fast and accurate, the traditional surface tension measurement may be replaced by partial specific volume determination to elucidate interactions between molecules in mixed micelles.

The partial specific volumes of DM from literature [23] have a 2.1% deviation in the case of experimental results and 3.3% in the case of theoretical evaluation. Since DM used in the literature is not specified as α, β or mixtures of α and β conformations and the tested temperature is not given, the result is reasonable. The partial specific volume of Triton N-101 from literature [16] is used for comparing with that of NP-10 and the deviation is only 0.3%. Triton N-101's chemical formula is $C_9\varphi EO_{9\text{-}10}$ while the NP-10's formula is $C_9\varphi EO_{10}$.

Temperature effect on partial specific volumes of surfactants

Temperature can have a marked effect on micellization, adsorption on rock and rheology of injected chemicals in the flooding process. The partial specific volumes of 1:1 mixtures at 25, 30, 36.8, 40, 45 and 50°C were further determined to elucidate the effect of temperature and determine the temperature coefficient. Usually temperature coefficients of surfactants range from to10×10^{-4} $cm^3g^{-1}K^{-1}$. The surfactant mixture may be a good sample for investigation partly due to the rigid two sugar rings connected by an oxygen atom and partly due to the mixing of n-dodecyl-β-D-maltoside(DM) with nonyl phenol ethoxylated decyl ether (NP-10).

The temperature coefficient is defined as:

$$f = \frac{d\bar{v}}{dt}$$

Here, f is temperature coefficient, $\frac{d\bar{v}}{dt}$ is slope of partial specific volume versus temperature.

Figure 15 shows the density of 1:1 mixtures at different temperatures. Higher the temperature, the lower is the density. Although the logarithm plots suggests sharp increase at high concentrations, densities are actually linear with concentration.

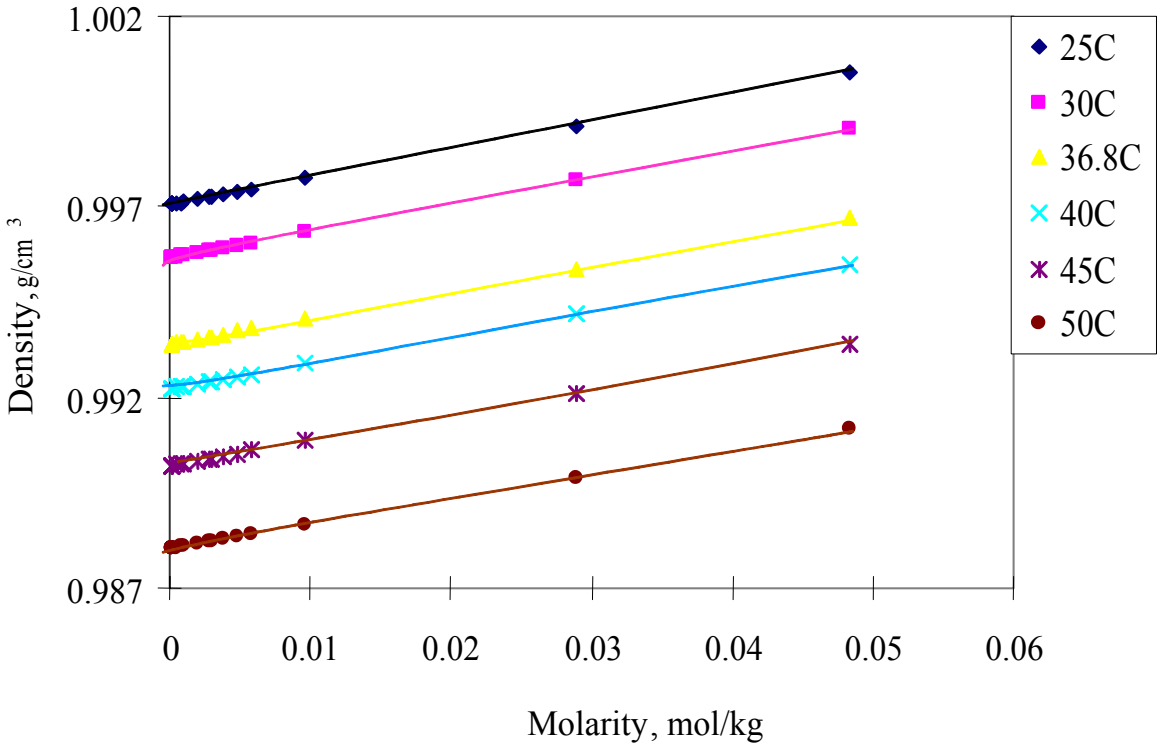

Figure 15. Density of 1:1 mixture of DM and NP-10 aqueous solutions at different temperatures

The data is analyzed with the above two methods: dρ/dc and V_σ. dρ/dc method was used first. Table 10 contains the partial specific volumes of 1:1 mixtures at different concentrations and different temperatures. The cmc at each temperature was not measured here. Thus the concentrations were divided to low, medium and high ranges. The low range consists of concentration of 10^{-5} to10^{-4}M and medium range covers 10^{-4} to10^{-3}M while high range starts from 5×10^{-3}M.

The trend agrees with those obtained for DM, NP-10 and 1:1 mixtures at 25°C. At the same temperature, the partial specific volume is smaller at low concentrations and higher at medium and high concentrations. Another trend is shown by the constant partial specific volume

at medium and high concentration ranges. The partial specific volume increases with concentration.

Table 10. The partial specific volumes analyzed for different concentrations and different temperatures by dρ/dc method.

Conc. Range	Temperature, °C					
	25	30	36.8	40	45	50
low	0.850	0.517		0.730	0.735	0.778
medium	0.879	0.884	0.888	0.892	0.895	0.898
high	0.879	0.884	0.889	0.891	0.895	0.899

When analyzed by V_σ method, the data for partial specific volumes are found to be scattered at low concentrations. The results are shown in Figure 16. It is clear that the partial specific volumes jump at low concentrations and become constant afterwards. The partial specific volumes at concentrations higher than 0.002 mol/kg are averaged and compared with the results obtained by dρ/dc method at high concentrations. Table 11 and Figure 17 show the values obtained.

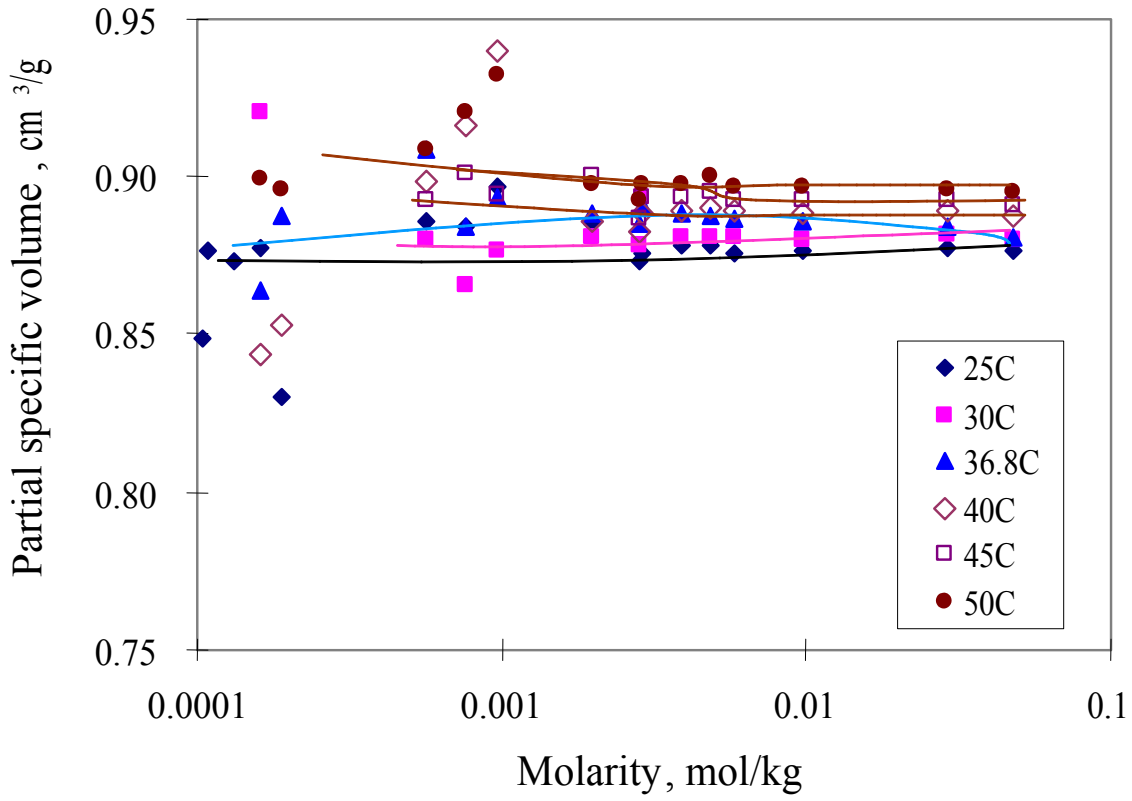

Figure 16. **Partial specific volume of 1:1 mixture at different temperature versus molarity.**

Table 11. Partial specific volumes of 1:1 mixtures by dρ/dc & V methods with deviations.

temp., °C	dρ/dc	V_σ	Δν%	temp.,°C	dρ/dc	V_σ	Δν%
25	0.879	0.876	0.4	40	0.891	0.888	0.4
30	0.884	0.880	0.5	45	0.895	0.892	0.3
36.8	0.889	0.885	0.4	50	0.899	0.897	0.2

The deviation between these two methods are within 0.2-0.5%. From the $d\bar{\nu}$ /d t, the temperature coefficients from both methods are obtained. Although there is a small difference between the values by dρ/dc & V_σ methods, the temperature coefficients are the same: $f = 8\times10^{-4}$ $cm^3g^{-1}K^{-1}$.

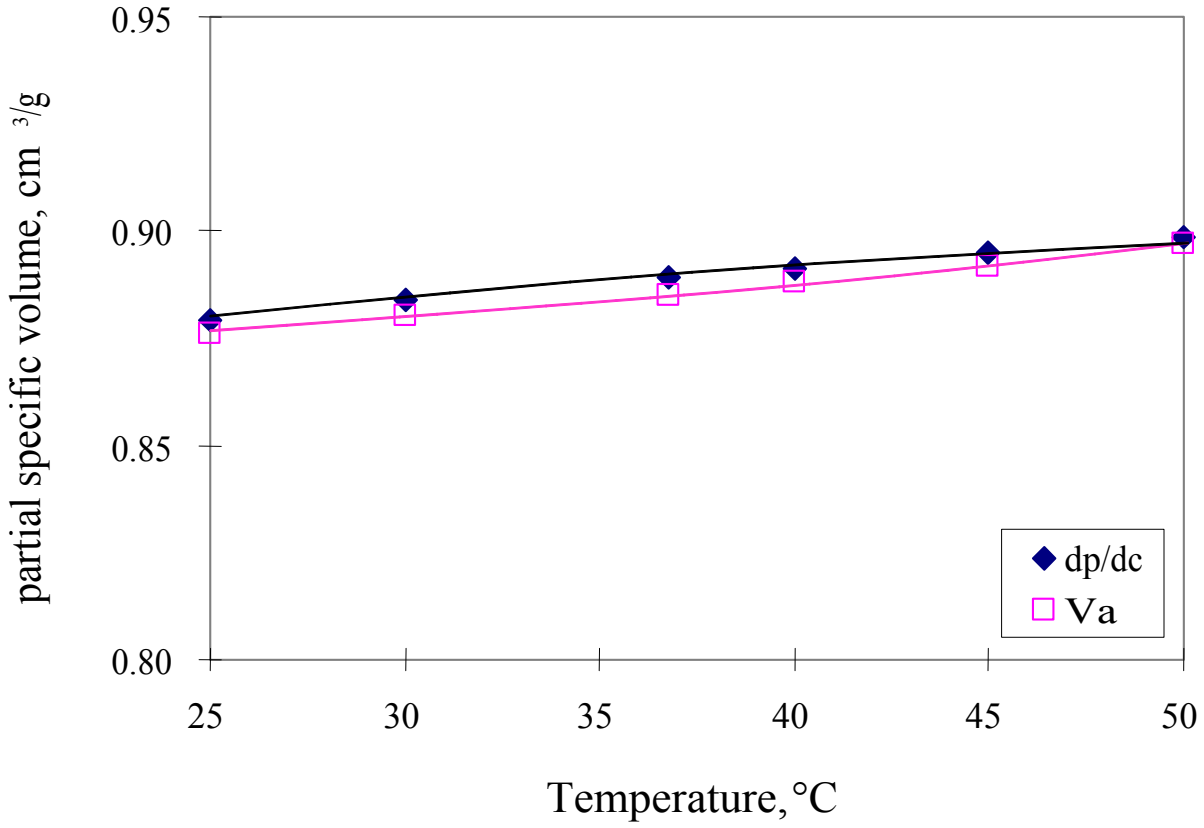

Figure 17. Partial specific volumes versus temperature by dρ/dc & V_σ methods.

The large temperature coefficient f indicates that the mixed DM and NP-10 micelles are sensitive to temperature gradients. In other words, mixed micelle has good fluidity at high temperatures, which will facilitate the EOR process.

Molar specific volume of different sugar-based surfactants

Information on partial specific volume of surfactants and their mixtures is required for treating analytical ultracentrifuge data. Previous results showed that the partial specific volume of n-dodecyl-β-D-maltoside determined by density gradient had a relatively large deviation (3%) from theoretical calculations based on Helmut Durchschlag's approach. To explore the reason for the discrepancy, the partial specific volumes of n-decyl-β-D-glucoside (C10G), n-decyl-β-D-

maltoside(C10M) and n-dodecyl-β-D-maltotrioside (C12TM) were determined to correlate with that for n-dodecyl-β-D-maltoside(C12M). N-dodecyl-β-D-glucoside was not chosen due to its low solubility in water.

The above four surfactants are different in molecular structures with N-decyl-β-D-glucoside with only one glucose group as hydrophilic part and ten-carbon chain as hydrophobic part, while N-dodecyl-β-D-maltoside has two glucose groups and n-dodecyl-β-D-maltotrioside three glucose groups, respectively (Figure 18). Both n-dodecyl-β-D-maltoside and n-dodecyl-β-D-maltotrioside contain twelve carbons in the hydrophobic parts. The molecular weights of n-decyl-β-D-glucoside, n-decyl-β-D-maltoside, n-dodecyl-β-D-maltoside and n-dodecyl-β-D-maltotrioside are 276.4, 482.6, 510.6 and 672.6, respectively.

The densities of the surfactant solutions are plotted as a function of concentration in Figure 19. The density of n-decyl-β-D-glucoside is composed of two parts represented by the solid and dashed lines. Phase transition occurred at concentrations over 0.015 g/cm^3. Hence the densities of turbid solutions are represented by a dashed line.

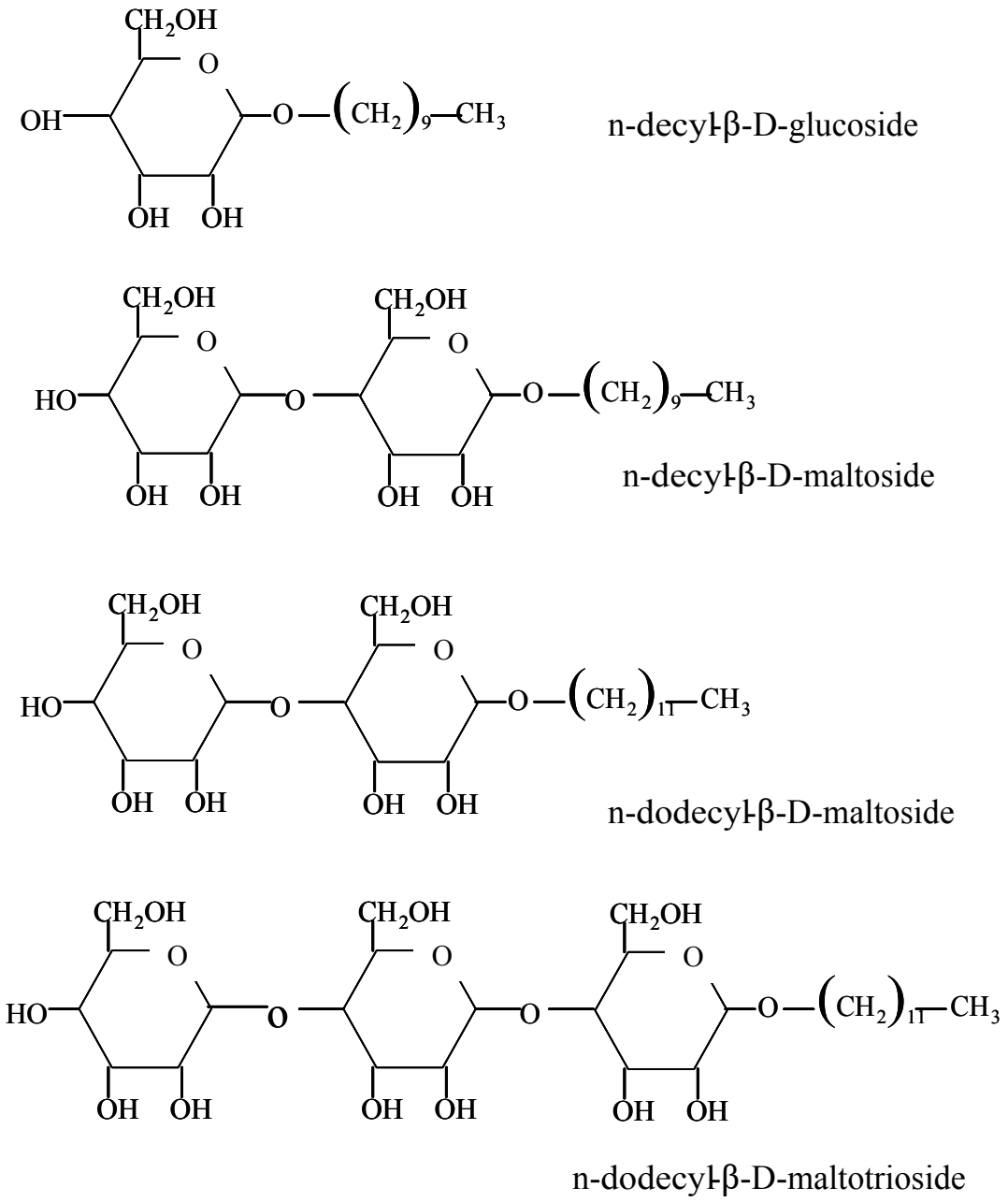

Figure 18. Schematic display of structures of n-decyl-β-D-glucoside, n-dodecyl-β-D-maltoside and n-dodecyl-β-D-maltotrioside.

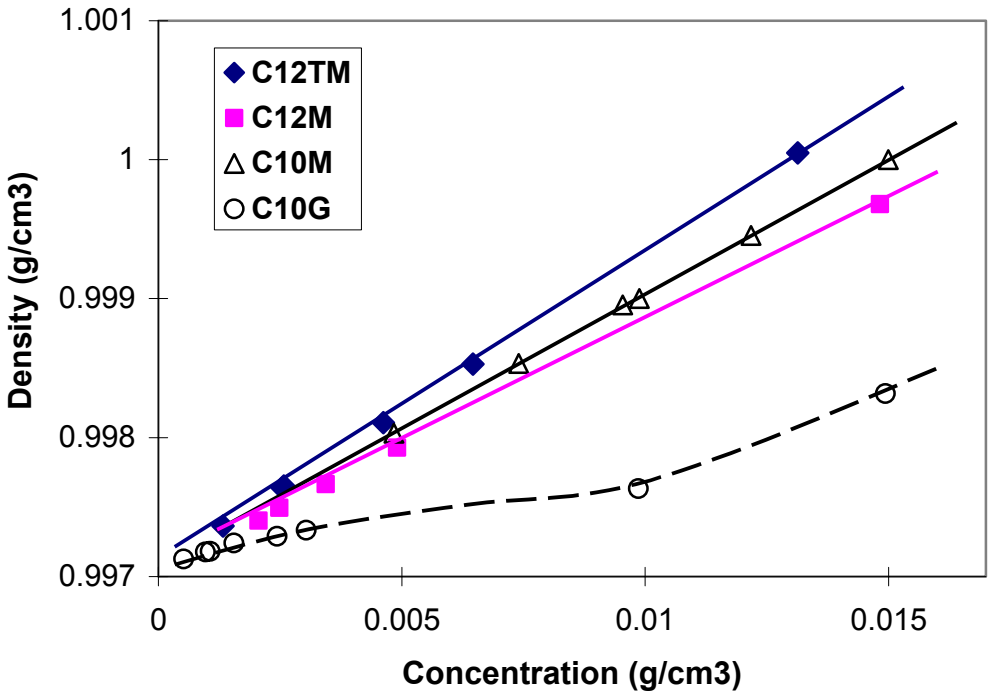

Figure 19. Plot of density vs. concentration for n-decyl-β-D-glucoside, n-decyl-β-D-maltoside, n-dodecyl-β-D-maltoside, and dodecyl-β-D-maltotrioside at pH 6 and at 25^{0}C.

The slopes were used to calculate partial specific volumes:

$$\bar{\nu} = \frac{1}{\rho_0}\left(1 - \frac{d\rho}{dC}\right)$$

where C is surfactant volumetric concentration in g/ml, ρ and ρ_0 are the densities of the solution and the solvent, respectively and the results obtained are 0.809 cm^3/g for n-decyl-β-D-glucoside, 0.820 cm^3/g for n-dodecyl-β-D-maltoside, 0.775 cm^3/g for n-decyl-β-D-maltoside and 0.892 for n-decyl-β-D-glucoside, respectively. It should be noted that only densities of clear solutions were used to obtain partial specific volumes for n-decyl-β-D-glucoside.

The experimental result was compared with the theoretical data based on the partial molar volume. Since the partial specific volume is obtained from:

$$\bar{\nu} = \bar{V}_C \; / \; M$$

The partial molar volume can be obtained by multiplying the partial specific volume with molecular weights. On the other hand, the partial molar volumes of surfactants at 25°C can be calculated using the equation:

$$\overline{V_c} = \sum V_i + V_{CV} + \sum V_{RF} - \sum V_{ES}$$

where, V_i is the volume increment for any atom or atomic group, V_{CV} is the correction for the co-volume, and V_{RF} and V_{ES} take into account the decrease in volume caused by ring formation and ionization (electrostriction), respectively.

The calculated and empirical results are compared in Table 12.

Table 12. List of theoretical and experimental results of partial molar volumes and related parameters for n-decyl-β-D-glucoside, n-decyl-β-D-maltoside, n-dodecyl-β-D-maltoside and n-dodecyl-β-D-maltotrioside at pH 6 at 25^0C

	C	H	O1	O2	O3	CV	RF	$\overline{V_c}$ (Theory)	$\overline{V_c}$ (Exp.)	Difference	V per ring
C10G	16	32	2	1	3	12.4	1	276.4	285.8	9.4	9.4
C10M	22	42	4	2	5	12.4	2	372.8	390.3	17.5	8.7
C12M	24	46	4	2	5	12.4	2	405	418.7	13.7	6.8
C12TM	30	57	6	3	7	12.4	3	504.5	521.3	16.8	5.6

In this table, C, H, O1, O2, O3 are the number of carbon, hydrogen, oxygen atoms in the ether and in the ring, first OH for carbon, tertiary OH for carbon, respectively. CV was co-volume. RF is for the ring formation. The next column was partial molar volume by theoretical calculation. $\overline{V_c}$ (Exp.) is the partial molar volume from experimental data. The discrepancy between $\overline{V_c}$ (theory) and $\overline{V_c}$ (exp.) is shown in the "difference", which is divided by number of sugar groups and the results are noted as in "V per ring".

It is interesting that V per ring followed the order: C10G>C10M>C12M>C12TM. The angle between two sugar groups with β-conformation was found to change from theoretical prediction. Both C10G and C10M have the same hydrocarbon chain with the difference resulting only from the glucose group. It is clear that the glucoside can be rotated more easily than maltoside with two glucose groups and maltoside is prone to bend over than maltotrioside with three glucose groups. In the case of C10M and C12M, while the glucose groups are the same, the hydrocarbon chain length varies. The larger difference in partial molar volumes for C10M than that for C12M is possibly due to the fact that short hydrocarbon chain gives glucose groups more free space to turn. In other words, the glucose groups with short hydrocarbon chain are less restrained. Since a 1% deviation in partial specific volume will result in a 4% difference in molecular weight and since the analytical ultracentrifugation data itself has ~ 10% error, this experimental method is considered reliable for systems containing sugar-based surfactants. The large deviation in partial molar volumes of sugar-based surfactants determined empirically from those obtained by theoretical calculation indirectly supports the bending conformation of glucose groups in aqueous solutions.

Analytical ultracentrifuge sedimentation equilibrium study of nonionic surfactant mixtures

A typical analytical diagram of sedimentation equilibrium experiment is exhibited in Figure 20. The graph is made up of four parts: subject (name of the material and rotor speed), residual vs. radius plot, sedimentation equilibrium results together with the fitted curve, analytical results and experimental conditions.

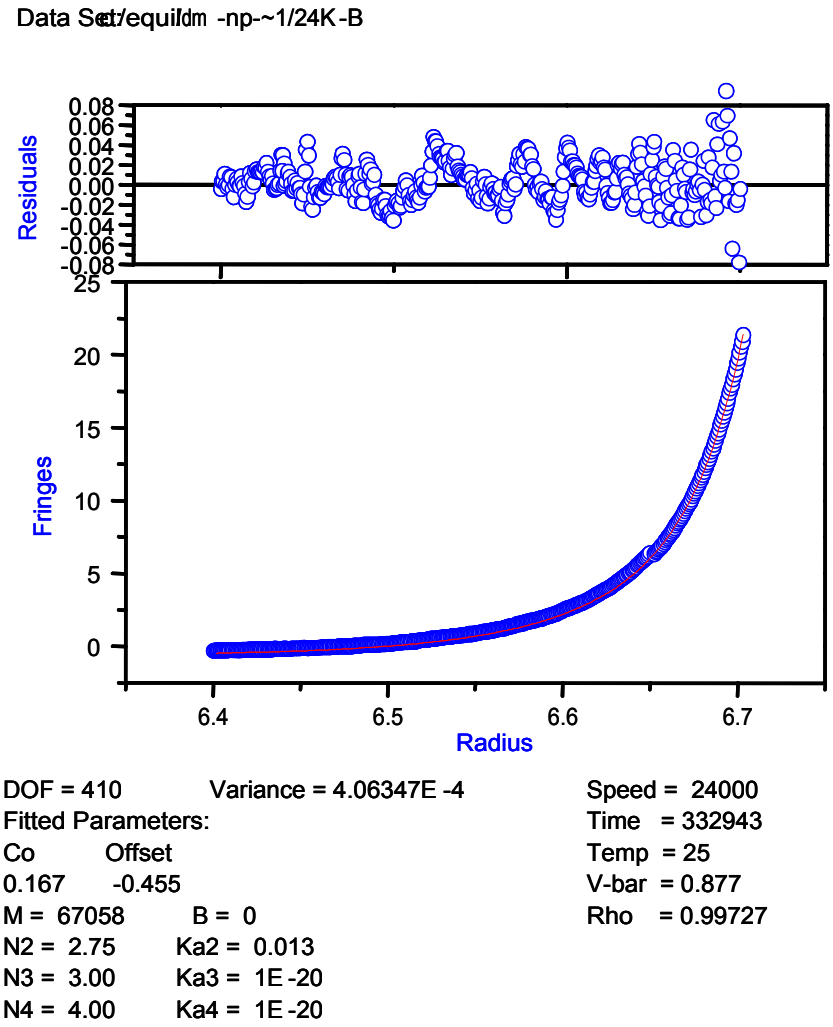

Figure 20. Data for 0.03 M mixed surfactant solution of n-dodecyl-β-D-maltoside and nonyl phenol ethoxylated decyl ether of 1:1 molar ratio at rotor speed of 24k and temperature of 25^0C.

DOF is the degree of freedom and the small variance suggests a successful fit. Among the fitted parameters, Co is the fitted concentration of micelle. The aggregation number is obtained by dividing micellar mass, M, by molecular weight of this surfactant. B is the second virial coefficient, N_2 the stoichiometry of species 2 and K_2 the association constant for transition from species 1 to species 2. N_3 and K_3 are similar to N and K for species 3.

In real cases, both nonideality and association are possible. They could be distinguished by checking the residuals and variance. As mentioned in the experimental section, the second virial coefficient is an indication of the nonideality and could be determined from the variation of apparent micellar mass with concentration. Here is an example.

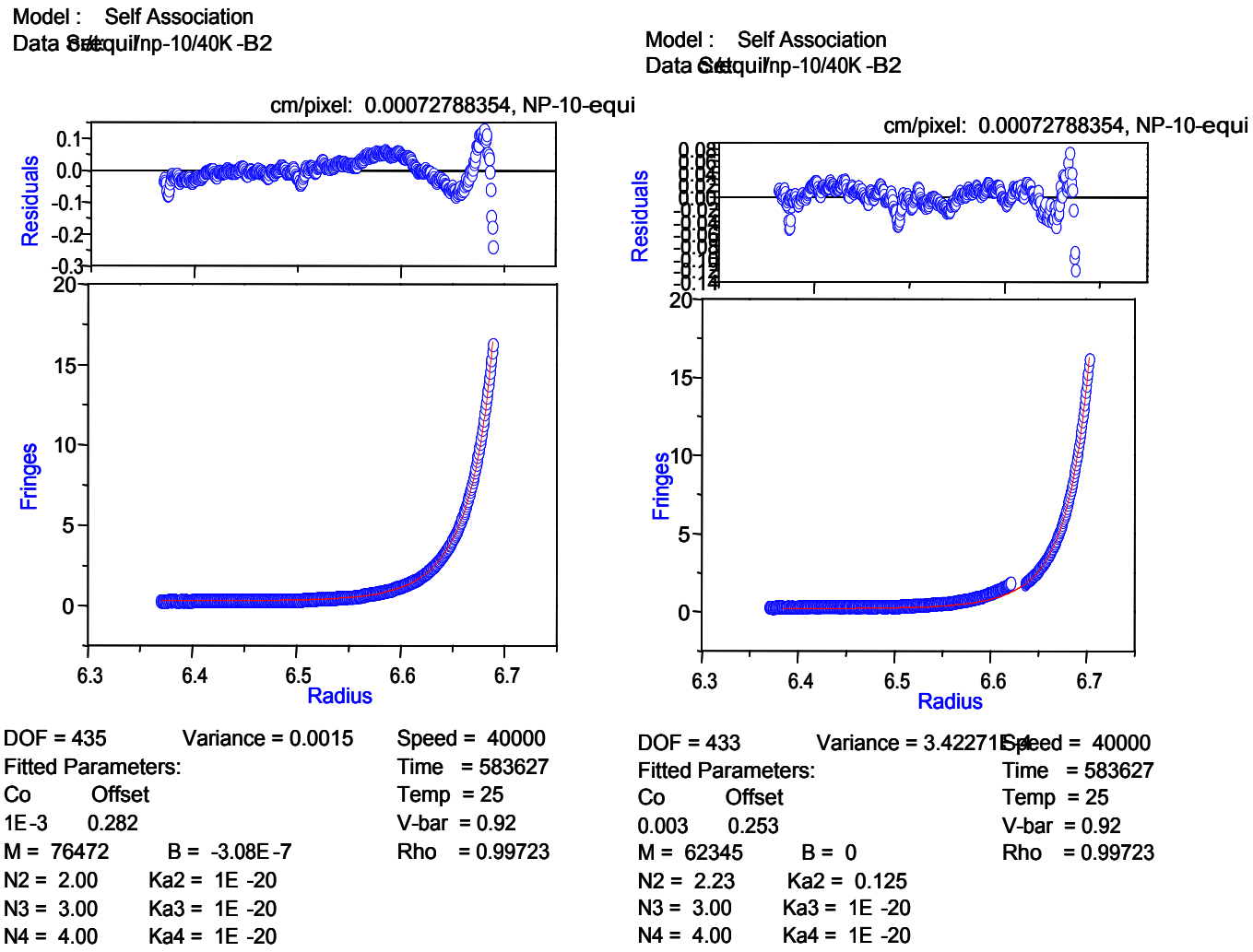

Figure 21. Data for the analysis of sedimentation equilibrium of nonyl phenol ethoxylated decyl ether at a concentration of 0.03M, rotor speed of 40k, at pH 6 and temperature of 25^{0}C. The left one fitted micellar mass and second virial coefficient and the right one used micellar mass and association.

Two different protocols were used for the analysis of data of 0.03M nonyl phenol ethoxylated decyl ether (Figure 21). Micellar mass and second virial coefficient was selected for the analysis shown on the left hand side, micellar mass and association for the same data shown on the right side. Evidently, the residual plot on the left shows less variation than the right one. In addition, the variance of the fit on the left is larger than that for the right. The nonideality was usually due to large excluded volume and charge of particles. Since nonyl phenol ethoxylated decyl ether has no charge, the second virial coefficient of its micelles is quite small, -3×10^{-7}. This value is lower than the minimum requirement for nonideality. Data for both residual plot and variance supports the presence of multi-species in nonyl phenol ethoxylated decyl ether aqueous solution at this concentration.

All sedimentation equilibrium analytical results are illustrated in Table 13. Different rotor speeds were tried for each surfactant concentration at several rotor speeds. The aggregation number of micelles is given next to the rotor speed. It should be noted that n-dodecyl-β-D-maltoside exihibits only one type of micelle. Two types of micelles were found for nonyl phenol ethoxylated decyl ether and for the 1:1 molar ratio mixture. Range of aggregation number for each species is specified in the table.

The average aggregation number of DM micelle is 148±9. The value reported from small angle neutron scattering studies for n-dodecyl-β-D-maltoside is 113-129 [24]. The effect of rotor speed on aggregation number of n-dodecyl-β-D-maltoside can be seen in Figure 22 to be small. Nonyl phenol ethoxylated decyl ether has the average aggregation number of 100±13 for species 1 and 299±73 for species 2. There are two different values in the literature for the aggregation number of nonyl phenol ethoxylated decyl ether. One was 100[25] and the other 276 [26]. Although both values were obtained using light scattering technique, only one value was

reported in each paper. Our data yields both of these two. Aggregation number of their 1:1 mixtures had relative large deviations, i.e., 92±27 for species 1 and 306±79 for species 2.

Table 13. Sedimentation equilibrium analytical results for n-dodecyl-β-D-maltoside, nonyl phenol ethoxylated decyl ether and their 1:1 mixture at different concentrations and rotor speeds.

DM	Rotor speed	C=0.024M Aggregation number	C=0.012M Aggregation number	C=0.004M Aggregation number
	16k	157	151	152
	32k	148	148	163
	40k	147	140	132

NP	Rotor speed	C=0.006M Aggregation number		C=0.003M Aggregation number		C=0.001M Aggregation number	
		I	II	I	II	I	II
	16k	118	406	121	356	78	N/A
	32k	106	312	101	246	98	N/A
	40k	91	264	94	210	95	N/A

1:1 Mixture	Rotor speed	C=0.006M Aggregation number		C=0.003M Aggregation number		C=0.001M Aggregation number	
		I	II	I	II	I	II
	16k	52	384	45	321	72	352
	24k	119	345	114	315	89	216
	32k	111	293	95	221	112	311
	40k	109	298	62	158	117	454

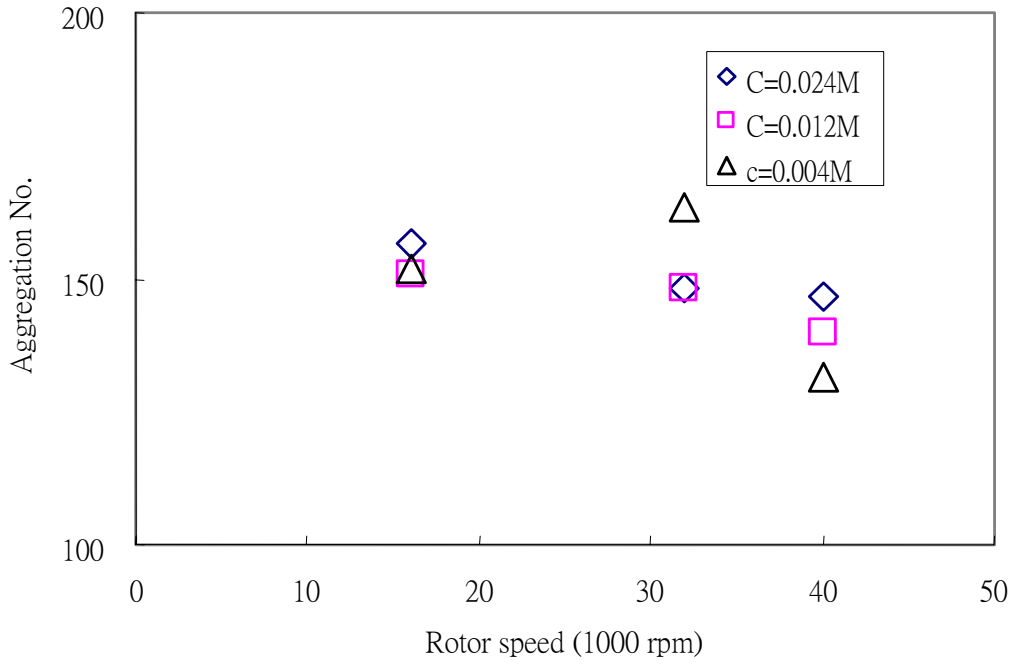

Figure 22. Aggregation number of n-dodecyl-β-D-maltoside at different rotor speeds at 25^0C.

The coexistence of two micellar species in the case of nonyl phenol ethoxylated decyl ether is attributed to its structure. A recent study has shown that polyethylene surfactant can form network structures in L_1 region [27]. Thus, the behavior of polyethylene surfactant is similar to that of polymers in certain concentration range. We propose the long flexible polyethylene chain to be responsible for the network formation and the polymer like behavior. Thermodynamic consideration suggests only one type of micelles to exist [28]. However, our study reveals, for the first time, the small micelles to coexist with the big micelles at high concentrations. The large size of the mixed micelles provides more space inside the micelles to trap crude oil. If the behavior of surfactant mixtures is similar to that of the polymer-like nonyl phenol ethoxylated decyl ether, the dosage of polymer for EOR may be reduced since the mixed surfactant itself can be adjusted for viscosity. In general, both the large micellar size and resulting polymer-like behavior could potentially benefit enhanced oil recovery process.

Dynamic light scattering study of nonionic surfactants and their mixtures

The apparent diffusion coefficients of DM, NP-10 and their 1:1 mixture were determined to change with concentration as shown in Figure 23 using the dynamic light scattering technique.

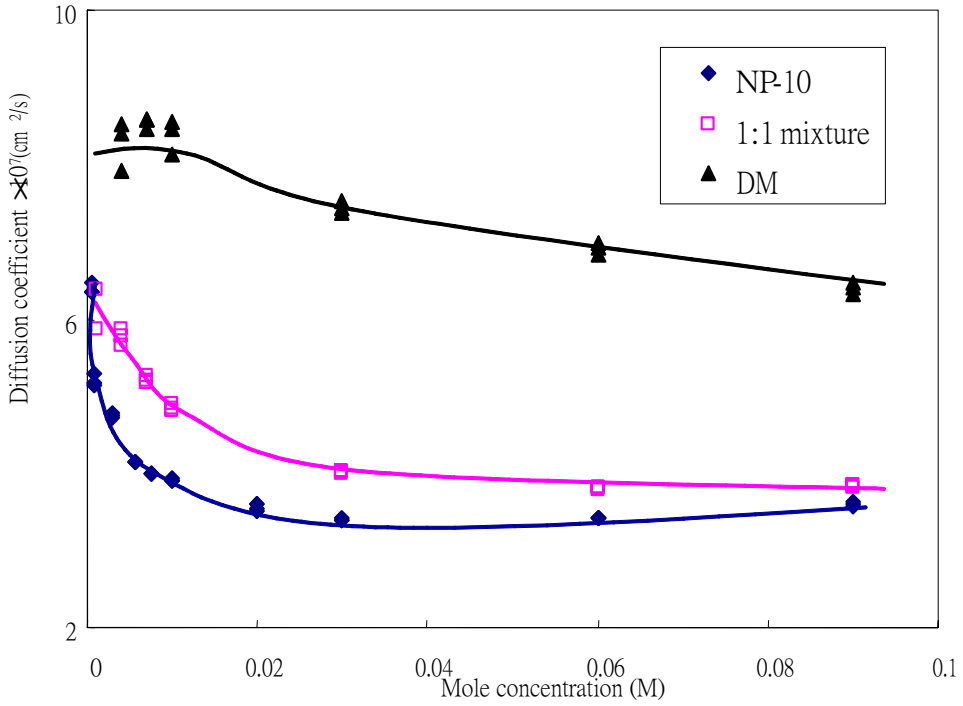

Figure 23. Diffusion coefficients of nonyl phenol ethoxylated decyl ether, n-dodecyl-β-D-maltoside and their 1:1 mixtures as a function of mole concentration at 25^0C.

Movement of n-dodecyl-β-D-maltoside micelles is faster than those of nonyl phenol ethoxylated decyl ether and their mixtures. Initially, apparent diffusion coefficient of n-dodecyl-β-D-maltoside micelles remains constant followed by a decrease at higher concentrations. Nonyl phenol ethoxylated decyl ether and their mixture exhibited different behaviors, the apparent diffusion coefficient decreases sharply at low concentrations itself. A negative slope of the D vs. C curve usually suggests formation of bigger aggregates. At high concentrations, the intermicellar interaction affects the micellar mobility. Such solutions should be treated as semi-dilute instead of dilute.

Phase diagram of nonyl phenol ethoxylated decyl ether

Above the cloud point, two isotropic phases coexist: the dilute aqueous phase and surfactant-rich phase. Below the cloud point, one isotropic phase is detected and is identified as micelle solution. The clouding phenomenon is attributed to the temperature dependence of intermicellar interactions. At elevated temperatures, the interactions change from repulsive at low temperatures to attractive, resulting in the dehydration of the hydrophobic groups in the micelles [29]. Another interpretation is based on the decreased local dipole moment at high temperatures resulting from the structure/conformational change of the micelles [30]. A series of properties, such as micelle size and shape are affected according to the mechanism. Attempts have been made to fit the phase boundary curves of polyoxyethylene surfactants to two theories, i.e. thermodynamic perturbation theory and Flory-Huggins solution theory [31]. The former describes spherical micelles with hydration shell so that the phase separation is due to the deterioration of the hydration shell, while the latter theory considers the growth of micelles to be responsible for the clouding phenomenon. The correlation of empirical results to the theoretical models suggests that a combination of hydration shell and elongation of the micelles account for the clouding behavior of polyoxyethylene surfactant with the low critical volumetric fraction.

We examined phase transition temperatures (cloud point) of polyoxyethylene surfactants [32] in dilute aqueous regime. Nonyl phenol ethoxylated decyl ether is denoted as NP-10. Figure 24 shows a partial phase diagram of the binary NP-10/H_2O system. Only isotropic micellar phase is present in dilute concentrations at the tested temperature of 25^0C.

N-dodecyl-β-D-maltoside does not exhibit clouding up to 45% concentration [33]. All the studied solutions of n-dodecyl-β-D-maltoside and its 1:1 mixtures with nonyl phenol ethoxylated decyl ether are in the L_1 region.

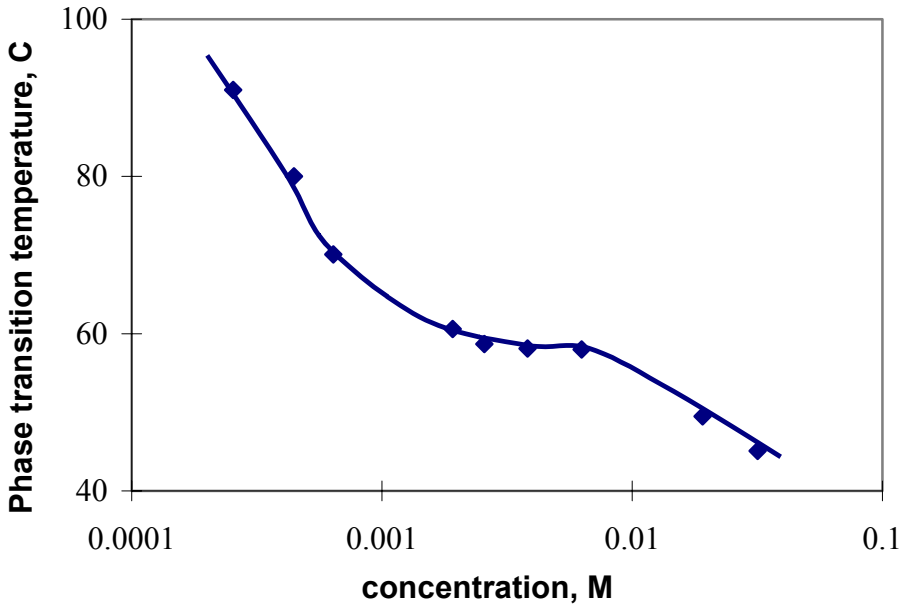

Figure 24. **Partial phase diagram of nonyl phenol ethoxylated decyl ether.**

Analytical ultracentrifuge sedimentation velocity study of size and shape of micelles

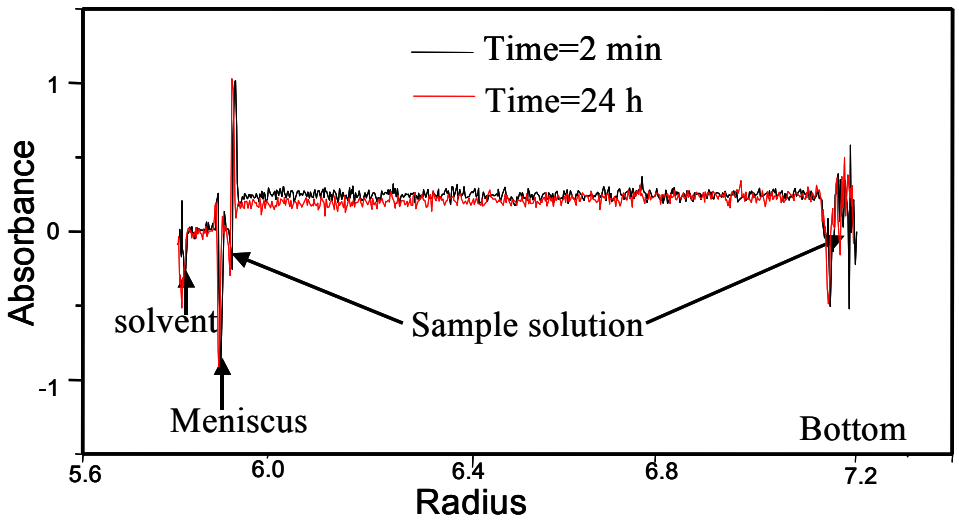

Figure 25. **Sedimentation velocity experiment of nonyl phenol ethoxylated decyl ether at premicellar concentration. Concentration: 4×10^{-5}M, detector: UV, wavelength: 274nm, rotor speed: 40,000 rpm. The black and red curves are scans at the beginning and after 24 hours, respectively.**

The velocity experiment of surfactants is studied first with the premicellar solutions (Figure 25). The concentration of the nonyl phenol ethoxylated decyl ether solution is 4×10^{-5}M, less than its cmc of 6.2×10^{-5}M. The boundary shifts very little during 24-hours of centrifugation. In contrast, a clear boundary between the solvent and the micellar solution is seen in Figure 26, moving with the centrifugation at a 4×10^{-5}M nonyl phenol ethoxylated decyl ether solution. The micelles are depleted from bulk solution in 17.5 hours.

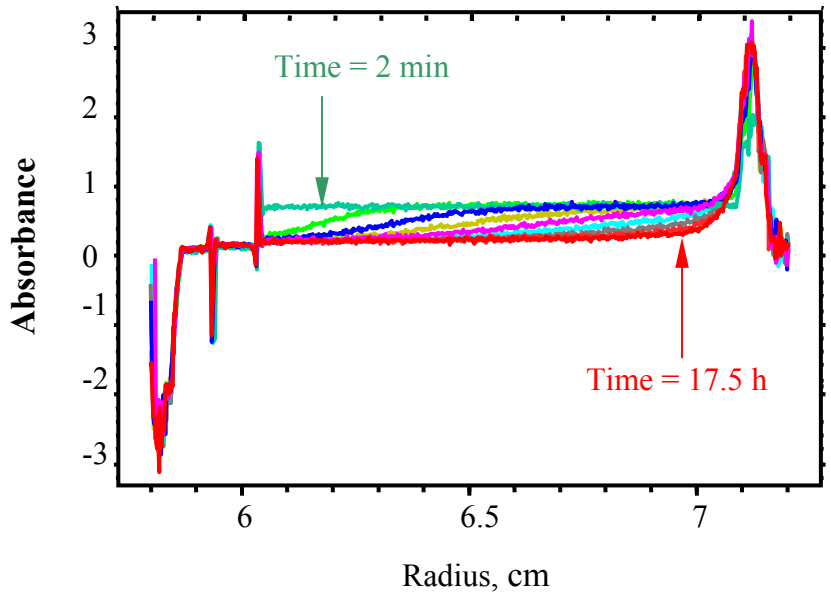

Figure 26. The sedimentation velocity experiment of nonyl phenol ethoxylated decyl ether at concentration above cmc. Experimental conditions: concentration: 4×10^{-4} M, detector: UV, wavelength: 300nm, rotor speed: 40,000 rpm. The scan interval is 2.5 hours.

The variation of sedimentation coefficients with concentration of n-dodecyl-β-D-maltoside, nonyl phenol ethoxylated decyl ether and their 1:1 mixtures is shown in Figure 27. These three surfactants used here exhibit an increasing trend, suggesting formation of larger aggregates [34, 35]. Sedimentation coefficients of n-dodecyl-β-D-maltoside increase from twice cmc and reach a plateau above 5 times cmc, showing a behavior different from that of sodium dodecyl sulfate

[36]. For ionic surfactants, the Gibbs free energy of electrostatic interaction between charged molecules predominate the packing interaction in the formation of micelles [37]. Nonyl phenol ethoxylated decyl ether reaches the plateau at 30 times cmc while the sedimentation coefficients of its mixtures with n-dodecyl-β-D-maltoside keep increasing up to 200 times cmc. Since the values of sedimentation coefficients of nonionic micelles depend only on properties such as micellar mass, size and shape, these micelles must experience growth governed by concentration. At low concentrations, the sedimentation coefficients for mixtures are close to those for nonyl phenol ethoxylated decyl ether, suggesting that nonyl phenol ethoxylated decyl ether plays a predominant role in the micellization. The value of sedimentation coefficients for mixtures are close to that for n-dodecyl-β-D-maltoside at higher concentrations, suggesting that the partition of n-dodecyl-β-D-maltoside in the mixed micelles have an effect on the size and shape of mixed micelles.

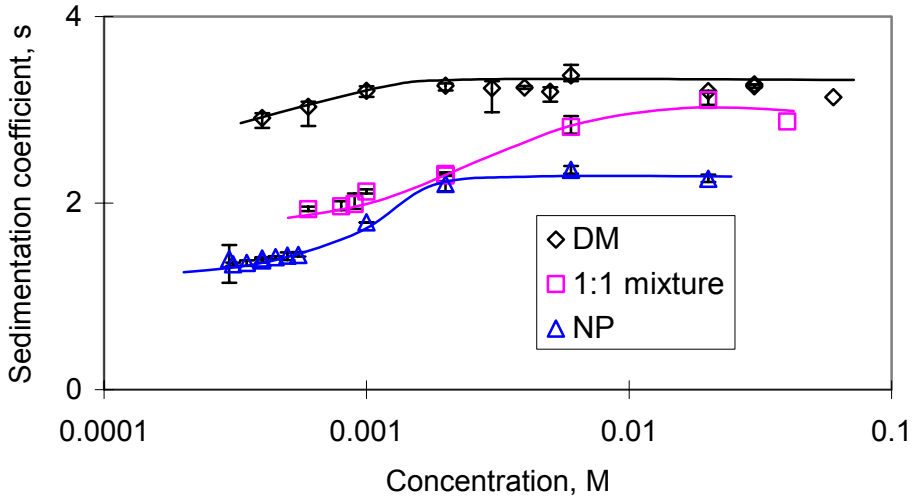

Figure 27. Sedimentation coefficients as functions of concentrations of n-dodecyl-β-D-maltoside, nonyl phenol ethoxylated decyl ether and their 1:1 mixtures.

A number of parameters can be derived from Figure 27 and these are given in Table 14. The standard sedimentation coefficients at 25^0C, S^0_{25}, and diffusion coefficients at cmcs, D_0 can be obtained by extrapolating the data at low surfactant concentrations close to cmcs using sedimentation velocity and dynamic light scattering techniques.

Table 14. Hydrodynamic parameters of n-dodecyl-β-D-maltoside, nonyl phenol ethoxylated decyl ether and 1:1 mixed micelles at cmc.

Parameters at cmc / Surfactant	$D_0 \times 10^{11}$ (m^2/s)	$S^0_{25} \times 10^{13}$ (s)	M_0 (kDa)	Agg. No.	R_H (nm)	r_0 (nm)	f/f_{shape}
N-dodecyl-β-D-maltoside	7.96	2.83	49.3	94	3.08	2.5	1.03
1:1 mixture	6.33	1.697	53.7	92	3.88	2.66	1.15
Nonyl phenol ethoxylated decyl ether	5.37	1.215	69.4	105	4.57	2.94	1.18

The aggregation numbers of n-dodecyl-β-D-maltoside and nonyl phenol ethoxylated decyl ether agree with those in the previous report and in the literature [38-42]. The concentration dependence of aggregation number is of particular interest. The aggregation number for n-dodecyl-β-D-maltoside in literature was found to be 94 at concentration of twice cmc while the value increases to 110 and then to 134 at higher concentrations [38-40]. Nonyl phenol ethoxylated decyl ether showed two distinct aggregation numbers of 125 and 276 [41,42].

The composition of mixed micelle is assumed to be the same as the mixing ratio, 1:1, to obtain the aggregation number, which is smaller than those of n-dodecyl-β-D-maltoside and nonyl phenol ethoxylated decyl ether. Since both surfactants are uncharged, the observed behavior is attributed to the geometric constraints, i.e. packing mode.

It is clear that all the hydrodynamic radii of the surfactants are larger than those of the hypothetical minimum radii. A single surfactant molecular length can be estimated as a sum of hydrophobic hydrocarbon chain length and hydrophilic head group radius. The hydrocarbon chain length of n-dodecyl-β-D-maltoside is taken as 1.67 nm in its fully stretched conformation following Tanford's equation [43]. Although the SAXS techniques yield the full length of two glucose units to be 1-1.2 nm [44, 45], the real length in the direction of hydrocarbon chain is only 0.62 nm [40]. The difference is due to both the hydrophilic head not aligning with the hydrophobic tail and the outside sugar ring bending towards the inner ring [40]. Thus the actual length of n-dodecyl-β-D-maltoside molecule is 2.29 nm. Nonyl phenol ethoxylated decyl ether has a length of 4.9 nm with a hydrophobic part of 1.8nm and a hydrophilic part of 3.1 nm [46].

The difference between the calculated surfactant molecular lengths and the hydrodynamic radii of micelles can provide information on the micellar shape as determined by asymmetry and hydration. Since the molecular length of nonyl phenol ethoxylated decyl ether is larger than the r_0, either oblate or prelate ellipsoid is feasible rather than the spherical shape.

In order to calculate the f/f_{shape} from the above equations, information on hydration is required. The hydration number per glucose unit is taken as 7.9 [39]. The hydration number per polyethylene glycol unit varies from 3 to 4.4 [47-50]. Since the surfactant molecules are solvated better at low concentrations and the polyethylene surfactants with phenol groups have a higher degree of hydration [50], a value of 4.4 is selected for nonyl phenol ethoxylated decyl ether.

The results show that the micelles are cylindrical at cmc. N-dodecyl-β-D-maltoside is found to have an axial ratio of 1.6 for both oblate and prelate cylinders, fitting well with 1.69 obtained using SANS technique [40]. The axial ratio for nonyl phenol ethoxylated decyl ether is 3.7 for the prelate and 4 for the oblate and for the mixture, 4 for the prelate and 4.4 for the oblate.

The literature value [51] from intrinsic viscosity is 5.4 for nonyl phenol ethoxylated decyl ether micelle for prelate and 1.9 for oblate. However, the hydration numbers obtained are negative for prelate and 1.8 for oblate, which deviates from the range described above.

To identify the micellar species in solutions at concentrations above cmc, the concentration distributions of sedimentation coefficient C(s) for n-dodecyl-β-D-maltoside, nonyl phenol ethoxylated decyl ether and their mixtures were examined as a function of the sedimentation coefficient at different concentrations (Figure 28). Two species are discovered to coexist for nonyl phenol ethoxylated decyl ether and its mixed solution with n-dodecyl-β-D-maltoside while only one species is present in the n-dodecyl-β-D-maltoside solution. The micellar species 1 of nonyl phenol ethoxylated decyl ether and its mixture with n-dodecyl-β-D-maltoside have the same sedimentation coefficients as those at concentration of cmc, indicating that the species 1 are the micelles at cmc.

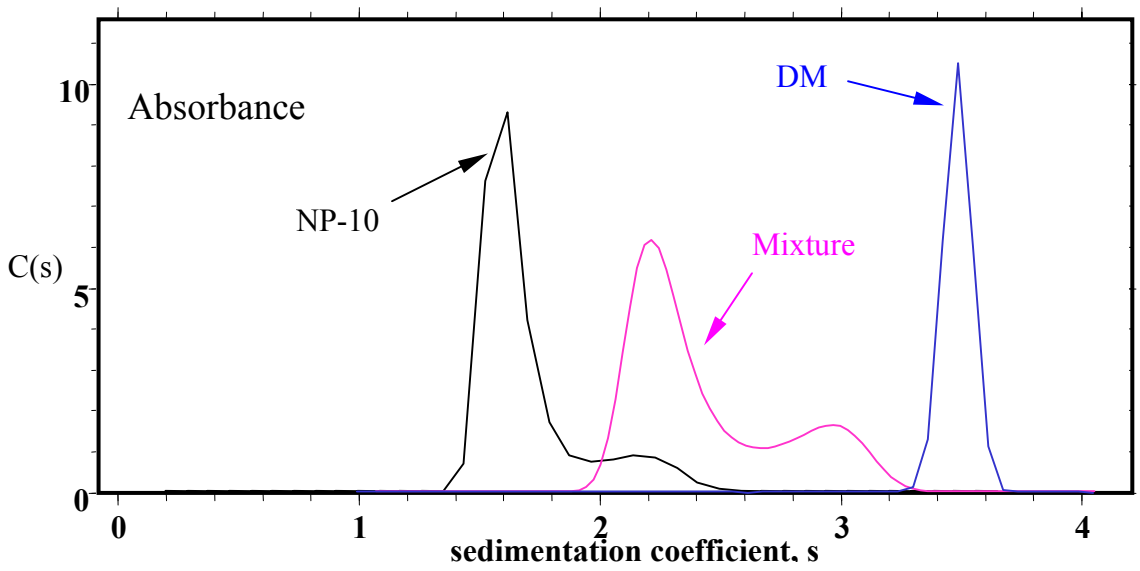

Figure 28. Micellar species in n-dodecyl-β-D-maltoside, nonyl phenol ethoxylated decyl ether and their 1:1 mixtures at 2×10^{-3}M. Experiment is conducted using RI detector at 40k rpm and temperature of 25^0C.

Study of micellar shape using Cryo-TEM technique

Typical micrographs of surfactant solutions of n-dodecyl-β-D-maltoside, nonyl phenol ethoxylated decyl ether and their 1:1 mixtures at concentration of 6×10^{-3}M are presented in Figure 29. Interestingly, the n-dodecyl-β-D-maltoside micelles form finger print structures. The coexistence of spheroidal and flexible cylindrical micelles was noticed for the nonyl phenol ethoxylated decyl ether and its mixtures with n-dodecyl-β-D-maltoside. Moreover, it is easy to identify the three-fold junction, suggesting the formation of network structures.

These findings account for the drastic increase in the micellar size of the mixed micelles with increased concentration using dynamic light scattering techniques mentioned above. Cryo-TEM images were taken to visualize the micelles, showing that both nonyl phenol ethoxylated decyl ether and its mixtures with n-dodecyl-β-D-maltoside micelles contain primary micelles and networks of elongated micelles while n-dodecyl-β-D-maltoside micelles are cylindrical.

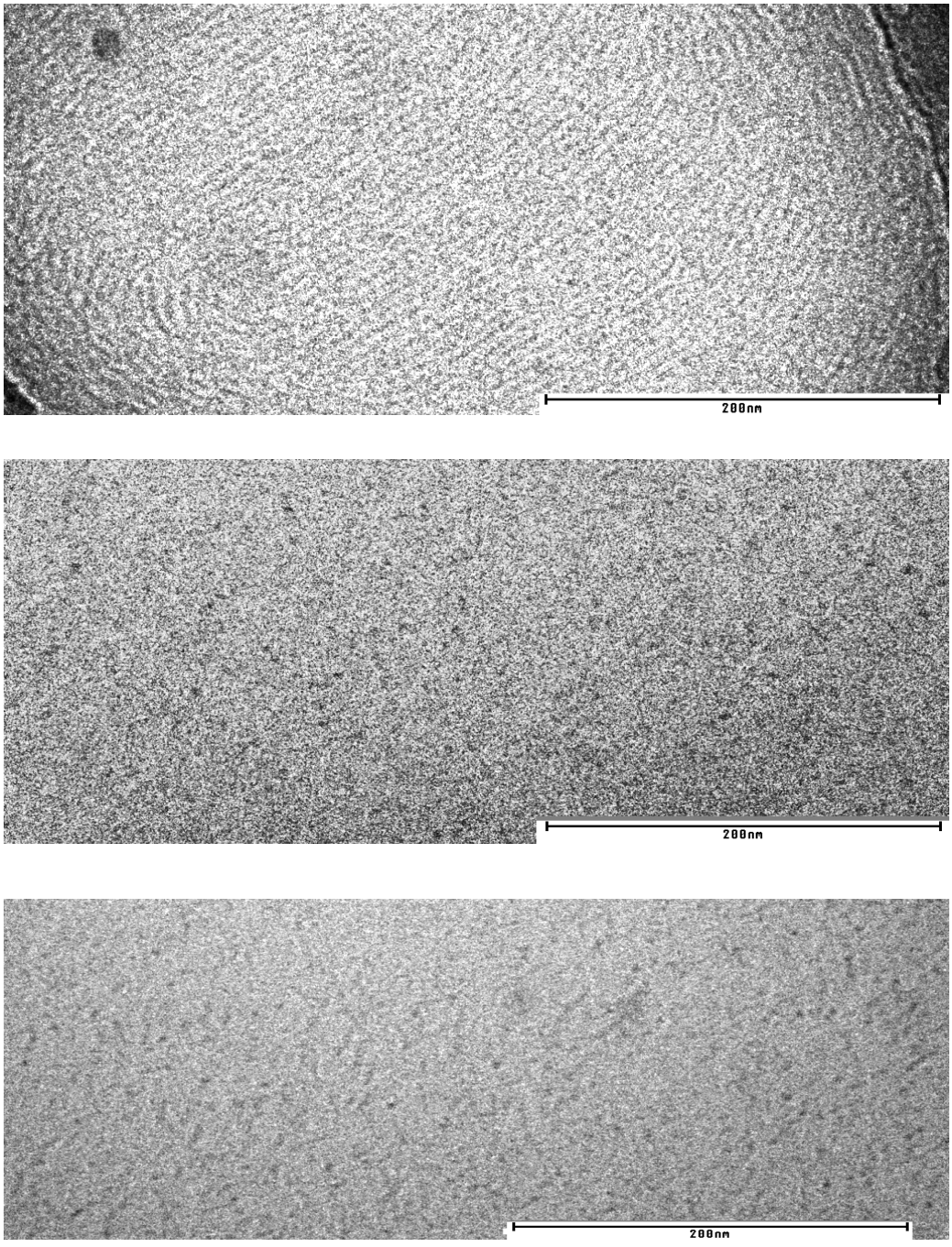

Figure 29. **Cryo-TEM images of surfactant solutions of n-dodecyl-β-D-maltoside (upper), its 1:1 molar ratio mixture with nonyl phenol ethoxylated decyl ether (middle) and nonyl phenol ethoxylated decyl ether (bottom) at concentration of 0.006M and temperature of 25^0C.**

Reasons for the difference in micellar size and shape

The difference in the micellar size and shape of sugar-based and polyethylene oxide surfactants can be accounted for considering their molecular structures. As mentioned in section 3.1, the hydrophobic part and the hydrophilic group form an angle of 58.9^{o} so that the ratio of hydrophobic over hydrophilic group is 2.7. In contrast to the n-dodecyl-β-D-maltoside, the hydrocarbon chain in n-dodecyl-β-D-maltoside molecule is connected to the flexible polyethylene groups and the ratio is 0.6. The micellar shape is governed by the packing free energy [52].

Ultrafiltration study of nonideality of mixture solutions

In our previous works, analytical ultracentrifugation has shown the coexistence of two types of mixed micelles in the mixtures of nonyl phenol ethoxylated decyl ether (NP-10) and n-dodecyl-β-D-maltoside (DM). In order to understand the role of mixing ratio in determining the formation of elongated micelles, the concentration and component composition of micellar species II (elongated micelles) were determined using ultrafiltration technique at a total surfactant concentration of 0.02M. Figure 30 shows the change in concentration of micellar species II with the increase in DM composition in the mixtures. In individual NP-10 solutions, over 40% of the surfactant forms large micelles (micellar species II). The amount of micellar species II decreases sharply with the addition of DM in the mixtures. Micellar species II was absent at DM composition of over 60% in the mixture. Obviously, NP-10 is responsible for the generation of micellar species II.

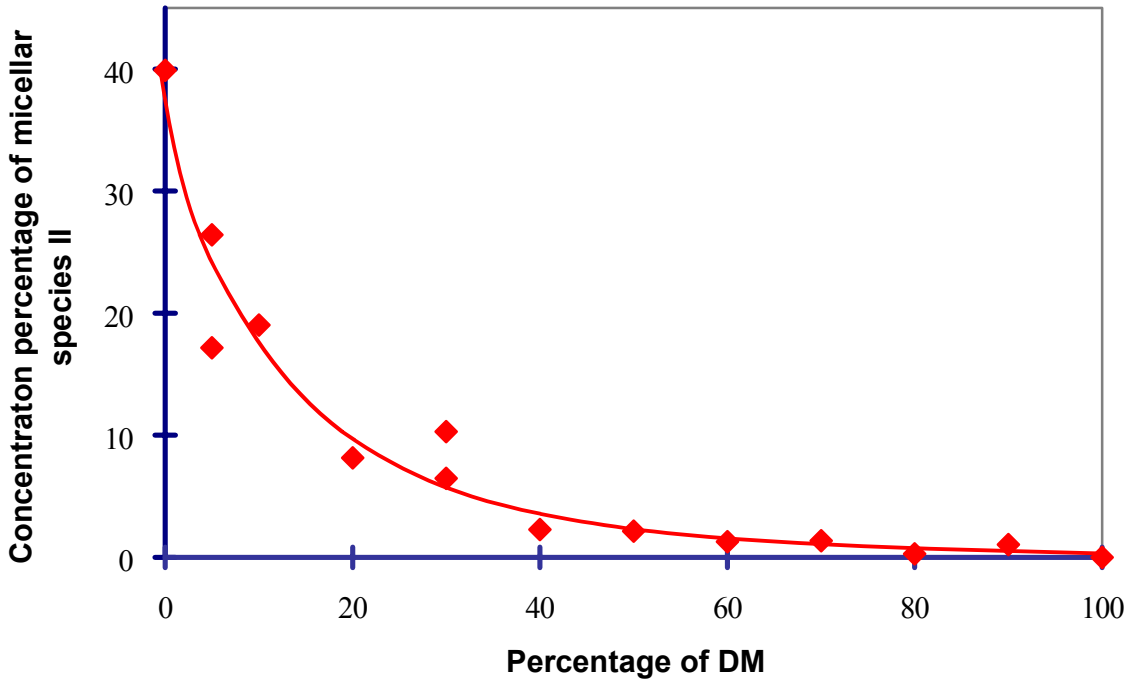

Figure 30. Change in the concentrations of micellar species II in the mixtures of nonyl phenol ethoxylated decyl ether (NP-10) and n-dodecyl-β-D-maltoside (DM) as a function of percentage of DM in mixtures.

NP-10 and DM contents in micellar species II were determined after separating micellar species by ultrafiltration. Results obtained are shown in Figure 31. Lower than ideal NP-10 composition was observed in the NP-10/DM solutions, for systems with appreciable amount of micellar species II, indicating the nonideality in the formation of nonionic mixed micelles.

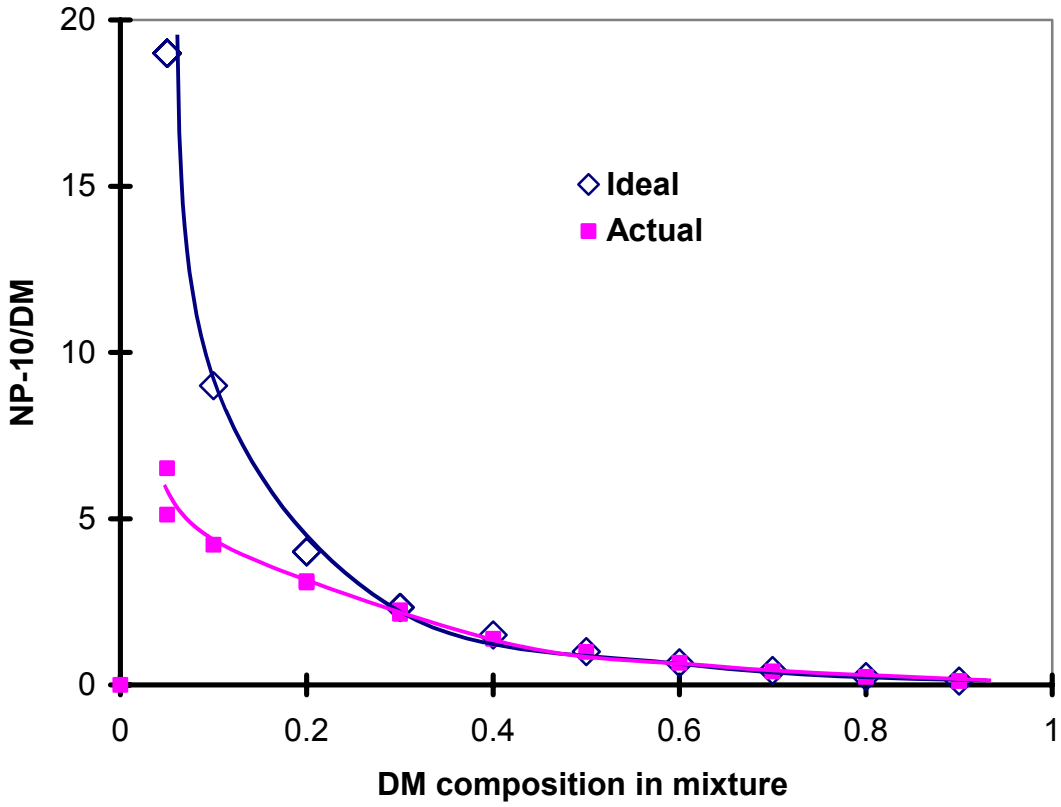

Figure 31. The comparison of actual mixing ratio of NP-10/DM in micellar species II to ideal mixing ratio (same as in bulk solution), as a function of DM composition.

Adsorption of sugar-based surfactant and anionic surfactant mixtures on alumina

Co-adsorption of n-dodecyl-β-D-maltoside (DM) and sodium dodecylsulfonate ($C_{12}SO_3$) on alumina was investigated under neutral pH condition (pH 7) when the negatively charged sulfonate can adsorb strongly on positively charged alumina. The results obtained for the adsorption of DM/$C_{12}SO_3$ 1:1 mixture on alumina at pH 7 are given in Figure 32. It is to be noted that at this pH, considerable amounts of both surfactants adsorb on alumina. In the very dilute concentration range, the adsorption of the mixture under these conditions is between that of DM and sodium dodecyl sulfonate, and the adsorption densities are almost the same for both the mixture and its individual components.

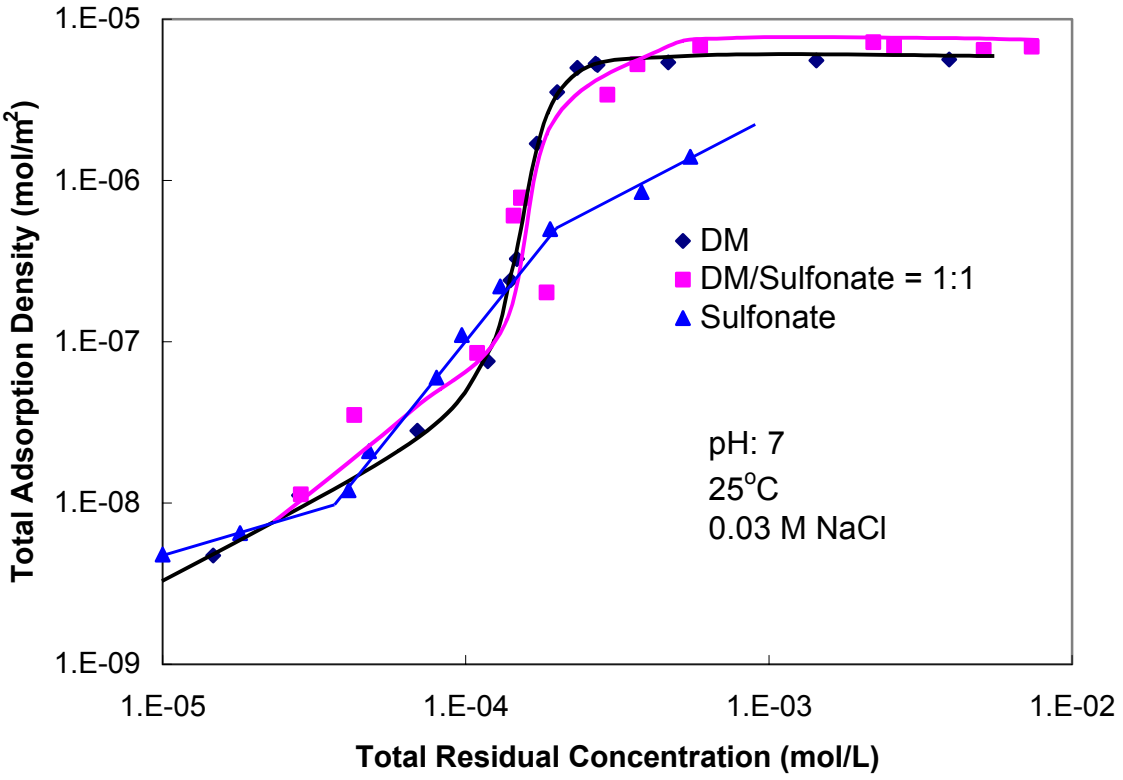

Figure 32. Adsorption of n-dodecyl-β-D-maltoside (DM), sodium dodecyl sulfonate and DM/Sulfonate 1:1 mixture on alumina at pH 7.

The effect of n-dodecyl-β-D-maltoside (DM) to sodium dodecylsulfonate ($C_{12}SO_3$) mixing ratios on the adsorption of DM, sulfonate and their mixtures is illustrated in Figure 33 for 3:1 and 1:1 ratios. The results show that there are synergistic effects between sulfonate and DM adsorption under these conditions, but the mixing ratio change from 1:1 to 3:1 show very little effect on the total adsorption density of the surfactant mixtures.

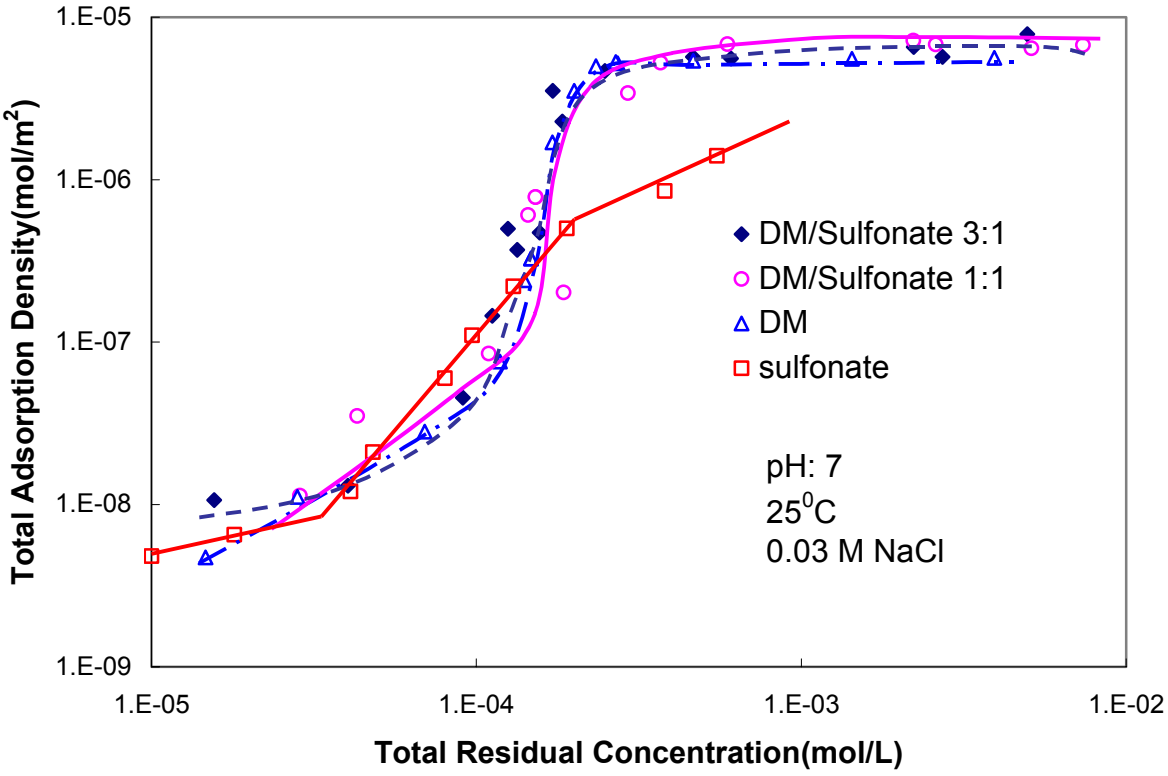

Figure 33. Adsorption of n-dodecyl-β-D-maltoside (DM), sodium dodecyl sulfonate and their 3:1 and 1:1 mixtures on alumina at pH 7.

The adsorption of sodium dodecyl sulfonate from its individual solution and from the DM/Sulfonate mixtures on alumina is plotted in Figure 34 as a function of the residual sulfonate concentration at pH 7. Adsorption of sulfonate from the mixtures is enhanced by the presence of DM in both the very high concentration regions (more obvious in the case of DM/Sulfonate=1:1) and dilute concentration regions (more obvious in the case of DM/Sulfonate=3:1). This is proposed to be due to the adsorbed DM functioning as anchor molecules for the sulfonate through hydrophobic chain-chain interactions. Thus for the sulfonate, there are obvious synergistic effects in adsorption from the surfactant mixtures with DM.

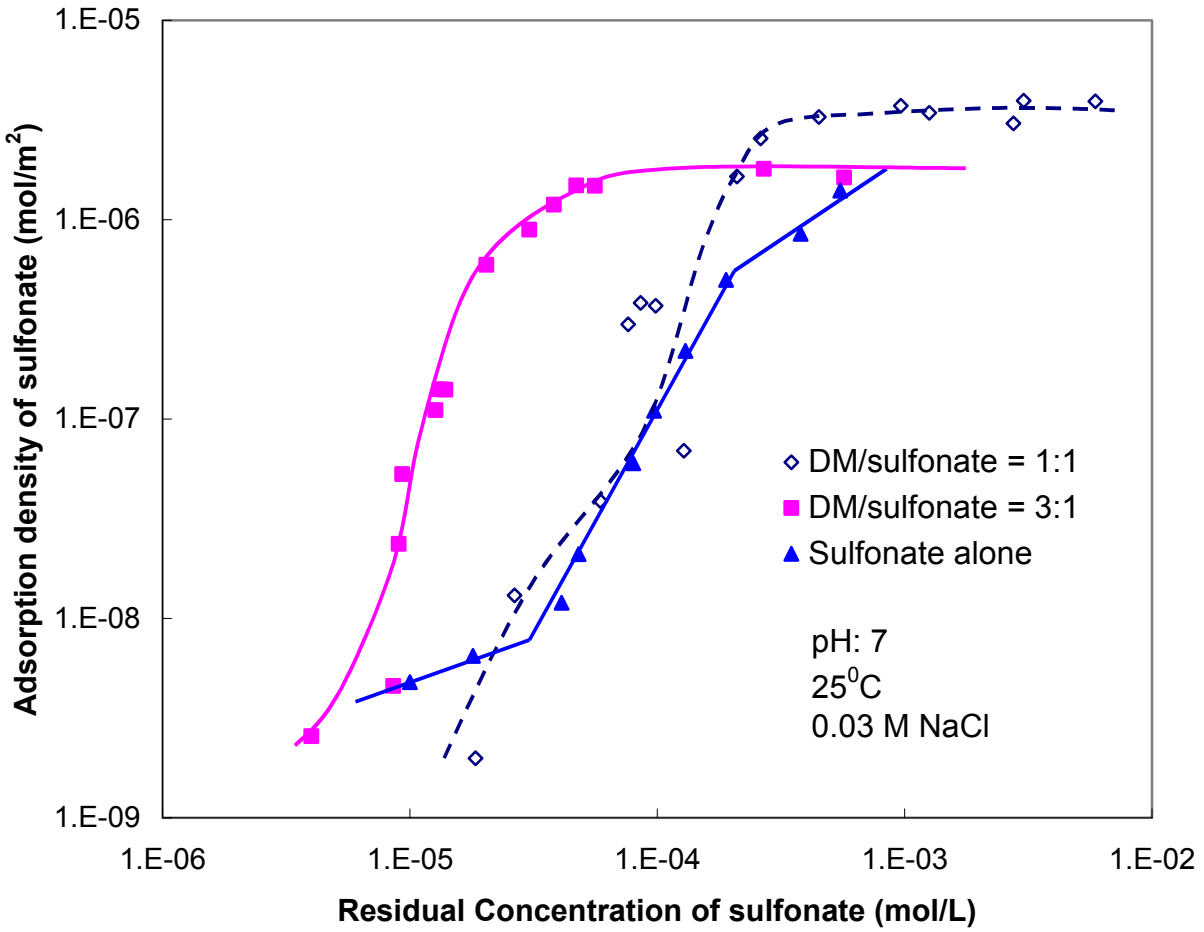

Figure 34. Adsorption of sodium dodecyl sulfonate on alumina at pH 7: Adsorption from sulfonate alone and from mixtures with DM.

In contrast to the above, it can be seen from Figure 35 that the DM adsorption is enhanced by sulfonate only in the dilute concentration range, and depressed slightly in the plateau region. More the sulfonate in the mixture, more is the effect on DM adsorption. At the 1:1 DM/Sulfonate mixture, DM adsorption begins to decrease slightly after reaching adsorption plateau, which could be due to the adsorption competition from sulfonate for adsorption sites. The resulting total adsorption, as shown above in Figure 33, does not decrease after plateau, and is slightly higher than DM alone. Therefore, it can be concluded that in this system at pH 7, there are synergistic

effects between DM and sulfonate. However, the decrease in adsorption obtained particularly in the high concentration region has implications for reducing surfactant loss in EOR processes.

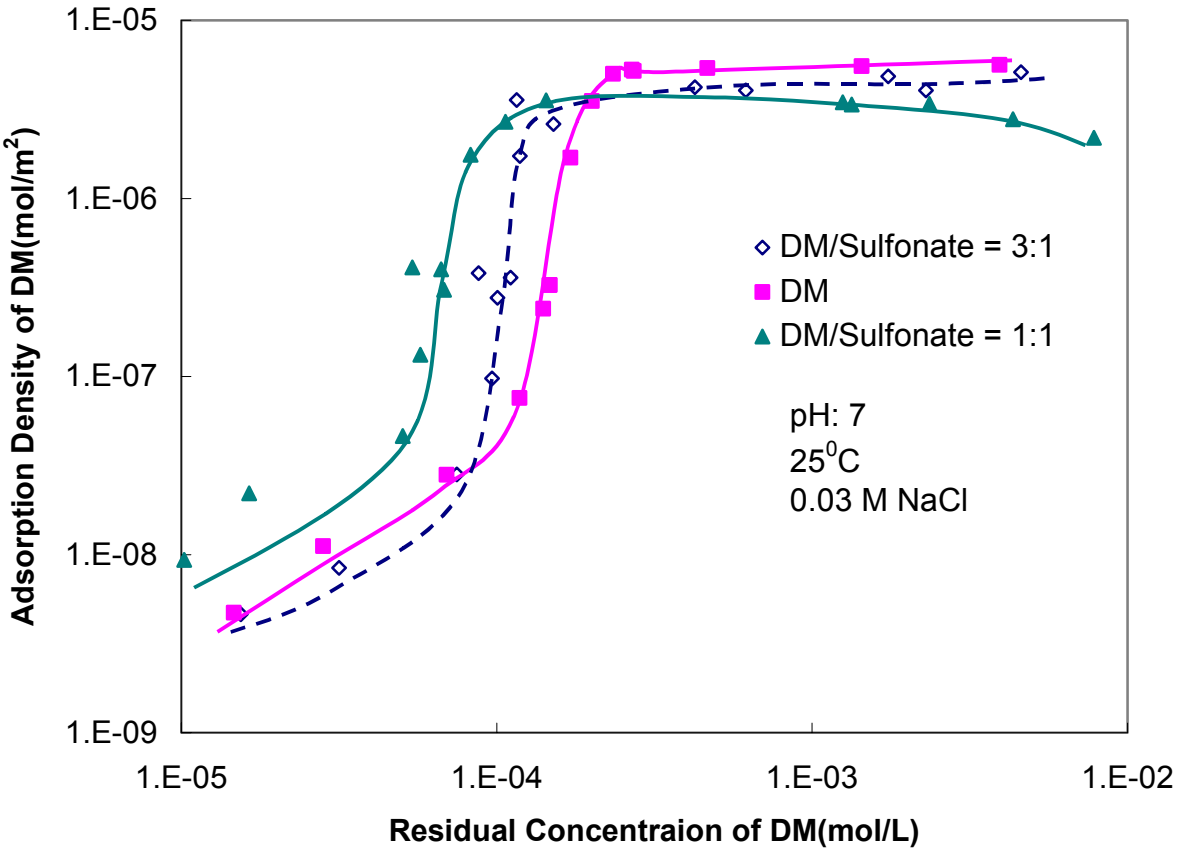

Figure 35. Adsorption of n-dodecyl-β-D-maltoside (DM) on alumina at pH 7: Adsorption from DM alone and from mixtures with sodium dodecyl sulfonate.

Effect of Ionic strength on surfactant adsorption on alumina

No significant effect of ionic strength change on adsorption of DM on alumina has been observed. Increase in the ionic strength in the solution tends to reduce the adsorption of anionic sodium dodecylsulfonate on alumina at pH 7 when alumina is positively charged. It is believed that the observed synergistic effects on the adsorption of DM/Sulfonate mixtures on alumina at pH 7 would be less and less visible and might be negligible with the increase in ionic strength,

which is ascribed to the effect of ionic strength on electrostatic adsorption of the sulfonate.

Effect of pH on the adsorption of DM/Sulfonate surfactant mixtures on alumina

As pH variation does change the form of actual active gradients in chemical flooding, it can also dramatically change and even reverse the surface charge properties of reservoir minerals. The mineral dissolution is also dependent on pH among other factors. Thus solution pH plays an important role in EOR efficiency. When it comes to the environmental impact from chemical waste in EOR, chemical pH adjustment through the addition of acidic or basic materials is another important factor to be considered. The adsorption of DM/Sulfonate surfactant mixtures on alumina has been studied further to take into account the effect of solution pH. From our previous studies, the adsorption of sodium dodecylsulfonate on alumina has been found to change dramatically with pH. Sulfonate adsorbs on alumina in much larger magnitude under acidic conditions than under neutral or basic conditions, with the difference being several orders of magnitude.

Figure 36 shows two adsorption isotherms of DM on alumina at different solution pH. Even though DM adsorbs onto positively charged alumina through the same mechanism at both pH 4 and 7 (with an initial adsorption step, a sharp increase and then a plateau), the magnitude of adsorption is different by orders of magnitude. Clearly, adsorption of DM on alumina varies dramatically, when the solution pH is increased from pH 4 to pH 7. In all the concentration ranges, the higher pH yields much higher DM adsorption on alumina, with only negligible adsorption at pH 4.

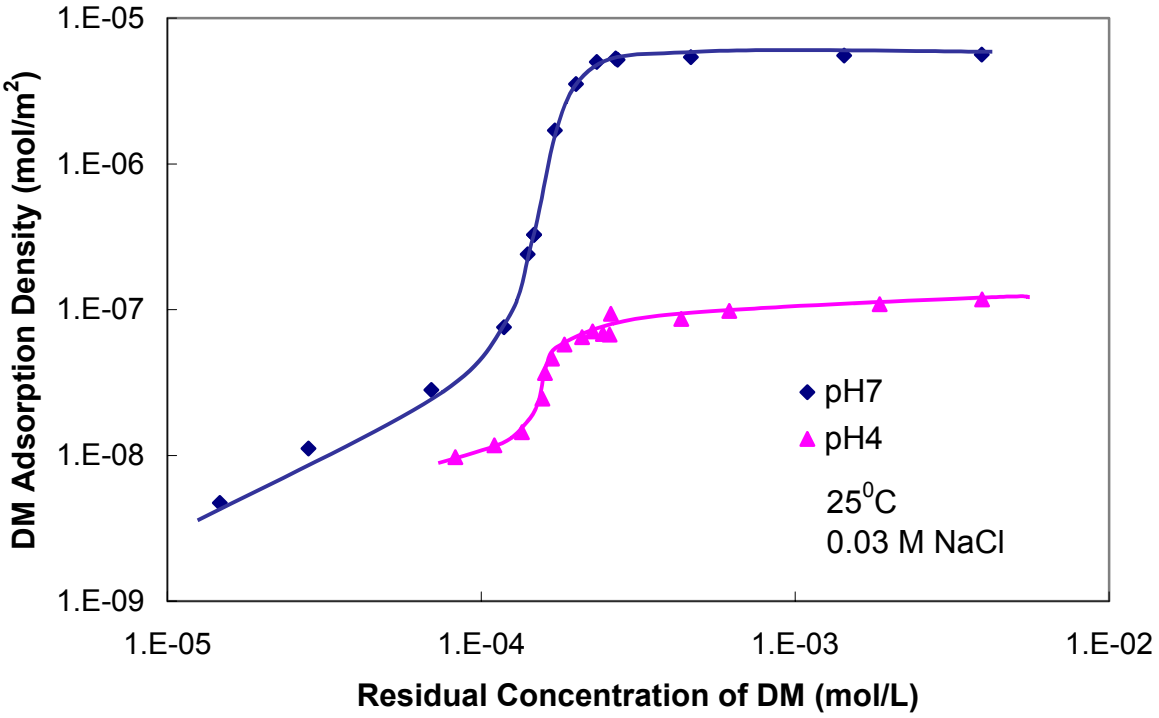

Figure 36. Adsorption isotherms of n-dodecyl-β-D-maltoside (DM) on alumina at pH 4 and 7.

Adsorption of DM alone and DM mixtures with sodium dodecylsulfonate is plotted in Figure 37 as a function of solution pH. In this set of experiments, the initial DM concentrations in all the test solutions have been kept at 4mM, which yields saturation adsorption for both individual surfactants and surfactant mixtures. From Figure 37, it can be seen that the adsorption density of DM increases sharply in the pH range of 4 to 7, with no further increase above pH 7. The adsorption density of DM at neutral and basic conditions is 30 to 40 times higher than that at pH 3 (from 3.5E-6 mol/m^2 to 1.0E-7 mol/m^2). The observed difference in adsorption of DM on alumina caused by pH change is proposed to be due to the hydrogen bonding between the hydroxyl groups in DM and those on the alumina surface.

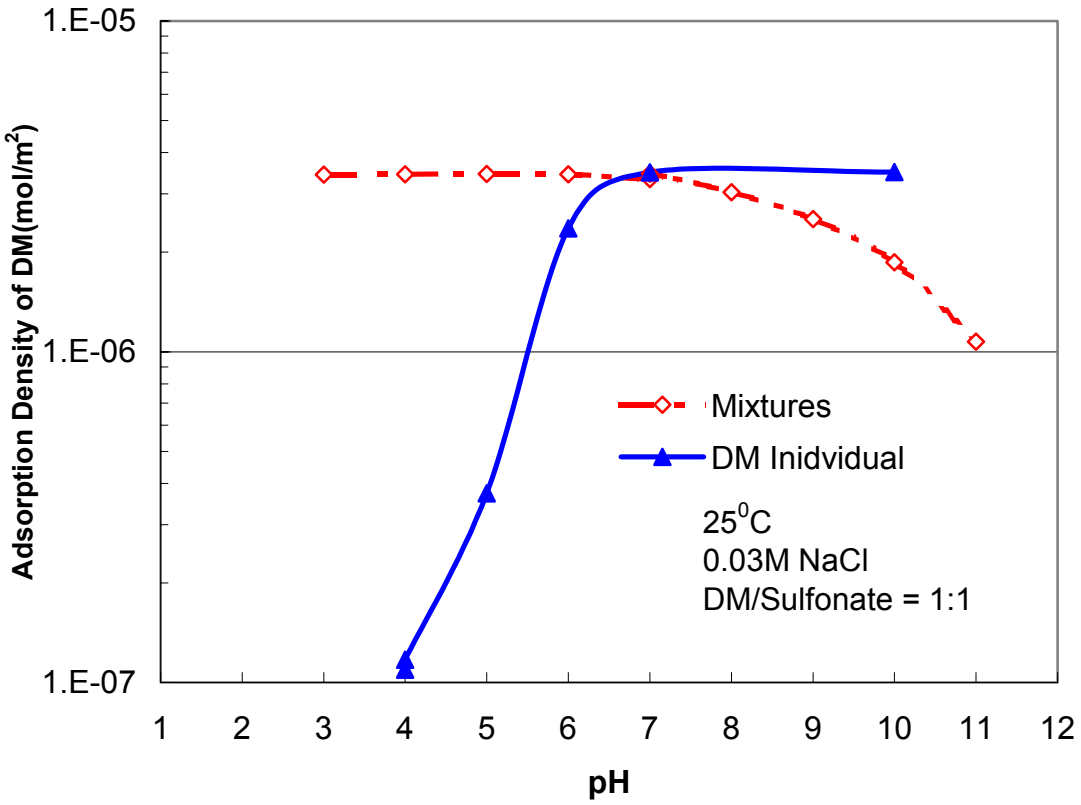

Figure 37. Adsorption of n-dodecyl-β-D-maltoside (DM) on alumina from DM alone and from its mixtures with sodium dodecylsulfonate as a function of pH. Initial DM concentration is 4mM, yielding saturation adsorption at all pH.

Interestingly, the effect of pH on the adsorption of DM from its mixtures with sodium dodecylsulfonate is the opposite to that of the adsorption of DM alone. The adsorption density of DM from its mixtures with sulfonate stays essentially the same from pH 3 to pH 7, and then decreases when pH becomes basic. Under acidic conditions, DM in the mixtures with sulfonate adsorbs more than from the single component DM system, while under basic conditions, DM alone shows greater adsorption than the DM from its mixtures with sulfonate. The completely opposite trend of the effect of pH strongly suggests that significant synergistic effects exists between DM and sulfonate under acidic conditions, and antagonistic effects under basic conditions. The adsorption synergism is attributed here to the hydrophobic chain-chain

interaction between DM and sulfonates, while the observed antagonism is due to competition for adsorption sites.

Theoretical study of adsorption of mixed surfactants at solid/liquid interfaces

A preliminary model is proposed in order to predict the mixed adsorption behavior. In this model, active surface site interacts with n_a monomers of species *a* and n_p monomers of species *p* to form hemimicelles. At equilibrium, an equation can be written as:

Site + n_a Monomer *a* + n_p Monomer *p* $\rightarrow$ Hemimicelle

With the equilibrium constant $k = a_{ss} / a_s a_a^{na} a_p^{np}$

Here, a_{ss}, a_s, a_a, and a_p are activities of hemimicelle, unoccupied active surface site, monomer concentration of species *a* and activity of species *p*, respectively. N_a and n_p are aggregation numbers of species *a* and species *p*, respectively. The total aggregation number of two species, *n,* is the sum of n_a and n_p.

The activities of a_a, and a_p can be replaced by C_a, solution concentration of species *a*, and C_p, solution concentration of monomer *p*, respectively. If one applies mass action law to use Γ and Γ_∞ instead of a_{ss} and a_s, the adsorption density Γ can be solved as a function of (k, n, *x*, α). Γ and Γ_∞ are adsorption densities at certain concentration and maximum adsorption density at high concentration respectively. *x* and α are the solution and surface compositions. The model contains two parameters to take into account the competition between micellization in solution and hemicelles at the solid/liquid interface. At low concentration (n=1), the model reduces to Langmuir form. Clearly there is a need for further development and test of the model.

Theoretical study of micellization of mixed surfactants in solutions

There exists no general theory yet that can adequately describe the composition

dependence of the excess thermodynamic properties of surfactant mixtures. Regular solution theory is one of the most popular models, which has been used so far to examine the behavior of surfactant mixtures. But comparison of experimental results with the expected behavior of the excess heat of mixing from the regular solution approximation shows poor agreement. The results demonstrate that, in spite of the success of this model for predicting critical micellar concentrations in non-ideal mixtures, it does not properly account for the heats of mixing in these systems. Synergism between different surfactant species is usually observed in the formation of mixed micelles. This apparently indicates that the interaction between different surfactant species is stronger than that between the same surfactant species. Due to this specific interaction, the mixing process in real systems is not completely random. On the other hand, the basic assumption of the regular solution theory is that the excess entropy of mixing is zero. This means that regular solution theory treats the mixed systems as ideal mixing from the viewpoint of randomness in mixing. Since the micellar phase is not a real separate phase, the aggregation number of micelles is limited. This fact will also make totally random mixing not valid for such cases. So when mixed surfactant systems are modeled, some constraints must be applied to account for the nonrandom mixing in the formation of mixed micelles.

Instead of using a very complex statistical thermodynamic model to treat this nonrandom mixing phenomenon, the concept of the relative solubility of each surfactant component in mixed micelles is considered. A packing constraint parameter is introduced to describe such nonrandom mixing. For example, for the case of a mixture of an ionic surfactant *A* and a nonionic surfactant *B*, where the latter is more surface active than the former, it is reasonable to assume that the nonionic surfactant *B* will form micelles first when the total concentration exceeds the mixture cmc, and then species *A* can dissolve in *B* micelles to form mixed micelles. When a small

quantity of *A* is dissolved in the *B*-rich mixed micelles, the formation of mixed micelles will be enhanced due to the synergism between the two surfactants. But a further increase in the *A* component in mixed micelles may then decrease the stability of mixed micelles, since excessive *A* in mixed micelles may cause packing problems and introduce strong electrostatic repulsion among head groups in the micelles. It is clear that there will be a packing limit for surfactant *A* in mixed micelles. When the *A* composition in the micelles is lower than this limit, the micellization process will be enhanced due to synergism between the two surfactants. On the other hand, when the *A* composition exceeds the packing limit in the micelles, the micellization process will become energetically unfavorable. Instead of surfactant *B*, if *A* can form micelles by itself, the solubility of nonionic *B* in A micelles can be treated as infinity. In other words, there is no packing limit for nonionic *B* species in *A* micelles. This hypothesis indicates that the micellization process is not a symmetrical process in terms of the micellar composition. The asymmetrical behavior in the mixed micellization process is an important aspect which should be taken into account in any attempt to model surfactant mixtures.

On the basis of the above analysis of mixed surfactant systems, several fundamental assumptions for modeling binary surfactant mixtures *A* and *B* are proposed:

(1) Interactions between two types of surfactant species can be represented using an interaction parameter, *W*. Here, the interaction will arise mainly from van der Waal's attractive forces, and *W* for binary surfactant mixtures is always $\leq$ 0. When $W = 0$, there is no special interaction between two different surfactant species, and the surfactant mixture can be treated as an ideal system.

(2) The formation of mixed micelles is affected by the packing properties of the surfactants. For binary surfactant mixtures, a packing parameter *P** can be employed to indicate

the packing constraint of surfactant *A* in surfactant *B*-rich micelles. This packing constraint is directly related to the nonrandom mixing in the system. On the other hand, the packing limit of surfactant *B* in surfactant *A*-rich micelles is taken as infinity, where the surfactant *B* is defined to be more surface active than the surfactant *A*.

(3) By adapting the equation in the lattice model for the enthalpy of mixing in liquid mixtures, the excess free energy G^E for the formation of mixed micelles can be represented by the following equation:

$$G^E = RTWX(1-X)\left(1-\frac{X}{f(\alpha)P^*}\right)$$

where α is the overall surfactant ratio of component *A* in the mixture, $f(\alpha)$ is a function of α, *X* is the molar fraction of surfactant *A* in mixed micelles, *W* is the interaction parameter, and *P** is the packing parameter. The function $f(\alpha)$ is used here to modify the possible change of the packing parameter as a function of the overall mixing ratio α. Similar to the relationship of packing density of two different particles as a function of mixing ratio, $f(\alpha)$ can be described by the following equation:

$$f(\alpha) = \begin{cases} \alpha, & \alpha > 0.5 \\ 1-\alpha, & a \le 0.5 \end{cases}$$

This equation indicates that the packing constraint will keep changing with any change in the overall surfactant mixing ratio. When the overall mixing ratio approaches 0 or 1, the packing ability in mixed micelles will be better than that when the ratio is about 0.5 (1:1 mixture). For the same total concentration of the binary mixture, the possibility for *A* and *B* surfactant to contact with each other will be maximum when the overall mixing ratio is 0.5, and the packing constraint will then become more significant.

To better understand the micellization behavior predicted by the proposed model, the excess free energy G^E is plotted at different levels of relevant parameters as a function of the

mole fraction of component *A* in mixed micelles. For the purpose of comparison, the excess free energy calculated from regular solution theory with the interaction parameter β = -3 is also plotted. The effect of the interaction parameter on the excess free energy G^E is presented in Figure 38. In this Figure, the packing parameter *P** is fixed at 1.2, and the overall mixing ratio of surfactant *A* is taken as 0.5 (1:1 mixture). It can be seen that the excess free energy G^E predicted is *not* symmetric with respect to the molar fraction of components in mixed micelles. Regular solution theory predicts that excess free energy is symmetric and will reach a minimum when the mole fraction of surfactant *A* is 0.5. But this is not the case with the model proposed here. According to the new model proposed here, the excess free energy G^E will reach a minimum when the mole fraction of component *A* in mixed micelles is about 0.25. In other words, the mole fraction corresponding to the minimum excess free energy is shifted to a lower value in this case. This suggests that by taking the packing effect into account the optimum mole fraction of component *A* in mixed micelles is lower than that predicted by the regular solution theory, thus the mixing of component *A* in mixed micelles is not as easily achieved as predicted by the regular solution theory. This is one of the reasons that regular solution theory cannot properly predict the micellization behavior above the cmc. It can also be seen from Figure 38 that the asymmetry of the excess free energy becomes more marked with a decrease in the interaction parameter *W*.

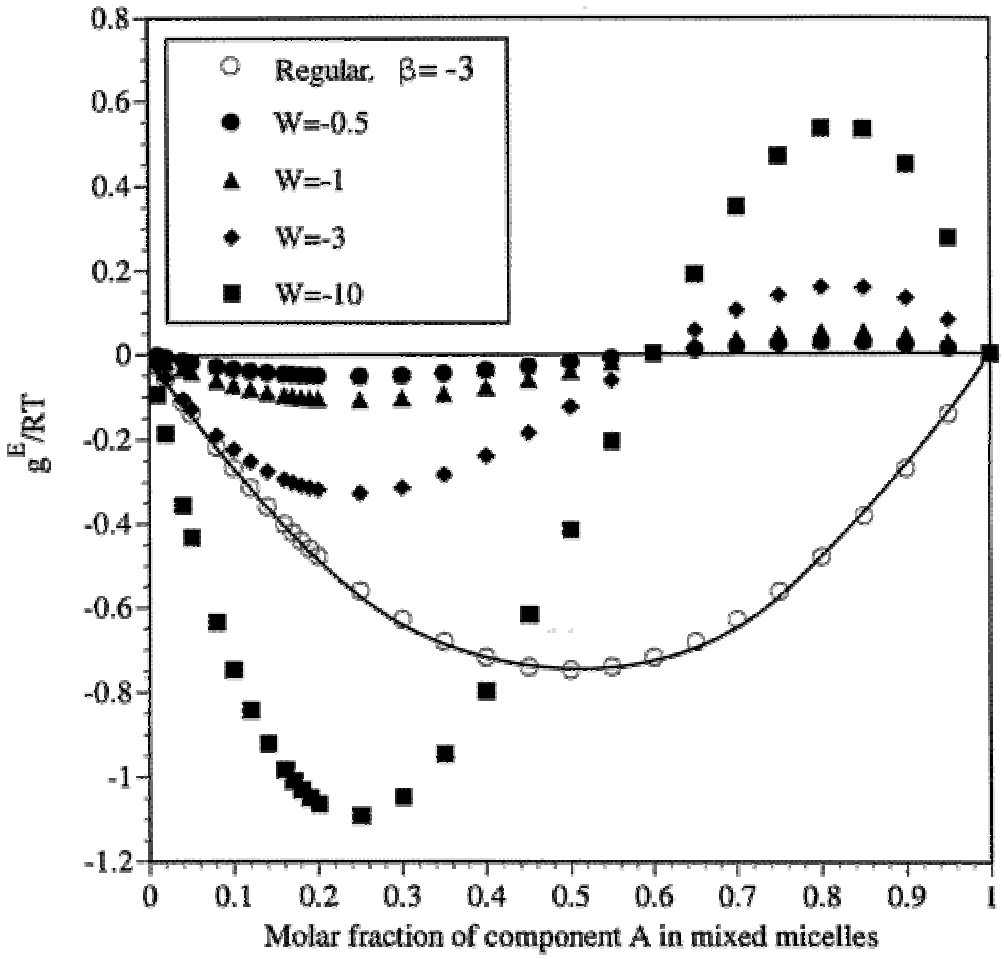

Figure 38. Effect of interaction parameter on the excess free energy.

The effect of packing parameter on the excess free energy is illustrated in Figure 39. In this plot, the interaction parameter W is fixed at -3, and the overall mixing ratio α at 0.5. It can be seen that the calculated excess free energy G^E decreases with an increase in packing parameter P^* and the G^E curve approaches the curve predicted by the regular solution theory ($\beta = -3$). It is clear that the asymmetry phenomenon in mixed micelles is controlled mainly by the packing parameter P^*. When the packing parameter approaches infinity, the proposed model will be same as that in the regular solution theory. Hence the model can be regarded as a generic equation for binary surfactant mixtures, and the regular solution theory, as only a special case of it. It is noted that the minimum excess free energy shifts to the lower mole fraction region of

component *A* in mixed micelles when the packing parameter for the mixture becomes smaller, and the negative value of the excess free energy becomes smaller also. This suggests that the formation of mixed micelles will be more difficult with a decrease in the packing parameter.

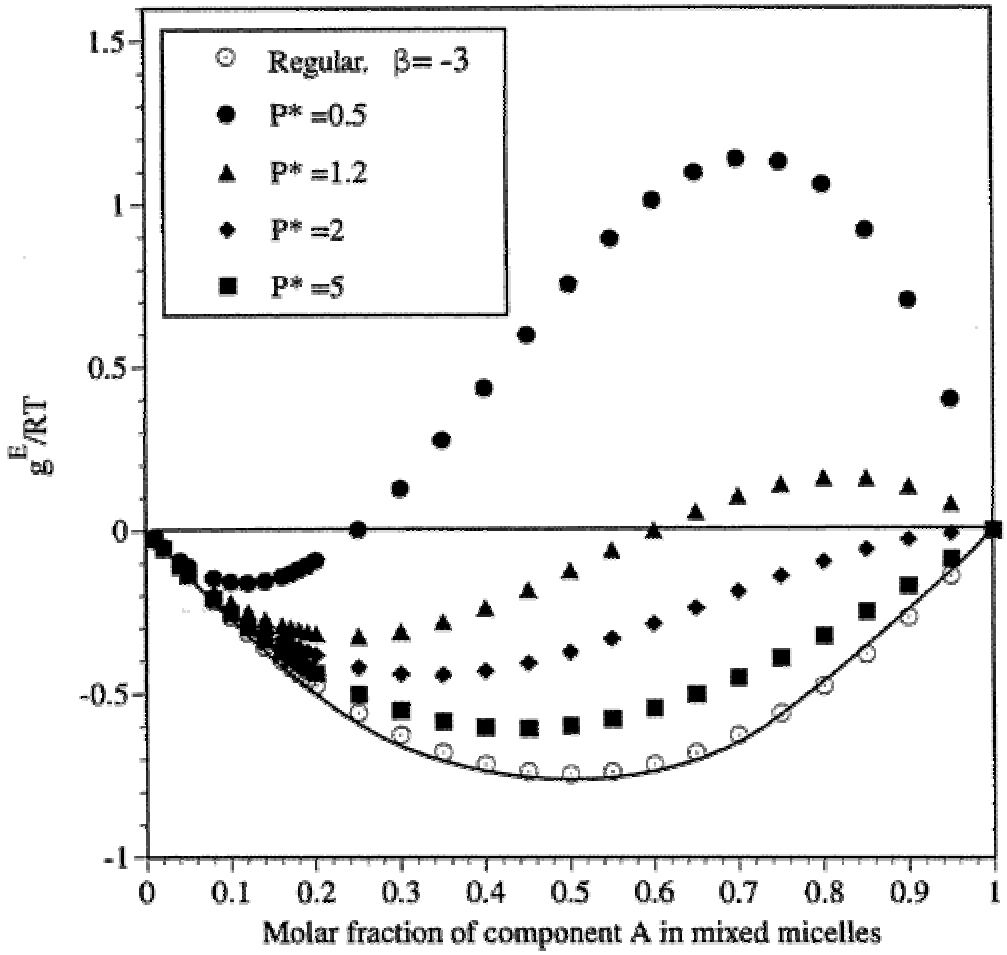

Figure 39. Effect of packing parameter on the excess free energy.

SUMMARY AND CONCLUSIONS

The aim of the project is to develop structure-relationships of surfactant mixtures in aqueous solutions and to facilitate optimization of formulations for enhanced oil recovery processes. In this project, aggregation and adsorption behaviors of sugar-based surfactants, especially their mixtures with other types of surfactants, in solutions and at solid/liquid interfaces have been investigated as a function of various parameters relevant to enhanced oil recovery (EOR). The major findings are summarized with scientific significance and industrial importance highlighted.

Analytical ultracentrifuge has been successfully applied for the investigation of surfactant micelles. The unique ability of this technique to separate particles and simultaneously monitor them made it possible for direct characterization of aggregate species, their size, shape and structures in mixed micellar solutions. Analytical ultracentrifuge has been shown to be powerful for investigating interactions in surfactant mixtures for enhanced oil recovery processes because it can distinguish individual components and different types of aggregates in complex systems. Also, the pressure generated by centrifugal force can be used to investigate the effect of pressure in deep oil well on the micellization of surfactant mixtures and surfactant-polymer interactions.

Partial specific volumes of sugar-based surfactants and their mixtures

For accurate results in analytic ultracentrifugation experiments, partial specific volumes of n-dodecyl-β-D-maltoside (DM), nonyl phenol ethoxylated decyl ether (NP-10) and their 1:1 mixture at 25°C were determined from density measurements. Theoretical calculation by Durchschlag's method was also applied to compare with experimental results. The calculated

partial specific volume of NP-10 is very close to that obtained experimentally for Triton-100, which has chemical-structure similar to NP-10.

Partial specific volume of DM was calculated using two empirical methods: $d\rho/dc$ and V_σ. The difference between data obtained using these two methods is within 0.5%. However, Durchschlag's theoretical calculation method has a deviation of -3.3 to -0.3% from experimental results. The rigid sugar group structure of DM is responsible for the large deviation. This reinforces the importance of packing of molecules in mixed micelles. Partial specific volume per sugar ring of n-decyl-β-D-glucoside (C10G), n-decyl-β-D-maltoside (C10M), n-dodecyl-β-D-maltoside (C12M) and n-dodecyl-β-D-maltotrioside (C12TM) followed the order: C10G > C10M > C12M > C12TM. The variation could be accounted for by considering the flexibility of β-conformation of sugar group in the solution. The easier the sugar-group can rotate, the larger the error.

Micellization has a larger effect on the partial specific volume. Below the cmc, the value is smaller than that above cmc. Deviation of the partial specific volume are 0.4%, 1.9% and 2.3% for DM, mixture and NP-10, respectively, when concentration is below 10 times cmc. Above that, the partial specific volumes are constant. The values are 0.820 for DM, 0.921 for NP-10, and 0.878 for their 1:1 mixture. No effect has been observed for mixing on partial specific volume of individual surfactant, suggesting that there is no interaction between the two surfactant components in the mixed micelles. This result was confirmed by determining their interaction parameters from surface tension measurements.

The temperature coefficient is computed to be 8×10^{-4} $cm^3g^{-1}K^{-1}$ using both $d\rho/dc$ and V_σ methods ranging from 25-50°C. This implies that the mixed micelle is sensitive to change in

temperature. The partial specific volume at high temperatures is larger than that at low temperatures. Thus the fluidity of surfactants mixed solutions is enhanced under reservoir temperature conditions, requiring reduced pressure for injecting chemicals in chemical flooding process.

Mixtures of sugar-based surfactants with other types of surfactants in solution

Mixtures of sugar-based n-dodecyl-β-D-maltoside (DM) with nonionic nonyl phenol ethoxylated decyl ether (NP-10) in solution were studied by surface tension and sedimentation velocity measurements. Critical micelle concentrations, maximum adsorption, cross sectional area per molecule and Gibbs free energy for micellization of DM, NP-10 and their 1:1 mixtures were calculated. Calculated interaction parameter, close to zero, indicates that there is no strong interaction between the two surfactants in mixed micelles.

Sedimentation velocity experiments were performed to determine the sedimentation coefficient and aggregation mass. Three software: OptimaTM XL-A/XL-I data analysis software, DCDT+, and Svedberg were applied for the data analysis in the sedimentation velocity experiments. Aggregation numbers obtained are 209, 127, 111 respectively. The last one is closest to the result from light scattering tests. The reasons why the three software gives different results are discussed. DCDT+ has a better resolution than OptimaTM XL-A/XL-I analysis software, and Svedberg is better than DCDT+ in that all data can be treated in analysis. The resolution by Svedberg analysis is better than that of DCDT+. Sometimes Svedberg is unable to yield results due to back diffusion effect.

Micellization behavior of the mixtures of sugar-based surfactant and nonionic surfactant

The nature and distribution of surfactant micelles in solutions was investigated using analytical ultracentrifugation. From sedimentation equilibrium experiments, both nonyl phenol ethoxylated decyl ether and its mixtures with n-dodecyl-β-D-maltoside were found to have two types of micelles. The average aggregation number of n-dodecyl-β-D-maltoside, nonyl phenol ethoxylated decyl ether and their mixtures are 148±9, 100±13 (species 1) and 299±73 (species 2) and 92±27 (species 1) and 306±79 (species 2), respectively. Two different aggregation numbers of 100 and 276 are reported in literatures for nonyl phenol ethoxylated decyl ether. Our study revealed, for the first time, that small micelles can coexist with larger micelles at high concentrations due to the unique structure of the surfactant. The implication of this finding lies in the fact that efficiency of oil recovery can be improved due to the large micellar size and its polymer-like viscosity and oil solubilization.

Mixed micelle formation in the DM/NP-10 surfactant mixtures was studied using ultrafiltration technique. The results suggest that NP-10 is responsible for the generation of elongated micellar species II. Lower than ideal NP-10 composition was observed in the NP-10/DM solutions, for systems with appreciable amount of micellar species II, suggesting the nonideality in the formation of nonionic mixed micelles. Analysis of the apparent diffusion coefficients of n-dodecyl-β-D-maltoside, nonyl phenol ethoxylated decyl ether and their 1:1 mixtures obtained using the dynamic light scattering technique indicates aggregate formation in solutions, supporting the sedimentation equilibrium results.

Aggregate structures of mixed surfactants in solutions

The micellar size and shape of sugar-based surfactant, n-dodecyl-β-D-maltoside, nonyl phenol ethoxylated decyl ether and their 1:1 molar ratio mixtures were determined in dilute

concentration regimes using analytical ultracentrifuge velocity experiment. The aggregation number of n-dodecyl-β-D-maltoside, nonyl phenol ethoxylated decyl ether and their 1:1 mixtures at cmcs were determined to be 94, 105 and 92, respectively. The micelles were not spherical in shape and the asymmetry at cmcs follows the order: n-dodecyl-β-D-maltoside <1:1 mixture <nonyl phenol ethoxylated decyl ether.

At concentrations above cmc, these nonionic micelles grow into cylindrical shapes. Two types of micelles are detected to coexist in nonyl phenol ethoxylated decyl ether solutions and its mixtures with n-dodecyl-β-D-maltoside while only one micellar species is present in n-dodecyl-β-D-maltoside solutions. For nonyl phenol ethoxylated decyl ether and its mixtures with n-dodecyl-β-D-maltoside, type I micelles were primary ellipsoidal micelles at cmc and type II micelles were elongated micelles. Cryo-TEM technique provided visualization of micellar size and shape, which support the results from analytical ultracentrifuge and dynamic light scattering techniques. The molecular structures of n-dodecyl-β-D-maltoside and nonyl phenol ethoxylated decyl ether are responsible for the differences in the micellar shapes of single surfactants and their mixtures. Both the relative hydrocarbon / hydrophilic chain length and the flexibility of the hydrophilic groups contribute to the packing parameters and hence the excess free energy.

Adsorption of mixtures of nonionic sugar-based surfactant with anionic surfactant on alumina

Co-adsorption of sugar-based n-dodecyl-β-D-maltoside (DM) on alumina from its mixtures with anionic sodium dodecylsulfonate ($C_{12}SO_3$) was investigated to identify adsorption synergism or antagonism. At pH 7 where alumina is positively charged, marked synergistic effects between DM/$C_{12}SO_3$ were observed, especially in the region where hydrophobic chain-chain interactions dominate the adsorption process as long as the surface is not saturated. In the

plateau region, there was competition for adsorption sites, with slight adsorption decrease of DM. At this pH, $C_{12}SO_3$ and DM promote the adsorption of each other and there exists mainly synergism. For the surfactant mixing ratios studied, higher the concentration of the other surfactant component in the mixtures, the stronger is the synergism in the rising part of the adsorption isotherms.

Solution pH plays an important role in determining the adsorption of both individual surfactants DM and $C_{12}SO_3$ on alumina. With the decreasing pH from acidic to basic range, there was reduced $C_{12}SO_3$ adsorption. On the other hand, increased adsorption of DM was observed with increasing pH from acidic to basic range. The overall effect of pH on the adsorption of DM/$C_{12}SO_3$ mixtures was marked. At lower pH conditions, significant synergistic effects exist between DM and $C_{12}SO_3$, due to the hydrophobic chain-chain interaction among surfactants. At higher pH (basic conditions), the presence of $C_{12}SO_3$ in the systems reduces the adsorption of sugar-based surfactants (DM) especially in the plateau region of the isotherm. In general there is mainly antagonistic effects between n-dodecyl-β-D-maltoside (DM) and sodium dodecylsulfonate ($C_{12}SO_3$) in this pH region, due to the competition for adsorption sites. The observed competitive adsorption between DM and $C_{12}SO_3$ on minerals at basic pH conditions provides us with valuable information for obtaining reduced surfactant loss in efficient chemical flooding EOR processes.

Theoretical studies of the adsorption of mixed surfactants at solid/liquid interfaces and micellization of mixed surfactants in solutions

A preliminary model was proposed to predict the mixed surfactant adsorption behavior. In the model, adsorption process was treated as a chemical reaction in equilibrium between

adsorbed mixed surfactant hemimicelles and active surface sites, monomers of species *a* and monomers of species *p* in solutions. From this model, the adsorption isotherm is fitted and information on aggregation number in surface aggregate and excess adsorption free energy (especially nonionic surfactant mixtures in our study) is generated as a function of mixing ratio, surfactant structure etc

A new model for binary surfactant mixtures and their micelles in solution has been proposed. Considering nonrandom mixing in the formation of mixed micelles, the concept of packing constraint is introduced, and this is represented by the packing parameter, P^*. The significant characteristic of this model is that it examines the asymmetric behavior of micellization in binary surfactant mixtures. This asymmetric behavior is controlled mainly by the value of the packing parameter. With an increase in the packing parameter, the formation of mixed micelles becomes more random. This new model can be considered as a generic model of binary surfactant mixtures with the regular solution theory being a special case of it, when the packing parameter approaches infinity.

Predictive model is used to examine the adsorption and aggregation behavior of surfactant especially mixed surfactant systems in solutions and at solid/liquid interfaces. It will be used to reveal the crucial role of surfactant aggregates, especially mixed aggregates, in controlling important interfacial properties such as wettability in enhanced oil recovery processes.

REFERENCES

1. Tom Wines, PhD thesis, Columbia University, 2002
2. Helmut Durchschlag and Peter Zipper, "calculation of the partial volumes of organic compounds and polymers", Progress in Colloid & Polymer Science, 94 (1994), 20-39
3. Helmut Durchschlag and Peter Zipper, "Calculation of partial specific volumes of detergents and lipids", Jorn. Com. Esp. Deterg., 26 (1995), 275-292
4. Beckman Coutler, User's manual
5. Allen Furst, Beckman Coutler's website, "Overview of sedimentation velocity for the Optima^{TM} XL-A analytical ultracentrifuge"
6. D. K. McRorie, and P. J. VoelkerAnalytical ultracentrifugation, Vol. 2: Self-associating systems in the analytical ultracentrifuge,1993
7. Allen T. Ansevin, Dennis E. Roark and David A. Yphantis, "Improved ultracentrifuge cells for high-speed sedimentation equilibrium studies with interference optics", Analytical biochemistry 34, 237-261, (1970)
8. Svedberg, T., Petersen, K. O., Bauer, J. H., The Ultracentrifuge, 1940, The Clarendon Press, Oxford
9. Tanford, Charles. Physical Chemistry of Macromolecules. (1961), John Wiley & Sons, New York
10. Peter Schuck, Biophys, 2000, Vol. 78, No. 3, 1606-1619
11. Peter Schuck; Matthew A. Perugini; Noreen R. Gonzales; Geoffrey J. Howlett; and Dieter Schubert, Biophysical Journal, 2002, Vol. 82, No. 2, 1096-1111
12. Philo, John S., Analytical Biochemistry, 2000, 279(2), 151-163.
13. Philo, John S., Biophysical Journal, 1997, 72(1), 435-444.

14. Philo, John S., Mod. Anal. Ultracentrifugation, 1994, 156-70.
15. Helmut Colfen, Critical reviews, Vol. CR 69, "Characterization of polymers and particles with the analytical ultracentrifuge"
16. Steele, J. C. H. Jr., Tanford, C., Reynolds, J. A., Methods Enzymol. 48 (1978), 11-23
17. Paul Becher, Journal of Colloid Science 16 (1961), 49-56
18. Calum J. Drummond, Gregory G. Warr, Franz Grieser, Barry W. Ninham and D. Fennell Evans, "Surface properties and micellar interfacial micrenvironment of n-dodecyl-β-D-maltoside ", J. Phys. Chem. B. 1985, 89, 2103-2109
19. J. A. Molina-Bolívar, J. Aguiar and C. Carnero Ruiz, "Growth and hydration of Triton X-100 micelles in monovalent alkali salts: a light scattering study", Molecular Physics, 2001, Vol. 99, No. 20, 1729-1741
20. A. González-Pérez, J. L. Del Castillo, J. Czapkiewicz, and J. R. Rodríguez, "Temperature dependence of equilibrium and transport properties of decyldimethylbenzylammonium chloride in aqueous solutions", J. Chem. Eng. Data 2001, 46, 709-711
21. C. Dupuy, X. Auvray, and C. Petipas, "Anomeric effects on the structure of micelles of alkyl maltosides in water" langmuir 1997, 13, 3965-3967.
22. K. S. Birdi, "The size, shape and hydration of micelles in aqueous medium", Progress in colloid & polymer science, 1985, 70, 23-29.
23. Timmins, P. A., Leonhard, M., Weltzien, H.U., Wacker, T., Welte, W., "A physical characterization of some detergents of potential use for membrane protein crystallization", FEBS Lett. 238, 361-368, 1988
24. S. Bucci, C. Fagotti, V. Degiorgio, and R. Pianza, Langmuir 7: 824 (1991)
25. J. Schick, J. Phys. Chem. 66, 1326, 1962

26. C. W. Dwiggins, J. Phys. Chem. 64, 1175 (1960)

27. Bernheim-Groswasser, A.; Wachtel, E.; Talmon, Y.; Langmuir; 2000; 16(9); 4131-4140

28. W. E. McMullen, W. M. Gelbert and A.Ben-Shaul in Micelles, membranes, microemulsions, and monolayer, (W. M Gelbart, A. Ben-Shaul, D. Roux Ed.), Springer-Verlag, 1994

29. R. Carabias-Martínez, E. Rodríguez-Gonzalo, B. Moreno-Cordero, J. L. Pérez-Pavón, C. García-Pinto and E. Fernández Laespada, J. Chromatography A., 2000, 251-265, 902

30. Lindman, Bjoern; Karlstroem, Gunnar. Zeitschrift fuer Physikalische Chemie (Muenchen, Germany), 1987, 155(1-2), 199-209.

31. Huw Evans, Dominic J. Tildesley, Christina A. Leng, Journal of the Chemical Society, Faraday Transactions 2: Molecular and Chemical Physics, 1987, 83(8), 1525-41.

32. Kenjo, Kazutoshi., Bull. Chem. Soc. Japan, 1966, 39(4), 685-94.

33. Benjamin James Boyd, "Structure-Property Relationships of Glucose Based Surfactants", PhD thesis, University of Melbourne, 1998

34. Karibyants, Natalia; Dautzenberg, Herbert; Coelfen, Helmut. Macromolecules, 1997, 30(25), 7803-7809.

35. Keiichi Kameyama and Toshio Takagi, JCIS, 137, 1, 1-10, 1990

36. W. L. Courchene, J. Phys. Chem., 1964, 68, 7, 1870-1874

37. W.M. Gelbart, "Micelles, Membranes, Microemulsions and Monolayers" W.M. Gelbart, A. Ben-Shaul, D. Roux ed., (Springer-Verlag New York, Inc.) 1994

38. J. Keith Wright; Ulrich Weigel; Ariel Lustig; Hubertus Bocklage; Martin Mieschendahl; Benno Miller-Hill and Peter Overath, FEBS Letters, 1983, 162, 1, 11-15

39. Gregory G. Warr; Calm J. Drummond; Franz Grieser; Barry W. Ninham; and D. Fennel1 Evans, J. Phys. Chem., 1986, 90, 4581-6

40. Dupuy, C.; Auvray, X.; Petipas, C.; Anthore, RicoLatters I.; and Lattes, A., Langmuir, 1997, 13, 3965-3967
41. C. W. Dwiggins, Jr.; R. J. Bolen and H. N. Dunning, J. Phys. Chem., 1960, 64, 1175-8
42. M. J. Schick; S. M. Atlas; and F. R. Eirich, J. Phys. Chem., 1962, 66, 1326-33
43. Tanford, Charles. The Hydrophobic Effect: Formation of Micelles and Biological Membranes. 2nd Ed.; 1980, Wiley, New York
44. Dupuy, C.; Auvray, X.; Petipas, C.; Anthore, R.; Costes F.; RicoLatters I. and Lattes, A., Langmuir, 1996, 12, 3162-3172
45. Christine Cecutti; Bonaventura Focher; Bruno Perly and Thomas Zemb, Langmuir, 1991, 7, 2580-5
46. German Urbina-villalba; Issac Reif; Mar a Lupe Mrquez and Estrella Rogel, Colloids and Surfaces A: Physicochemical and Engineering Aspects, 1995, 99, 207-220
47. Sedev, R.; Langmuir; (Technical Note); 2001; 17(2); 562-564.
48. George D. J. Phillies and Jeniffer E. Yambert, Langmuir, 1996, 12, 3431-3436
49. Harada, S.; T. Nakajima; T. Komatsu; and T. Nakagawa, J. Solut. Chem., 1978, 7, 463-474
50. V. A. Kolkov, Colloid J. of USSR, 1975, 37, (1), 107-110
51. K. S. Birdi, Progress in Colloid & Polymer Science, 1985, 70, 23-29
52. Shiloach, Anat; Blankschtein, Daniel., Langmuir, 1998, 14(25), 7166-7182

PUBLICATIONS AND PRESENTATIONS

1. A. D. Campbell, Z. Pan and P.Somasundaran. in V. Hackley, P.Somasundaran and J. A. Lewis, eds. "Polymers in Particular Systems - Properties and Applications", Marcel Dekker, Inc, New York, 2001.

2. L. Zhang, P. Somasundaran, J. Mielczarski, and E. Mielczarski, "Adsorption mechanism of n-dodecyl-β-D-maltoside on alumina", Journal of Colloid and interface science 256, 16-22, 2002.

3. Q. Qiang and P. Somasundaran. Journal of Colloid and Interface Science, 253, 231-237, 2002.

4. L. Zhang and P. Somasundaran, "Adsorption of Mixtures of Nonionic Sugar-based Surfactants", presented at the 76th ACS Colloid & Surface Science Symposium, June 23-26, 2002. Ann Arbor, Michigan.

5. P. Somasundaran and Qiong Zhou, "Environmentally Benign Surfactants For Efficient Enhanced Oil Recovery", *Second Joint DOE U.S.-People's Republic of China (PRC) Conference on Clean Energy,* Washington DC, November 2003.

6. R. Zhang, L. Zhang and P. Somasundaran, "Study of mixtures of n-dodecyl-β-D-maltoside with anionic, cationic and nonionic surfactant in aqueous solutions using surface tension and fluorescence techniques", Journal of Colloid and Interface Science, 278, 453-460, 2004.

7. R. Zhang, P. Somasundaran, "Abnormal micellar growth in sugar-based and ethoxylated nonionic surfactant and their mixtures in dilute regimes using analytical ultracentrifugation", Langmuir, 20, 8552-8558, 2004.

8. P. Somasundaran and Lei Zhang, "Mineral-Surfactant Interactions and Environmentally Benign Surfactants for Efficient Enhanced Oil Recovery", 8th International Symposium on Reservoir Wettability, Houston, TX, May 2004.

9. R. Zhang, P. Somasundaran, X.Y. Hua and K.P. Ananthapadmanabhan, "Study of Mixed Micellar Growth of Nonionic Surfactants using Analytical Ultracentrifuge", 78th ACS Colloid and Surface Science Symposium, New Haven, CT, June, 2004.

10. R. Zhang, Q. Zhou and P. Somasundaran, "Complexations of Poly(vinylcaprolactam) with Anionic Surfactants: Impact of Surfactant Molecular Structures", 78th ACS Colloid and Surface Science Symposium, New Haven, CT, June, 2004.